Earliest Embrithopod Mammals (Afrotheria, Tethytheria) from the Early Eocene of Morocco: Anatomy, Systematics and Phylogenetic Significance

Emmanuel Gheerbrant, Fatima Khaldoune, Arnaud Schmitt, Rodolphe Tabuce

Earliest embrithopod mammals (Afrotheria, Tethytheria) from the Early Eocene of Morocco: anatomy, systematics and phylogenetic significance

EMMANUEL GHEERBRANT[1], FATIMA KHALDOUNE[2], ARNAUD SCHMITT[1], and RODOLPHE TABUCE[3]

[1] CR2P, Centre de Recherche en Paléontologie, Paris, UMR 7207 (CNRS, MNHN, UPMC, Sorbonne Universités), Paris, France

[2] Office Chérifien des Phosphates (OCP Group S.A.), Khouribga, Morocco

[3]Institut des Sciences de l'Évolution (UM, CNRS, IRD, EPHE), Université Montpellier, France

Corresponding author: Emmanuel Gheerbrant, emmanuel.gheerbrant@mnhn.fr

Abstract We provide detailed morphological description, including enamel microstructure, of the earliest known embrithopod mammals (Afrotheria, Paenungulata), *Stylolophus minor* and *S. major*, n. sp., recently discovered in the early Eocene of the Ouled Abdoun phosphate basin, Morocco. *Stylolophus minor* and *S. major*, n. sp., show close morphological affinity, and the enamel microstructure supports their congeneric status. *Stylolophus major*, which comes from an upper level (middle Ypresian) of the Ouled Abdoun phosphate series, has more derived features than *S. minor* in addition to a larger size. This argues that *S. minor* and *S. major* are chronospecies. This new mammal lineage recognized in the Ouled Abdoun phosphate series is characterized by a rapid size increase, as for the proboscideans and probably in correlation with early-middle Ypresian global climatic warming events. We investigated relationships of *Stylolophus* in a new cladistic analysis based on an extended and revised matrix that includes new enamel microstructural features studied in *Stylolophus*. Resulting MPTs recover 1) basal relationships of *Stylolophus* within the Embrithopoda; 2) sister-group

relationship of the Embrithopoda to the crown Tethytheria (Proboscidea, Sirenia); and 3) the clades Tethytheria and Paenungulata. It supports in particular that the order Embrithopoda is a basal tethytherian offshoot that rapidly evolved and specialized in parallel to the splitting and early evolution of extant tethytherian orders. *Stylolophus* shows that the ancestral embrithopod morphotype was already well specialized in the early Eocene and quite distinctive with respect to other paenungulates (e.g., hyperdilambdodonty, lingual hypoconulid, cristid obliqua very lingual on the trigonid, small and lingual hypoconulid lobe on M_3, large paranasal sinuses, concave palate), even with respect to their earliest representatives. *Stylolophus minor* was larger than the contemporary proboscidean *Phosphatherium escuilliei*. Together with the stem tethytherian relationship of the Embrithopoda, it supports an old origin of the order, at least early in the Paleocene. This relationship is also most consistent with the evolution of the embrithopod hyperdilambdodont pattern from the dilambdodont and selenodont ancestral morphotype of the paenungulates, which is known in early hyracoids but not in proboscideans and sirenians, which have reduced the ectoloph. The most specialized embrithopods evolved hyperdilambdodonty in a pseudolophodont state in parallel to the true lophodonty of crown tethytherians. The Ouled Abdoun embrithopods further help indeed to show that the early Tertiary herbivorous niches of the African island favored convergent evolution of the folivorous diet in several paenungulate and tethytherian clades. At higher scale, convergence of African and Laurasian “ungulates” is supported by enamel microstructure of *Stylolophus*. The early and basalmost embrithopods *S. minor* and *S. major*, n. sp., are new evidence of the Arabo-African origin of the order.

Electronic supplementary material The online version of this article (doi: XXXXXX) contains supplementary material, which is available to authorized users.

Keywords *Stylolophus*, Embrithopoda, Tethytheria, Paenungulata, Ypresian, Eocene, Morocco, Africa

Introduction

The placental order Embrithopoda was named by Andrews (1906) for the amazing, superficially rhino-like African mammal *Arsinoitherium zitteli* Beadnell, 1902*,* the skeleton of which was entirely reconstructed based on the well-preserved material from the early Oligocene of the Fayum (Egypt). Since its discovery, the genus *Arsinoitherium* has also been found in several late Eocene-early Oligocene Arabo-African sites from Libya (Wight 1980), Oman (Thomas et al. 1989, 1999; Pickford 2015), Angola (Pickford 1986), and Tunisia (Vialle et al. 2013; Pickford 2017). Additionally, the giant species *A. giganteum* Sanders et al., 2004, was described from the late Oligocene of Ethiopia and Kenya (Sanders et al. 2004; Rasmussen and Guttierez 2009). *Arsinoitherium* is included in the endemic African family Arsinoitheriidae (Andrews 1904). *Namatherium* Pickford et al., 2008, from the Lutetian of Namibia, is the only other known arsinoitheriid genus, and the oldest known of the family. Other embrithopods belonging to the family Palaeoamasiidae were discovered in the Eocene of the North Tethyan shores, in Romania (*Crivadiatherium* Radulesco et al., 1976; Radulesco and Sudre 1985; Radulesco and Samson 1987) and in Turkey (*Palaeoamasia* Ozansoy, 1966, and *Hypsamasia* Maas et al., 1998; Ozansoy, 1966; Sen and Heintz, 1979; Kappelman et al. 1996; Maas et al., 1998; Sen 2013; Erdal et al. 2016). More recently, *Stylolophus* Gheerbrant, 2018, from the early Eocene of the Ouled Abdoun, Morocco, was reported as the oldest known African embrithopod (Gheerbrant et al. 2018).

Palaeoamasiids remain very poorly known, mostly by dental remains, but they are clearly more primitive than the arsinoitheriids, suggesting a possible North Tethyan origin of the order Embrithopoda (e.g., Erdal et al. 2016). The interordinal relationships of the Embrithopoda remained debated since the discovery of *Arsinoitherium* because of its

remarkable specializations such as the hyperdilambdodont molars (Court 1992a). However, the current view is that the order is an extinct branch of the afrotherian paenungulates (e.g., Simpson 1945), aside to the extant hyracoids, proboscideans, and sirenians. The relationship of the order within Paenungulata has long been debated. The order was initially related to the Hyracoidea by Andrews (1906). Later, it was considered as the sister group to Tethytheria (Gheerbrant et al. 2005; Gheerbrant 2009; Tabuce et al. 2007), sirenians (Seiffert 2007; Gheerbrant et al. 2014), or proboscideans (Tassy and Shoshani 1988; Court 1990, 1992b; Fischer and Tassy 1993; Asher et al. 2003; Benoit et al. 2013b). A sister group relationship of the Embrithopoda to the Proboscidea was for long time the most consensual hypothesis; this hypothesis has been challenged with the discovery of *Stylolophus* (Gheerbrant et al. 2018).

We here describe in detail the new material of *Stylolophus* from the early Eocene (Ypresian) of Morocco reported in Gheerbrant et al.'s (2018) preliminary paper. This material belongs to two species, *Stylolophus minor* Gheerbrant, 2018, and the new species *Stylolophus major*, n. sp., which are the most primitive known embrithopods. Their stratigraphic age is detailed and discussed in Gheerbrant et al. (2018).

Methods and abbreviations

CT Scan, 3D modelization, softwares

All studied specimen here were subjected to X-ray Computed Tomographic (CT) imaging at the AST-RX platform of the MNHN, using a GE Sensing and Inspection Technologies phoenix|x-ray v|tome|x L240-180 CT scanner. We used the microfocus RX source 240 kV, detector 400x400 mm with a matrix of 2024 pixels (pixel size: 200x200 mm).

The table 1 summarizes the scan parameters of studied specimens.

Table 1 here

Data were reconstructed using datos|x reconstruction software (Phoenix|x-ray, release 2.0) and then exported into a 16 bits TIFF image stack of 1717 virtual slices in transversal view. We used MIMICS Innovation Suite software (Materialise, Research Edition, release 19-21) for the analysis, 3D modelling, and measurements on the 3D model. Corrections for reconstructions were also made with the help of the software VG studio Max Cinema 4D (Maxon, release 19-20).

Measurements of the bony labyrinth were conducted using ARIADNE software developed by David et al. (2016). The average thickness ratio of the crus commune is calculated using this formula: average section radius / crus commune length * 100. The average thickness ratio of the semicircular canals is calculated using this formula: average section radius / semicircular canals length * 100.

Enamel microstructure

Enamel microstructure of *Stylolophus minor* and *S. major*, n. sp., was studied combining light and SEM microscopy, following the protocol detailed in Tabuce et al. (2017). Observations are based on:

- *Stylolophus minor*: OCP DEK/GE 667, left M^1, vertical section on the labial flank of the parastyle (UM-ENAM 584).
- *Stylolophus major*, n. sp.: MNHN.F PM53 (holotype), right M^1, vertical section on the distal flank of the mesostyle (UM-ENAM 583); MNHN.F PM53 (holotype), right M^3, transverse section on the mesial flank of the metacone (UM-ENAM 582).

Institutional abbreviations

OCP DEK/GE: collections of the Office Chérifien des Phosphates, Direction des Exploitations, Service Géologique, Khouribga, Morocco; MNHN.F: paleontological collections of the Museum national d'Histoire Naturelle, Paris, France; MHNM.KHG: collection of the natural history of Marrakech, Marrakech, Morocco; UM-ENAM: collection of enamel specimens from the Université de Montpellier.

Data availability

All data generated or analyzed during this study are included in this published article and its supplementary information files.

SYSTEMATIC PALEONTOTOLOGY

INFRACLASS PLACENTALIA OWEN, 1837

SUPERCOHORT AFROTHERIA Stanhope et al., 1998

SUPERORDER PAENUNGULATA Simpson, 1945

MIRORDER TETHYTHERIA Mckenna, 1975

ORDER EMBRITHOPODA Andrews, 1906

STYLOLOPHIDAE, n. fam. Gheerbrant

LSID urn:lsid:zoobank.org:act:6EE2EBBC-4036-4E73-A6D0-1AE83877EB3A
Type and only genus: *Stylolophus*.

Diagnosis: small-sized embrithopods with low, brachydont and poorly advanced hyperdilambdodont molars that have short pseudolophs (preparacrista, premetacrista) and retain a postparacrista, a postmetacrista and a metaconular pseudohypocone; anterior premolars small and simple.

GENUS ***STYLOLOPHUS*** Gheerbrant in Gheerbrant et al., 2018

LSID URN: LSID: ZOOBANK.ORG: ACT: 9B31342F-7FBA-44E7-8B46-4C5D5341FBA5

Etymology: generic name derived from stylos (gr.: pillar), styles, and lophos (gr.: crest), lophs, in reference to the peculiar lophs corresponding to the transverse development of the labial crests linking the enlarged parastyle and mesostyle in the upper molars.

Type-species: S*. minor*

Included species: S*. minor, S. major*, n. sp.

Distribution: early and middle Ypresian of the Ouled Abdoun basin, Morocco.

Diagnosis of the genus

Stylolophus shows the following morphotypic molar features of the Embrithopoda: hyperdilambdodont pattern; hypoconulid cingular-like and lingually located; hypoconulid lobe on M_3 small, compressed laterally, and lingually set; cristid obliqua lingual on the trigonid; entocristid reduced and postfossid open lingually. *Stylolophus* differs from all other embrithopods, including *Palaeoamasia,* by its very small size and other plesiomorphic traits such as: primitive state of hyperdilambdodonty with less lingual paracone and metacone and

shorter pseudolophs (preparacrista, premetacrista), and retention of larger postparacrista, postmetacrista and metaconular pseudohypocone; low and brachyodont cheek teeth; M^{1-2} with only one lingual root and with separated paracone and protocone roots; P_2 one-rooted and simple ; P^2 two-rooted, transversely narrow and simple. The unique enamel microstructure of *S. minor* and *S. major*, characterized by radial enamel with prisms having irregular and sinuous trajectories, is an autapomorphic feature of the genus *Stylolophus* within the Embrithopoda. Palaeoamasiids differ from *Stylolophus* by specializations such as a higher bunodonty, the molar trigonid less compressed and more selenodont with a stronger paracristid and paraconid, the molar cristid obliqua more lingual on the trigonid, the molar metaconid more inflated and mesio-distally expanded, the P_4 selenodont, and the labial hypsodonty. Lower molars of *Crivadiatherium* further differ from *Stylolophus* in the well-developed labial and distal cingulid and the wider trigonid with respect to the talonid. Higher bunodonty of *Palaeoamasia* is illustrated by the large and voluminous paracone and metacone with convex labial spur, and the inflated distal crest and flank of the protocone (infilling the interloph). It also has a more posteriorly detached zygomatic arch. *Namatherium* and *Arsinoitherium* have an advanced hyperdilambdodonty (e.g., lost pseudohypocone), P^{3-4} with postcingulum extended posteriorly, and M^3 more offset lingually with respect to M^{1-2}. In addition, *Namatherium* has a lingual cingulum on the upper premolars, and a more anterior zygomatic process, and *Arsinoitherium* has much more molarized premolars with a large hypocone on P^{2-4}.

Stylolophus minor Gheerbrant in Gheerbrant et al., 2018

(Text-figs. 1-15)

LSID urn: lsid: zoobank.org: act: B4367769-7BE7-4EBF-A9EA-2E18E409D80E

Etymology: minor (lat.), by reference to its small size.

Holotype: OCP DEK/GE 668, right dentary preserving M_{1-3}, P_{3-4}, P_1, anterior alveoli, and roots of I_{1-2} (specimen donated to OCP by S. Xerri). Morocco, Ouled Abdoun Basin, Sidi Chennane mining area, exact locality unknown; Early Ypresian, intercalary beds II/I, *Otodus obliquus* Bone Bed.

Hypodigm

- Holotype
- MNHN.F PM30, fragment of left dentary with broken dP_4 and M_1, and unerupted tooth germs of P_4 and M_2. Morocco, Ouled Abdoun Basin, Grand Daoui mining area, exact locality unknown.
- OCP DEK/GE 667 (PM96), several fragments of skull rostrum of the same individual: Right maxilla with M^{1-3}, P^4; right premaxilla with alveoli of I^{1-3}; left maxilla with P^{2-3} and alveoli of P^1 and C^1 and with attached left nasal; and the isolated left M^1. Morocco, Ouled Abdoun Basin, Sidi Chennane mining area; exact locality unknown; Early Ypresian. Specimen donated to OCP by F. Escuillié.

Referred specimen: MHNM.KHG.228, posterior fragment of right dentary bearing M_3. The larger size of this specimen with respect to OCP DEK/GE 668 suggests that it belongs to a

large, presumably male individual. This specimen was donated by N. Longrich to the collections of the Natural History Museum of Marrakech (Morocco).

Type locality: Ouled Abdoun Basin, Sidi Chennane mining area, intercalary phosphate Beds II/I and possibly Bed I, early Ypresian.

Localities and Age: Morocco, NE Ouled Abdoun basin (Grand Daoui and Sidi Chennane quarries), early Ypresian. Specimens of this species were found by local people (as for most mammal material from Ouled Abdoun basin), and hence the exact quarries where they have been found remain unknown. Available information indicates that the known material of *S. minor* comes from the *Otodus obliquus* Bone Bed in intercalary phosphate Beds II/I and possibly the phosphate Bed I, both of early Ypresian age (Yans et al. 2014; Gheerbrant et al. 2018). The matrix of the specimen of OCP DEK/GE 668 closely resembles the *Otodus obliquus* Bone Bed by both its lithological facies and its selachian content (Table 2). The matrix of specimen MNHN.F PM30 also yielded a tooth of the selachian *Abdounia baugei* (Ypresian). The geochemical analysis of the matrix of the specimens of *S. minor* supports its early Ypresian age (Gheerbrant et al. 2018). The Ce/Ce* values overlap with those of *Phosphatherium escuilliei* Gheerbrant et al., 1996 (Gheerbrant et al. 2018) and they are in the range of the lower Ypresian phosphate levels too such as Intercalary Beds II/I and Bed I (Kocsis et al. 2016). All these data support the Early Ypresian age of *S. minor*, ca. 56 to 54 ma (Gheerbrant et al. 2018).

Table 2 here

Diagnosis: Smallest known embrithopod species, with a molar row about 40 mm long. Anterior incisors, especially I^1_1, enlarged with hypertrophied root. I_1 was at least partially hypsodont.

Description

Fig 1 here

Skull and upper dentition

The specimen OCP DEK/GE 667 referred to this species corresponds to several fragments of the rostral part of a single skull; they include the fragment of a right maxilla with P^4 and M^{1-3}, the right premaxilla with empty incisor alveoli, part of the left maxilla with P^{2-3}, and alveoli of P^1 and C^1, and the isolated left M^1. The CT scans of the various fragments of OCP DEK/GE 667 were used to make the 3D models and a reconstruction of the snout that is illustrated in Fig. 14 and in Suppl. Fig. S3.

Premaxilla (Fig. 1)

Most of the right premaxilla is preserved. It is high (>33 mm) and long (17 mm). It was probably widely joined to the nasal so that the maxilla was restricted distally far from the nasal opening rim. In addition, the premaxilla does not bear an extended posterior process between the nasal and the maxilla: the suture with the maxilla is subvertical in contrast to *Arsinoitherium*. The premaxilla was also consequently well separated from the frontal by the nasal. The lateral margin of the right nasal fossa is preserved. It shows that the nasal fossa is large and high. It is slightly retracted at the level of I^2. The premaxillary-maxillary suture is subvertical, and it extends at least 30 mm high. It crosses the alveolar border between I^3 and

C^1. The suture is located more anteriorly in *Arsinoitherium,* on the posterior side of C^1 according to Court (1992b: 9).

Maxilla (Fig. 2, 3, 4)

A fragment of the left maxilla with premolars (Fig.2), and another fragment of the right maxilla with molars (Fig. 3) are preserved. The zygomatic process of the maxilla expands laterally not very high above the tooth row. Its root is located above M^{2-3} level, i.e., slightly more posteriorly than in *Phosphatherium*. The snout was significantly narrowed at the level of P^{1-2}. The processus frontalis was rather high on the snout. The partially preserved infraorbital foramen opens about 15 mm above P^2. The tuber maxillae is flat and it is slightly extended behind the zygomatic process of the maxilla, but not significantly behind M^3. The rim of the orbit is not preserved. The nasal fossa is large. The palate is distinctly concave and arched between the premolars (Figs. 2, 4). In palatal view the maxilla extends far anteriorly, up to the level of I^2 (Fig. 4). This means that if the incisive foramen was present, it was located much more anteriorly than in *Arsinoitherium*, between the anterior right and left incisors. The presence of this foramen in *Stylolophus* still remains uncertain.

Fig 2 here

Fig. 4 illustrates a reconstruction of the palate and the upper dentition in ventral view, made from the CT scans modelling of maxillary and premaxillary fragments of specimen OCP DEK/GE 667.

Figs 3-4 here

Nasal (Fig. 5)

A fragment of the left nasal is preserved. Its broken lateral and posterior margins preserve part of the suture for at least the maxilla and possibly the frontal. The suture with the frontal is slightly convex posteriorly as in *Phosphatherium*. The ethmoidal crest for the attachment of the dorsal nasal turbinate is present.

Upper dentition (Figs. 2, 3, 4)

Fig 5 here

The reconstruction of the upper tooth row provided in Fig. 4 shows that *S. minor* has the generalized placental upper dental formula: I^{1-3}, C^1, P^{1-4}, M^{1-3}.

The left premaxilla bears three alveoli that decrease in size posteriorly (Fig. 1). I^1 was a very large tooth, much larger than I^2; I^3 is smaller than I^2 but slightly larger than C^1. These incisors proportions are reminiscent of *Arsinoitherium* in which Andrews (1906: 9) described the first pair of incisor alveoli for I^1 as "considerably the largest." The 3D digital reconstruction (Fig. 4) of the palate shows that the two I^1 are separated at the midline of the snout by a significant median diastema at the premaxillary suture as was observed by Andrews (1906) and Court (1992b: pl. 2) in *Arsinoitherium*.

As seen from the preserved alveolus, I^1 has a long and large root extending high, below the floor of the nasal fossa and above the root of I^2 (Fig. 14); its long root suggests that the tooth was hypsodont as for the lower first incisor. The premaxilla is inflated lateral to the root of I^1. The other incisor alveoli indicate subvertical teeth. Like the lower dentition, the upper dentition lacks any significant diastema. The canine is small. Its root is compressed laterally, and the tooth was possibly slightly procumbent according to the orientation of its alveolus.

P^1 is small, uniradicular and probably simple. It is the smallest upper tooth, like P_1 in lower tooth row. P^2 has two roots; it is a small, laterally compressed tooth with a low and elongated crown. The crown is dominated by one main cusp located anteriorly (paracone), and flanked by one small anterior cusp (parastyle) in low position, one long posterior crest, and one small posterolingual cusp (protocone). The distal root is larger (wider) than the mesial one.

In contrast to P^1 and P^2, P^3 and P^4 have a large protocone and are wide transversely. The labial cusps include a large and laterally compressed paracone that bears a long posterior crest on which is present a small crestiform metacone that is appressed to the paracone. The high labial crest between the paracone and metacone and the strong and high parastyle all define a high and sharp ectoloph. The postmetacrista joins the distal cingulum. The paracone and metacone are separated by a small groove on the lingual side; it is distinctly more developed on P^4 than on P^3. There is a large and inflated parastyle on the mesial side of the tooth, which is the third main cusp of the tooth. This cusp is salient on the mesial flank of the tooth. The large protocone is located lingually, in front of the lingual notch between the paracone and metacone. The protocone has a distinct preprotocrista that joins the mesiolingual base of the paracone. There is no postprotocrista, so that the protofossa is widely open distally. P^3 and P^4 have a large lingual root and two smaller labial roots. On P^3 the cingulum is restricted to the distal side of the crown; on P^4 the distal cingulum is well developed and it bears a small cuspule at mid crown width, and the precingulum is weak and short.

P^4 is significantly larger and more extended transversely than P^3. The occlusal outline of P^4 is rectangular with the labial and lingual sides of comparable length, in contrast to P^3 in which the labial side is proportionally much longer. The parastyle is very large on P^4, and even slightly larger than the paracone. The metacone is more inflated than on P^3, but it is still widely fused with the paracone. The preprotocrista is transverse and joins the lingual flank of the paracone. The protocone of P^4 is wider mesiodistally.

The upper molars (Figs. 2, 4) are characterized by a sub-square occlusal outline, a quadritubercular morphology, and an hyperdilambdodont ectoloph with development of two predominant transverse shearing crests formed by the preparacrista and premetacrista linking the paracone to the parastyle and the metacone to the mesostyle, respectively. The

elongated preparacrista and premetacrista are specialized loph-like structure for transverse shearing with the protolophid and hypolophid of lower molars. The resulting molar pattern is basically bilophodont. However, the morphology is not homologous with the classical bilophodonty of extant “ungulates” such as proboscideans and perissodactyls. The upper molars of the Moroccan species do not have true lingual lophs, but they instead have “pseudolophs” made by the preparacrista and premetacrista that are lingually extended and transverse in orientation.

The molar crests are well developed, but the cusp base is inflated, denoting noticeable residual bunodonty. The ectoflexus excavates the labial flank of the molars between the parastyle and mesostyle. There is no distinct labial cingulum. Parastyle and mesostyle are remarkably large, high, and bulbous; they are slightly larger than the paracone and metacone, and are located transversely more or less aligned to paracone and metacone. The parastyle is the larger molar cusp. It forms a large parastylar lobe that is salient mesio-labially. Its lingual side is excavated by a large groove for protoconid occlusion. Extensive wear, especially on M^1, indicates that the protoconid groove is functional. As the result of the hyperdilambdodont morphology, the paracone and metacone are located very lingually, i.e., closer to the lingual flank than to the labial flank: they are lingually appressed to the protocone and metaconular pseudohypocone (see Gheerbrant et al. 2016) from which they are separated only by a narrow groove. The postmetacrista is weak and residual. The postparacrista is a little more developed. Whereas both postmetacrista and postparacrista are reduced, the premetacrista and preparacrista are strong and marked by an extensive shearing wear facet, indicating they are the main functional structures of the molars. The wear extends transversely on the lingual side of the mesostyle, as on the parastyle. The premetacrista is longer than the preparacrista, as a result of a slightly more lingual position of the metacone than the paracone. These transverse crests are aligned with the closely

appressed lingual cusps. A large and deep interloph valley extends transversely between the mesial and distal cusps and between the pseudolophs.

The metaconular pseudohypocone and the protocone are the smallest and lowest molar cusps. They are bunodont with reduced crests. The protocone is distinctly larger than the pseudohypocone (especially in lingual view). The protocone has a small anterior crest; it lacks a distinct postprotocrista, but the distal flank of the protocone is inflated and convex posteriorly. In M^{1-2} the pseudohypocone is linked by a short posterolingual crest to a distal cingulum that also joins the postmetacrista and the mesostyle base; this crest is absent in M^3. There is a well-developed mesial cingulum that is linked to the parastyle. It shows in front of the paracone a minute crest linked to the mesial flank of M^2 and M^3. The lingual cingulum is weak to absent. The conules are absent.

The molars increase in size posteriorly. Besides the size difference, M^{1-3} have similar morphology. M^3 has more markedly wrinkled enamel, a smaller and more lingual mesostyle and a deeper ectoflexus. The molars bear two labial roots, and a lingual root that is enlarged below the protocone. M^3 bears an additional root below the pseudohypocone (Fig. 3C). This root is continuous labially with the root of the metacone and mesostyle (Suppl. Inf. Fig. 1). The pseudohypocone root of *Stylolophus* corresponds indeed to the lingual extension of the posterolabial root of the tooth as seen also in *Phosphatherium* and *Eritherium*, instead of the longitudinal division of the lingual root of the tooth as seen for the hypocone of lophodont euungulates.

Examination of the CT scans and the 3D models shows that the molar roots have distinct vertical radicular grooves on their interradicular side for bony crests attachment of the teeth in the alveolus (Suppl. Inf. Fig. 1). They also show that the roots of M^3 are still open, especially the protocone and metacone roots. Other molars do not show open roots. This is indicative of a delayed development of the last molar, that can be observed here

because the specimen belongs to a young individual (e.g., weak tooth wear). Cheek teeth with open roots related to delayed development have also been reported in *Arsinoitherium* by Sanders et al. (2010).

Measurements of the upper dentition: Tables 3-4.

Tables 3-4 here

Fig 6 here

Lower dentition (Figs. 6-12)

The lower dentition of *S. minor* is documented by a nearly complete right lower jaw (specimen OCP DEK/GE 668; Figs. 6-7, 9, 12), a fragment of dentary of a juvenile individual bearing the erupted M_1 and damaged dP_4 (specimen MNHN.F PM30; Figs. 11, 12), and a partial lower jaw with M_3 (MHNH.KHG.228, Fig. 8). The lower dental formula of *Stylolophus minor* is that of generalized placentals: I_{1-3}, C_1, P_{1-4}, M_{1-3}. The tooth row has no developed diastema.

In the anterior dentition, the incisors and canine are documented at least by their tooth alveoli. The crowns of the two anterior incisors I_{1-2} are broken, but their long and large roots are preserved.

Fig 7 here

I_1 and I_2 are noticeably procumbent and enlarged with hypertrophied roots (Fig. 6D, 7C). The root of I_1 is at least 24 mm long. The overall size of I_1 preserved in OCP DEK/GE 668, is similar to that of the I_1 of *Phosphatherium* (specimen MNHN.F PM11; Gheerbrant et al. 2005). The roots of I_1 and I_2 seen in OCP DEK/GE 668 are large and extend far distally on the dentary (Fig. 7). The root of I_1 extends up to the level of P_2. One remarkable feature of I_1 is that it has a large root apex with widely open pulp canal (the ratio of the diameter of the canal opening to the root section is about 50%; Figs. 6E, 7; Suppl. Inf. Fig. 2). As on the same specimen the M_3 is fully erupted and already worn, this means that I_1 was still growing during adult life: I_1 was hypsodont (root hypsodonty) at least for some time in this species. The CT scans show that the root of I_2 is thinner and closed at its apex; I_2 was not hypsodont as I_1.

The roots of I_1 and I_2 are compressed laterally and closely appressed (Fig. 6); these two incisors probably formed a single functional protruding dental structure. I_1 was only slightly larger than I_2. The enamel is present on part of the preserved root of I_1. I_3 was much

smaller than I_1 and I_2 and probably procumbent. Its root was smaller and probably not open. According to the alveoli, C_1 was of similar development than I_3 and was slightly larger than P_1. It was probably slightly procumbent.

The lower cheek teeth series increases in size posteriorly, with a strong step between the small and simple P_{1-2} and the large posterior teeth. Four premolars were present, although only P_1, P_3, and P_4 are preserved in specimen OCP DEK/GE 668.

P_1 is small and uniradicular. Both its root and crown are slightly procumbent. The crown is small, simple, and elongated. It is supported by a large, deep, and robust root. The length of the root is only slightly smaller than that of the crown. The crown bears one large cusp that is compressed laterally and flanked by a small anterior cusp and a small talonid cusp in low position. The anterior cusp is small but well inflated. It is located remarkably high, close to the main median cusp. P_2 has only one root.

P_3 and P_4 are robust and bunodont, and submolariform. They have two long roots, like the lower molars. However, they show no trace of lophs. P_3 is large. The trigonid is elongated. The talonid is wider but shorter than the trigonid. The paraconid is large and inflated and located high on the crown, mesial to the protoconid. The metaconid is weak to absent. The talonid is separated from the trigonid by a distinct hypoflexid. It bears well-developed hypoconid and cristid obliqua. The latter extends lingually onto the trigonid and has a noticeable shearing function, as shown by a well-developed wear facet that extends onto the protocristid. Posterolingual to the hypoconid, there is a distinct cusp probably corresponding to the entoconid. There is no entocristid and the talonid is open lingually. There are no traces of cingulids. P_4 is larger than P_3, and is significantly more molarized with a three-cusped trigonid, and a larger and basined talonid. The trigonid is wider. The metaconid is well developed, high, and posterolingual to the protoconid. The cristid obliqua is longer than in P_3. The entoconid is more developed and distolingual rather than distal. P_4

is significantly smaller than M_1. The germ of P_4 preserved in MNHN.F PM30 is very similar in size and morphology to the erupted P_4 in OCP DEK/GE 668 (Fig. 11).

The lower molars are preserved in the right dentaries MNHN.F PM30 and OCP DEK/GE 668. They increase in size posteriorly. The crown is high on both the labial and the lingual sides. The talonid is in particular high, as high as the trigonid. The lingual cusps are significantly higher than the labial cusps. The lower molars show an advanced bilophodont pattern with two continuous and sharp lophs. The lophs are strongly transverse (not oblique) and they show a typical transversely extended and semilunar wear facet. The hypolophid in particular is well developed and high, as high as the protolophid. The trigonid and talonid are compressed mesiodistally, in relation to the development of the lophs and the bilophodont morphology. The hypoflexid is deep, resulting in a typical two-lobed shape of the crown in occlusal view. There is no labial cingulid.

Fig 8 here

The trigonid is strongly compressed. It is as wide or wider than the talonid in M_1, but narrower in M_{2-3}. The paraconid is absent. The paracristid is thin but well distinct. It extends lingually up to the mesiolabial base of the metaconid. A thin precingulid extends onto most of the mesial flank of the trigonid (from protoconid to metaconid level), and well below the paracristid. It is located at the mid height of the mesial flank of the crown. The prefossid is shallow and more elongate transversely than longitudinally. The metaconid is larger and higher than the protoconid. It shows traces of anterior and posterior crests, and especially of a postmetacristid. However, there is no postmetastylid. The protolophid is longer than the hypolophid. The hypolophid is more deeply notched than the protolophid. The entocristid is reduced and the postfossid is widely open lingually. The postfossid is longer than wide. The cristid obliqua is well differentiated and long; it joins the trigonid in its lingual side, below the metaconid, so that the hypoflexid is very deep transversely. The cristid obliqua rises slightly on the trigonid. There is no distinct mesoconid. All posterior parts of the tooth distal

to hypolophid (hypoconulid, postcristid) are vestigial and reduced to a low and cingular-like structure that is short transversely and restricted to the distolingual side of the tooth. In M_3 (Figs. 6, 8), the distal part of the tooth is larger and it forms an elongate oblique hypoconulid lobe that is made by the vestigial and cingular-like hypoconulid and postcristid. It bears a narrow and small basin, and shows a minute distolingual cusp (postentoconulid) and a small distolabial hypoconulid**.** The talonid of M_3 is noticeably narrower and longer than in $M_{1\text{-}2}$. All molars bear two deep roots.

The juvenile specimen MNHN.F PM30 preserves the germ of unerupted P_4, part of dP_4 (talonid), the M_1, and the germ of unerupted M_2 (Fig. 11). The broken talonid of the dP_4 preserved in MNHN.F PM30 is characterized by a lighter color (i.e., thinner enamel). Its fully molariform talonid is very close in shape and size to the M_1 which is the only erupted molar in MNHN.F PM30.

Fig 9-10

Individual variation - The reconstruction of the occlusion of the upper dentition preserved in OCP DEK/GE 667 and the lower dentition preserved in OCP DEK/GE 668, shows that the latter individual is slightly smaller by 10%. The referred specimen MHNM.KHG.228 to *S. minor* has a larger size than the hypodigm material. M_3 of MHNM.KHG.228 (Table 4) is larger than that of OCP DEK/GE 668 by 115-120%; it is closer in size to the maxilla OCP DEK/GE 667, which is 10% larger than the dentary OCP DEK/GE 668. It should be noted that the size disparity is stronger for the mandibular corpus than for the preserved tooth (M_3). Actually, the M_3 of MHNM.KHG.228 occludes with the $M^{3\text{-}2}$ of OCP DEK/GE 667 with only a minor size difference: the best occlusal fitting of M^3 and M_3 of the two specimens is obtained following a reduction of the size of MHNM.KHG.228 by 6.3%, based on their 3D digital reconstructions (Suppl. Fig. 6). The larger size of MHNM.KHG.228, and especially of the mandibular corpus, might be related to a sexual dimorphism in *S. minor*, with the specimen MHNM.KHG.228 belonging to a male individual, and OCP DEK/GE 668 belonging to a female

individual. An alternative interpretation would be that this specimen belongs to a slightly more recent population of the same species from a higher horizon in the Bed I from the Ouled Abdoun phosphate series.

The M_1 and the germ of M_2 in MNHN.F PM30 are nearly identical in size and morphology to those teeth in OCP DEK/GE 668 (Fig. 11). Molars of OCP DEK/GE 668 have a slightly more developed labial cingulum, especially at the hypoflexid level.

Figs 11-12

Measurements of the lower dentition: Tables 5-6.

Tables 5-6 here

Lower jaw (Figs 6-10; Suppl. Inf. Figs. 2, 4-5, 7)

The lower jaw of *S. minor* is documented by specimens OCP DEK/GE 668 and MHNM.KHG.228. The specimen OCP DEK/GE 668 preserves most of the corpus, but only a small part of the vertical ramus (Figs. 6-7). In OCP DEK/GE 668 the corpus is moderately inflated and not deep below the teeth (H= 26 mm below M_2; MNHN.F PM30: H=18 mm below M_2; which is 1.5-2 times M_2 length). MHNM.KHG.228 has a significantly deeper corpus than OCP DEK/GE 668, by 29 % (H=36.5 mm below M_3). The vertical ramus is subvertical behind M_3. There is a small retromolar fovea (coronoid fossa) on the mesial side of the coronoid process, but it is clearly less excavated and less marked than in the early proboscideans *Phosphatherium* and *Eritherium*. No distinct coronoid foramen is present in either OCP DEK/GE 668 or MHNM.KHG.228. CT scan observations of these specimens confirm the absence of a coronoid foramen in *S. minor* (Suppl. Inf. Fig. 5). *Palaeoamasia* also lacks a coronoid foramen. This is a noticeable difference of these embrithopods from the proboscideans, sirenians, and hyraxes.

Only one large mental foramen is seen below the P_2 alveoli. It is widely open anteriorly. The masseteric crest is sharp. It extends just labial to the talonid of M_3. There is

also a bony crest on the lingual side of the anterior side of the coronoid process; this crest and the masseteric crest delimit a small coronoid fossa behind the M_3. The mandibular symphysis extends to the P_2 level.

The mandibular foramen, best preserved in MHNM.KHG.228 (Fig. 8), opens as an oblique (at about 45 °) and straight (not crescent-like) slit; it is located well below (10 mm below) and behind (17.6 mm behind) the tooth row. Its length is about 12.2 mm. This shape, position and development of the mandibular foramen in *S*. *minor* is very similar to that seen in *Palaeoamasia kansui* (e.g., specimen MNHN.F EC-3); it differs from the latter, mostly by a slightly more tilted orientation. Such a low position and slit-like shape of the mandibular foramen seen in early embrithopods noticeably differs from proboscideans such as *Phosphatherium, Daouitherium* and *Numidotherium*; these proboscideans have a distinctive crescent-like and vertically oriented mandibular foramen that is located at the level of the tooth row. A low mandibular foramen is also seen in the stem paenungulates *Abdounodus* and *Ocepeia*: this is probably a plesiomorphic trait in the embrithopods. There is no horizontal inflated bony ridge or medial buttress above the mandibular foramen as in early proboscideans such as *Phosphatherium* and *Daouitherium*. The ascending ramus is broken in MHNM.KHG.228, but the masseteric crest rises labially at the level of the posterior part of the talonid of M_3. It is labially shifted with respect to M_3 and the tooth row. The mandibular condyle is not preserved. However, the notch anterior to the mandibular condyle partially preserved in OCP DEK/GE 668 indicates that the condyle was located slightly above the tooth row (at least as high as the M_2 length).

The deeper corpus (by 129 %) in MHNM.KHG.228 than OCP DEK/GE 668, in addition to its larger size, indicates that it belongs to a larger and a male individual.

Figs. 9-10 provide a reconstruction of the whole lower jaw of *S*. *minor.*

Measurements of the lower jaw: Table 7.

Table 7 here

Enamel microstructure (Fig. 13)

The upper molar OCP DEK/GE 667 of *S. minor* presents a one-layered Schmelzmuster formed by radial enamel (RE) with an important amount of interprismatic matrix (IPM) that completely encloses prisms. Prisms are not densely packed and have a slightly curved course from the enamel dentine junction (EDJ) to the outer enamel surface (OES). Prisms also present irregular deviations for short distances from the general order. The angle between the crystallites of the IPM and prisms varies from ~45° near EDJ to 0° in the outer part of the enamel layer.

Fig 13 here

Size and body mass estimations of *S. minor*

We estimated the body mass of *S. minor* and *S. major* based on the allometric equations provided by Damuth (1990) for dental measurements (molars) of non-selenodont ungulates. Our estimated widest range of the body mass of *S. minor* (Table 8) is 20-40 kg (based on measurements of individual molars and molar series length). A median body mass of about **30 kg** based on the length of the upper molar series seems to be the best estimate (best estimates of body mass from dental measurements are based on the length of molar rows; see Gheerbrant et al. 2014). This is the body mass of a small goat.

Table 8 here

We estimated the length of the reconstructed snout (premaxilla + maxilla) as 9.5 cm based on the 3D digital reconstruction of the skull fragments belonging to specimen OCP DEK/GE 667 (Fig. 14). The upper series P^4-M^3 of *S. minor* is about 20 % longer than that of *Phosphatherium escuilliei* (Gheerbrant et al. 2005). Based on this ratio and assuming similar

skull proportions, the comparison with the skull length of *Phosphatherium* (about 18 cm) indicates an estimated skull length of **22 cm** for *S. minor.*

Reconstruction of the rostrum and dentition of *S. minor* (Fig. 14, Suppl. Inf. Fig. 3)

The composite reconstruction illustrated in Fig. 14 and in Electronic Supplementary material Figure 3 was made virtually with the help of the software VG studio Max (Volume Graphics, release 2.2) and Cinema 4D (Maxon, release 13), and using the 3D digital models reconstructed from the CT scans of the different fragments of the right and left maxilla and premaxilla of the specimen OCP DEK/GE 667, and of the lower jaw OCP DEK/GE 668 (fitted in occlusion). We additionally reconstructed in Fig. 15 the upper and lower jaws in occlusion using the specimens OCP DEK/GE 667 and OCP DEK/GE 668. In both reconstructions, the lower jaw OCP DEK/GE 668 was enlarged by 10% to get the best occlusal fit with the upper dentition preserved in OCP DEK/GE 667. The individual OCP DEK/GE 667 is indeed slightly larger than the individual OCP DEK/GE 668.

Fig 14 here

Fig 15 here

Stylolophus major, n. sp. Gheerbrant

(Figs. 16-23)

LSID urn:lsid:zoobank.org:act:F4660036-9D09-4983-9345-FE5853440A19

Holotype: MNHN.F PM53, several pieces of a broken skull of an adult individual including a fragment of the snout with the anterior part of the parietals and the right frontal and nasal, the left maxilla with M^{1-3} and broken P^4, the isolated left P^2, the isolated right M^3 (broken), one isolated broken right M^1, and several fragments of the left and right petrosal.

Hypodigm and referred material: MNHN.F PM53, holotype and only known specimen.

Type locality and age: Morocco, NE Ouled Abdoun Basin (unknown quarry), upper phosphate levels, middle Ypresian. The holotype MNHN.F PM53, was found by Moroccan people living close to the phosphate quarries. Although it is from an unknown locality of the North-Eastern Ouled Abdoun phosphate quarries, its matrix indicates it comes from phosphate Bed 0 or "sillons." The presence of encrusting chert on the surface of the bone of MNHN.F PM53 is more usual in the upper levels of the Ouled Abdoun phosphate series, such as the Bed 0 and the "sillons" that are dated middle Ypresian (Gheerbrant et al. 1998; Yans et al. 2014). The matrix of MNHN.F PM53 also yielded a small but significant selachian assemblage including *Coupatezia* sp., *Archeomanta* sp., the carcharhiniform cf. *Galeorhinus* and several dermal denticles (determinations H. Cappetta). Although all these taxa are known in the whole Ypresian stage, most, especially *Archeomanta*, are more frequent in phosphate Bed 0 and the "sillons", and their association is most characteristic of these levels (H. Cappetta, pers. com. to E.G.).

The geochemical analysis of the matrix of MNHN.F PM53 provides data on its stratigraphic provenance (Gheerbrant et al. 2018). Kocsis et al. (2016) demonstrated a shift towards lower Ce/Ce* values from older to younger beds in the Ouled Abdoun phosphate series, a trend that slightly reverses towards the youngest phosphate level. Values obtained for MNHN.F PM53 (see Gheerbrant et al. 2018: Supp. Info.) are found in the upper levels of the Ouled Abdoun phosphate series, in particular in the sillons A and B of Sidi Chennane and Sidi Daoui (Kocsis et al. 2016; Gheerbrant et al. 2018). This is consistent with the selachian assemblage and occurrence of chert deposit on the bone. The Ouled Abdoun phosphate sillons A and B levels are correlated with the beginning of the EECO global climatic event (Yans et al. 2014; Kocsis et al. 2014), which postdates the ETM 2 and 3 hyperthermal events, and is dated 53-49 Ma (Westerhold et al. 2018). This supports a middle Ypresian age of *S. major* (Gheerbrant et al. 2018). All these elements indicate that the age of *S. major* is younger than that of *S. minor,* which is in accordance with their relative evolutionary state (e.g., size difference).

Diagnosis: Dental morphology most closely relates to the Embrithopoda and within the order to *S. minor. Stylolophus major* most remarkably differs from *S. minor* in its larger size, being 30-40% larger in tooth size. Also differs in some morphological details of upper molar such as the posterior molars (M^{2-3}) that are 10-20% larger and more elongated proportionally to M^1, the paracone and metacone more lingually located and the related longer pseudolophs (preparacrista, premetacrista), and the smaller postparacrista, postmetacrista, and metaconular pseudohypocone. P^2 is wider than in *S. minor*. Other skull features of *S. major* distinct from *S. minor* include a more developed submaxillary fossa, and a more posterior infraorbital foramen. Most differences of *S. major* from *S. minor* relate to its more derived morphology. *Stylolophus major* differs from *Arsinoitherium* in lacking any

trace of horn on the nasal and frontal and in having a separate fenestra cochleae and aqueductus cochleae rather than a perilymphatic foramen.

Fig 16 here

Description

Maxilla (Figs. 16, 17; Suppl. Fig. 7)

The maximal preserved length of the left maxilla MNHN.F PM53 is 10.4 cm. The lower rim of the orbit opens high, at about 35 mm above the alveolar border of the teeth. It is also noticeably salient laterally above the teeth, so that there is a distinct submaxillary fossa that is more developed and deeper than in *S. minor* and *Phosphatherium*. As a consequence, the orbit is located significantly laterally with respect to the tooth row on a maxillary process, like in *Namatherium* for instance. The height of the maxilla in this area suggests that this bone has a very high processus frontalis in front of the orbit on the snout.

The maximal length of the orbit preserved in MNHN.F PM53 is 36 mm. The anterior rim of the orbit is located above P^4, as in *Phosphatherium* and *Palaeoamasia,* but more anteriorly than in *Namatherium* (M^1) and *Arsinoitherium* (M^2 or M^3). The infraorbital foramen is large and especially high (L max= 7 mm; H= 10 mm). It opens about 25 mm above P^3, and close in height (about 2 mm) and length (about 4 mm) to the orbit. This is a closer morphology to *Namatherium* and *Arsinoitherium* than to *Phosphatherium* and *S. minor* in which the infraorbital foramen is much lower above the teeth (20-25 mm) and more anterior (above P^3-P^2). The infraorbital canal was consequently short (L ~ 15 mm) similar to *Namatherium* and *Arsinoitherium.* The large infraorbital foramen and the high maxilla indicate a well-developed snout and a large and very flexible (prehensile) upper lip, as in *Phosphatherium* (Gheerbrant et al. 2005: 254). The lacrimal area is broken away. No foramina are preserved in the orbital area.

The floor of the orbit is wide transversely (ca. 30 mm at its widest). The zygomatic process of the maxilla is robust and located posteriorly: it extends antero-posteriorly between M^2 and M^3, and its posterior root diverges above the anterior loph of M^3 as in *S. minor*. By contrast, it is located more anteriorly between M^1 and M^2 in *Namatherium*, and between M^2 and P^4 in *Phosphatherium*. The lacrimal (facial part) is not preserved, but the lacrimal foramen is present and located within the orbit. The suture of the jugal and the maxilla lateral to the orbit is not distinct. The posterior part of the maxillary zygomatic process is broken above M^2, suggesting a possible suture of the jugal at this level. It is unknown if the jugal was extended more anteriorly, but the area of broken bone on the anterior margin of the orbit might have been part of the place of the lacrimal and maxillary suture. The tuber maxillae is moderately inflated and extends a little behind the zygomatic process of the maxilla (5.5 mm behind M^3), in contrast to *Phosphatherium*.

Fig 17 here

In ventral view a large major palatine foramen is present at the longitudinal level between M^2 and M^3 (Fig. 17). The preserved part of the palatine-maxillary suture extends indeed from M^3 to M^2 and nearly parallel to the molar alignment (not oblique posteriorly as in *Phosphatherium* and *Arsinoitherium*). This is similar to *Namatherium*. The posterior position of the major palatine foramen and the relative anterior extension of the palatine are similar or slightly more posterior than in *Phosphatherium.*

Fig 18 here

Skull roof (mostly naso-frontal) (Fig. 18)

A large broken fragment of the skull roof with the snout preserves the right nasal, the right frontal, the anterior part of the right parietal, and part of the right orbitotemporal fossa.

The nasal extends far anteriorly, which indicates that the nasal fossa was located anteriorly in contrast to *Arsinoitherium*. Its dorsal surface is wide and flat in contrast to *Arsinoitherium* in which it is inflated vertically as a large nasal horn core. The nasal had a

long contact with the processus frontalis of the maxilla. The elongated nasal indicates the absence of a premaxillary-frontal contact, unlike *Arsinoitherium*. This is correlative to the fact that the nasal openings are not retracted in *Stylolophus*.

The broken side of the specimen at the level of the mid-line suture with the left nasal shows the semilunar cross sections of four well developed paranasal sinuses for anterior turbinal (Fig. 18, C1) that are centimetric in length. The internal structures of the nasal and frontal of this specimen remain poorly distinct on the CT scans of this specimen because it is silicified. However, the tomographies also show several well-developed sinuses in the frontal. The large development of such anterior sinuses is unusual among placentals. This character of *Stylolophus* might be a remarkable homology with the "enormous nasal sinus" developed in the nasal horn of *Arsinoitherium* (Andrews 1906).

The naso-frontal suture was located at about the same level as in *Phosphatherium*, i.e., above the orbits. It is less concave posteriorly than in *Phosphatherium.* Part of the left frontal is preserved so that the metopic suture between the two frontals is distinct on the specimen. The shape and relative extension of the frontal closely recall the morphology of *Phosphatherium*. Its dorsal surface is in continuity with that of the nasal, both forming a flat skull roof, without any trace of horn.

The postorbital process of the frontal was developed in front of a strong postorbital constriction indicating a small cerebrum. The temporal fossa was deep and wide. The specimen preserves the fronto-parietal suture above the postorbital constriction and the anterior part of the right parietal. The anterior part of the orbitosphenoid is possibly preserved. No well-distinct skull foramina are seen.

Unfortunately, no point of contact of this fragment of right rostrum with the left maxilla has been recognized to help with the reconstruction of the snout of *S. major.*

Maximal length of the right fronto-nasal-anterior part of parietal in MNHN.F PM53: 15.5 cm. In *Phosphatherium*, this measurement corresponds to about 50-55% of the skull length.

Petrosal (Figs. 19-21)

Figs 19-21 here

The left maxilla and the rostrum of *S. major* are associated with an isolated left petrosal belonging to the same individual. It is broken and very incomplete (e.g., absence of most of the cochlea). It has been CT-scanned for description of the bony labyrinth. Some small fragments of the right petrosal are also present in the material, but they preserve very few features; the description of the petrosal of *S. major* is based on its left petrosal.

The overall morphology of both the middle and inner ear of *S. major* is reminiscent of early paenungulates such as *Phosphatherium*, *Eritherium* (Schmitt and Gheerbrant 2016), and *Seggeurius* (Benoit et al. 2016), as seen from Figs. 20 and 21. Hence, the general pattern of the petrosal seen in *S. major* is plesiomorphic at least among paenungulates.

In cerebellar view, the internal acoustical meatus is broken but its outline is still preserved. It has the shape of a mediolaterally elongated ellipse. The outlines of the foramen acusticum inferius and foramen superius are lost, but their anterior margin with part of the crista transversa can be seen. It indicates the narrow (ellipsoid) outline and anterior location of the foramen acusticum superius, in the same disposition as in *Phosphatherium*. The meatus is bordered by a thick prefacial commissure also similar to *Phosphatherium*. The broken subarcuate fossa is located posterolateral to the meatus and is moderately deep; this is distinctive from *Arsinoitherium*, which lacks the fossa. The fossa is very similar to that of *Phosphatherium* in depth and shape. A foramen can be observed within the subarcuate fossa (Fig. 15A); it is the point of entry of an internal canal oriented towards the anterior semicircular canal. This is probably the petromastoid canal that

contains the subarcuate artery in life. This feature has been observed in primates, artiodactyls, and notoungulates (Gannon et al. 1988; Krombach et al. 2002; O'Leary 2010; Billet and Muizon 2013). The aquaeductus vestibuli has the shape of a thin slit that opens in the medial side of the petrosal. In *S. major*, the area containing the fenestrae is broken, hence the *fenestra cochleae* is not preserved. However, the posterior part of the opening of the aquaeductus cochleae is visible in MNHN.F PM53. This aquaeductus cochleae is located near the aquaeductus vestibuli. This is indicative of the presence of divided foramina aquaeductus cochleae and fenestra cochleae in *S. major,* because the unique perilymphatic foramen is usually located on the tympanic surface near the promontorium and fenestra vestibuli (Ekdale 2011; Benoit et al. 2013b). Conversely, the two foramina are not separated in *Arsinoitherium,* which displays a unique perilymphatic foramen. *Stylolophus major* provides indeed new evidence of the convergent evolution of a unique perilymphatic foramen in the Embrithopoda, Sirenia, and Proboscidea (Court 1991, 1994; Savage et al. 1994; Gheerbrant et al. 2005; Benoit et al. 2013b).

In tympanic view (Fig. 19B) the pars cochlearis is broken, showing a remnant of the bony labyrinth. Part of the cochlea is preserved and the bony crest for the lamina secundaria is present and directly visible on the broken petrosal. Lateral to the cochlea lies a groove that is probably the sulcus facialis given its location, although its determination needs to be confirmed. The vestibule is also visible in tympanic view. It is broken at the level of the lateral and posterior ampullae. The base of the crus commune is clearly visible at the center of the broken vestibule. Close to the vestibule, but located more posteriorly, lies a depression that looks like part of the cochlea (Fig. 19B, d?). However, given its location and the absence of the secondary laminar crest this is unlikely homologous with the cochlear canal. Moreover, a foramen opening just posteriorly to the depression is clearly part of the broken lateral semicircular canal. This depression might correspond to an internal bony

canal of uncertain identification. Its location corresponds either to the facial canal or to the fossa for the stapedius muscle. The region of the tegmen tympani is broken but it is reminiscent of the inflated tegmen tympani observed in *Eritherium* and to a lesser extent in Sirenia (Benoit et al. 2013a). Its morphology is also close to that of *Seggeurius* (Benoit et al. 2016). In contrast to Benoit et al. (2016), we identify the tegmen tympani in *Seggeurius* as corresponding to the kidney-shaped bulge located ventrolateral in rostral view. It is quite similar in shape and location to the tegmen tympani seen in both *Eritherium* and *Ocepeia*.

Bony labyrinth (Fig. 20)

The ampullae are well defined and inflated. They are smooth and display neither ridges nor bumps. The crus commune is elongated as in *Arsinoitherium* (Benoit et al. 2013b). However, there is a sharp ridge along the crus commune in *Arsinoitherium* that is absent *in S. major.* It is smooth and displays no ridges. The average section radius of the crus commune is 0.53 mm and its length is approximately 3.92 mm. Our comparisons show that the crus commune of *S. major* has a remarkably low thickness ratio. The anterior and posterior semicircular canals meet very high (at more than 85% of the anterior canal height) as in *Arsinoitherium* and the crus commune is not inclined.

The outline of the anterior semicircular canal is sub-circular as in *Arsinoitherium* (Benoit et al. 2013b). The central streamline length of this canal is 12.63 mm and its average section radius is 0.22 mm. Therefore, the thickness ratio of this canal is 1.72, making it very slender. The anterior canal is the largest in *S. major* and its radius of curvature is 3.26. The posterior semicircular canal is round as well but less than the anterior canal (this canal is more oval in *Arsinoitherium*). The central streamline length of the posterior canal is 13.38 mm, which is longer than the anterior canal. The average section radius of the posterior canal is very similar to the anterior one (0.21 mm). Hence the thickness ratio of the posterior

canal (1.57) is very close to the ratio of the anterior canal. The radius of curvature of the posterior canal is similar to the radius of the anterior canal but slightly smaller (3.13). The lateral semicircular canal is incomplete because the petrosal is broken at this level but it seems to be oval. The estimated length of the central streamline of the lateral canal is 10.96 mm but this is an approximation. The average section radius of the lateral canal is lower than the other canals (0.12 mm). Hence the thickness ratio is clearly lower (1.08) for the lateral canal than for the anterior and posterior canals. The estimated radius of curvature of the lateral canal is 2.29.

The angles between the semicircular canals are always around 90°. The highest angle in *S. major* is between the lateral and posterior canals (98.6°), which is very large. This angle is much larger than in *Arsinoitherium* (83°). This is well marked and clearly visible on the 3D reconstruction (Fig. 20). The angle between the anterior and lateral canals is the lowest (83.4°) while the angle between the anterior and posterior canals is in the middle range (86°). The radius of curvature of the lateral canal is smaller (2.29) than those of the anterior (3.26) and posterior canals (3.13). The smaller size of the lateral canal is obvious on the 3D reconstruction. The anterior canal apex is located roughly at the same level as the posterior canal apex. In *S. major,* the semicircular canals are remarkably thin with an average thickness ratio of 1.46, which contrasts with the stocky canals of *Arsinoitherium*. In cross-section, the canals appear to be circular with no particular flattening, while there is a flattening observed in cross-section in the anterior and posterior canals of *Arsinoitherium* (Benoit et al. 2013b). The slender part of the lateral semicircular canal is connected to the vestibule at a quite high position. This is illustrated by a partial fusion of the bony lateral canal with the posterior ampulla, as in *Ocepeia* and to a lesser extent *Eritherium;* the fusion of the bony lateral canal with the posterior ampulla in *S. major* remains less advanced than

in *Phosphatherium*. Neither ridges nor marked undulations were observed on the semicircular canals.

Only a very small fraction of the cochlea is preserved. The number of turns is unknown but it displays more than one and a half turns. This is indicated in our reconstruction by the presence of a second cochlear turn. However, it is unknown if this second turn was complete *in S. major*. The lamina secundaria is preserved in MNHN.F PM53 on the part of the first turn. This is observed both in the 3D reconstruction and directly on the broken petrosal. *Stylolophus major* is distinctive in this feature from *Arsinoitherium* which lacks the lamina secundaria (Benoit et al. 2013b). The presence of a lamina secundaria in *S. major* is a plesiomorphic character also known in several early paenungulates (*Eritherium*, *Phosphatherium*, *Ocepeia*, *Seggeurius*) and other placentals.

Table 9 summarizes our comparison of the main features of the petrosal of *S. major*. It shows that *S. major* shares several primitive petrosal characters with other early paenungulates.

Table 9 here

Fig 22 here

Upper dentition (Figs. 15, 16; Suppl. Fig. 7)

The dental morphology of *S. major* is very similar to that of *S. minor*. *Stylolophus major* is most remarkably distinctive from *S. minor* by its much larger size: it is 30-40% larger in tooth size.

The premolars of *S. major* are only represented by the broken lingual part of the left P^4 and the isolated right P^2. P^2 was probably biradicular as in *S. minor*. The P^2 of *S. major* differs from *S. minor* in its less elongated and rounder occlusal outline with a more developed disto-lingual talon that supports a wider and more distinct basin. The parastyle is a little larger and the cingula are more inflated. The mesial and distal crests are more developed. In *S. major* the distal crest of the paracone of P^2 shows a strong shearing lingual wear facet; it is much less developed in *S. minor*. *Stylolophus minor* has a small cusp on the distolingual talon of the tooth that is weaker and blunter in *S. major*.

The molars of *S. major* are very similar to those of *S. minor.* The few morphological differences of *Stylolophus major* are the following:

- The occlusal outline is less transverse, and in particular the posterior molars M^2 and M^3 are proportionally more elongated; *S. minor* retains a comparatively primitive wider occlusal outline;
- M^2 and more markedly M^3 are slightly larger with respect to M^1;
- The paracone and metacone are more lingually located and the pseudolophs (preparacrista, premetacrista) are consequently transversely longer;
- The postparacrista and postmetacrista are more reduced and lower, in particular they do not join the cusp apex;
- The pseudohypocone is smaller;

- The styles are mesiodistally more compressed;
- The lingual cusps and their lingual flank are slightly more vertical and higher;
- The lingual cingulum is more differentiated;
- The anterior cingulum is thicker at the mid-width of the tooth.

Most of these distinct features indicate a more advanced state of *S. major*: all can be derived from the morphology of *S. minor*. This is consistent with the larger size of *S. major*. The two species are indeed considered to represents two successive chronospecies of the same generic lineage in accordance with their relative evolutionary stage, their age and locality (both are from Ouled Abdoun basin). Their congeneric position is supported by the enamel microstructure (see Comparisons).

Measurements of the upper dentition of *S. major*: Tables 10-11.

Table 10-11 here

Enamel microstructure (Fig. 23)

The enamel microstructure of an undetermined broken right premolar of *S. major* was examined. The Schmelzmuster is one-layered, formed by radial enamel (RE). Prisms have a slightly curved course from the enamel-dentine junction (EDJ) to the outer enamel surface (OES); as in *S. minor* they present irregular deviations for short distance from the general order. Prisms are densely packed and completely enclosed by interprismatric matrix (IPM). The IPM crystallites show the same orientation as the long axis of prisms from the EDJ to the OES.

Size and body mass estimations of *S. major*

We estimated the body mass of *S. minor* and *S. major* based on the allometric equations provided by Damuth (1990) for dental measurements for non-selenodont ungulates. Our body mass estimate for *S. major* (Table 12) gives a maximum range of 60 –128 kg (based on molars series length and individual molars measurements), and a median estimate of 88 kg (based on length of the molar series). It corresponds to the body mass of a medium-sized individual of the common warthog (*Phacochoerus africanus*) and the wild boar (*Sus scrofa*), and also to a large individual of *Orycteropus afer*. These mammals have a body length ranging from 1 to 1.5 meters, and a skull length of about 30 cm.

Stylolophus major is about 35-40 % larger than *S. minor* in tooth measurements (e.g., length of molar series), and two to three times heavier in body mass estimates. The length of the fronto-nasal preserved in MNHN.F PM53 is 15.5 cm, i.e., about 165% that of *Phosphatherium.* By comparison *Palaeoamasia kansui* is four to five times larger than *S. major* with an estimated body weight of 275 kg, as estimated from the allometric equation

calculated on the M^1 surface of specimen MNHN-EC 4 (Sen and Heintz 1979; Eski Celtek coll.).

Table 12 here

Comparison of *Stylolophus* (*S. minor*, *S. major*) with embrithopods

Palaeoamasia kansui (Palaeoamasiidae)

Palaeoamasia kansui from the Ypresian-Lutetian of Anatolia, Turkey (Sen and Heintz 1979; Koc and Türkmen 2002; Erdal et al. 2016) is the type species of the family Palaeoamasiidae that also includes the Eocene genera *Hypsamasia* and *Crivadiatherium*. *Palaeoamasia kansui* shows the closest dental morphology to both *S.minor* and *S. major.* The upper molars of *Stylolophus* most noticeably display the same early stage of the hyperdilambdodonty retaining the well distinct protocone and metaconular pseudohypocone (separated from the lingual cusps by a short valley), and also the posterior crests of the ectoloph (postparacrista and postmetacrista).

The most noticeable shared derived features related to the hyperdilambdodont upper molar pattern include the very large and inflated parastyle and mesostyle (largest cusps of the tooth), the lingual position of the paracone and metacone, and the two sharp pseudolophs made by the anterior crest of the paracone (preparacrista) and of the metacone (premetacrista) that links to the inflated styles. Other shared traits of upper molars include the protocone with a short anterior crest, the precingulum inflated as an accessory cusp in front of the paracone, the lingual cingulum present at the level of the entoflexus, and the M^3 lingually offset with respect to other teeth (*Stylolophus*: Figs. 3, 16, 22; weakly in *P.kansui*). P^3 and P^4 of *Stylolophus* and *Palaeoamasia* are similarly extended transversely and submolariform, with the presence of a paracone and metacone, a large parastyle and a protocone. The lower molars of *Stylolophus* and *Palaeoamasia* share the following remarkable traits: presence of two sharp continuous lophs; postfossid lingually

open (reduced entocristid) with a narrow valley between the entoconid and metaconid; hypoconulid small, cingular and lingually located; and cristid obliqua very lingual on the trigonid. The hypoconulid lobe of M_3 of *S. minor* is also very similar in development and morphology: it is narrow and long, and lingually located being restricted behind the entoconid; it bears a narrow basin, a posteriorly pointed hypoconulid, and a small vestigial entoconulid; and it is linked to the postcingulid. Additionally, P_1 is uniradicular in both *Stylolophus* and *Palaeoamasia*.

Most of the shared features of *Stylolophus* and *Palaeoamasia kansui* are derived embrithopod traits among the Paenungulata, but are generalized within the order. There is indeed no exclusive shared derived feature of the two genera.

Stylolophus is well distinct from *Palaeoamasia* in several traits that are for most primitive:

- Upper molars: Paracone and metacone more labial and, relatedly, lophs shorter; postparacrista and postmetacrista more developed; posterolabial flank of the paracone and metacone concave (it is inflated as a convex labial spur in *Palaeoamasia*); posterior crest of the protocone reduced; occlusal outline squared in *S. minor* in contrast to the elongated one in *Palaeoamasia*; crown of lower height on the labial side (incipient unilateral labial hypsodonty in *Palaeoamasia)*;
- Lower molar: trigonid mesiodistally more compressed, with less developed prefossid (shorter and shallower); ectostylid and ectocingulid less distinct labially in the hypoflexid; metaconid smaller, less extended mesiodistally; postmetacristid more developed; talonid of M_3 narrower with respect to the trigonid;
- Premolars: P_2 one-rooted, and P^2 two-rooted (two and three roots respectively in *Palaeomasia*);
- Zygomatic arch detached more anteriorly;

- Size much smaller.

Some of these differences might indicate divergent autapomorphic specializations in *Palaeoamasia.* This includes a specialized bunodonty illustrated by the large and voluminous paracone and metacone with convex labial spur, the inflated distal crest and flank of the protocone (infilling the interloph), and the large, mesiodistally inflated metaconid.

Most of the distinctive features of *Palaeoamasia kansui* unambiguously indicate that its dentition is more derived with respect to *Stylolophus.* However, some remarkable distinct traits of *P. kansui* are either primitive or more likely secondary: the more developed paracristid and paraconid, the M^3 weakly offset lingually with respect to M^{1-2} (if not resulting from distortion), and the two-rooted P_2. P_2 has only one root in early sirenians and proboscideans, and in *S. minor*, which suggests a reversal in *Palaeoamasia* and more advanced embrithopods (this is supported by our cladistic analysis, see below). The lower teeth remain unknown in *S. major.*

Comparison of *S. minor* and *S. major* with *Palaeoamasia* shows that *S. minor* is clearly more distinct and primitive with respect to *Palaeoamasia*, than is *S. major*. *Stylolophus major* is closer to *Palaeoamasia* in the following derived traits with respect to *S. minor*: a more reduced postparacrista and postmetacrista, the pseudohypocone smaller than in *S. minor*, and an upper molar occlusal outline elongated with respect to *S. minor* (Fig. 22).

The unnamed new species of *Palaeoamasia* described by Sanders et al. (2014) from the Eocene-Oligocene transition of the Boyabat Basin, in Turkey, remains poorly known, only by the upper dentition. With respect to *Stylolophus* it is much larger and more derived for instance in the longer pseudolophs, the more reduced protocone and pseudohypocone, the roots extended transversely, and the strong hypsodonty. Interestingly, it is apparently closer to *Stylolophus* than to *Palaeoamasia kansui* in the M^3 more lingually offset (M^3 weakly lingually offset in *P. kansui*).

Hypsamasia seni (Palaeoamasiidae)

Hypsamasia seni was described from the early/middle Eocene of the Uzunçarşidere Formation in central Anatolia, Turkey (Maas et al. 1998; Maas et al. 2001; Sen 2013; Metais et al. 2017). It is only known by broken upper cheek teeth. It departs more from *Stylolophus* than *Palaeoamasia*, with additional distinct traits such as more molarized upper premolars (e.g., more developed postprotocrista, metacone, and lingual cingulum in P^{2-4}, protocone present in P^2), and more hypsodont molars.

Crivadiatherium (Palaeoamasiidae)

Crivadiatherium is only known by its lower dentition. Two species, *C. mackennai* Radulesco et al., 1976 and *C. iliescui* Radulesco and Sudre, 1985, have been described from the middle-late Eocene of Romania (Radulesco et al. 1976; Radulesco and Sudre 1985; Radulesco and Samson 1987). Most remarkably, *Crivadiatherium* differs from *Stylolophus* in its large size, larger than that of all species of *Palaeoamasia* (e.g., Sanders et al. 2014). Other distinctions in the lower dentition of *S. minor* are the followings: more compressed trigonid, metaconid inflated and more expanded mesiodistally, paracristid and paraconid reduced (trigonid more selenodont in *Crivadiatherium*), absence of ectocingulid in premolars and molars, labial cusps less compressed mesiodistally, cristid obliqua less lingual on the trigonid, and crown much less hypsodont. Additionally, the premolars of *Crivadiatherium* are selenodont and have high crowns. Many of these differences also distinguish *Crivadiatherium* from *Palaeoamasia*.

Namatherium (Arsinoitheriidae)

The African species *Namatherium blackcrowense* Pickford et al., 2008 from the Lutetian of Black Crow (Namibia) is known by a single skull (Pickford et al. 2008). *Stylolophus* shares with *Namatherium* many features related to the hyperdilambdodonty that are also known in *Palaeoamasia.* It retains a molar protocone. It also has brachydont teeth, and

transversely extended P^{3-4}, bearing a paracone and metacone, a large parastyle, and a protocone. All these characters are plesiomorphic within the Embrithopoda. Some interesting traits are shared by *Stylolophus* and *Namatherium*, but are absent in *P. kansui*: the more anterior zygomatic arch and the lower bunodonty as seen for instance in the labial flank of the paracone that is not inflated.

Namatherium differs from *Stylolophus* in several derived features. The most noticeable correspond to the more advanced hyperdilambdodont pattern of the upper molars: metaconular pseudohypocone absent (fused with the cingulum below the metacone), paracone and metacone more lingual and pseudolophs longer transversely, paracone more appressed lingually to the protocone, postparacrista very weak and postmetacrista fully absent. *Namatherium* upper molars also differ in the larger and more lingual accessory cusp on the precingulum, the M^3 more lingually shifted with respect to M^{1-2} and the presence of at least four well-developed roots on upper molars. The P^{3-4} have a larger postcingulum that extends posteriorly, making the distal flank convex posteriorly. The ectocingulum is slightly more developed on molars and premolars. The distal part of the zygomatic arch is detached more anteriorly in *Namatherium,* at the level of the posterior loph of M^2.

Arsinoitherium (Arsinoitheriidae)

We compared the Moroccan material of *S. minor* and *S. major* with the MNHN and NHM collections of *Arsinoitherium zitelli* from the Jebel Qatrani Formation (Rupelian), Fayum, Egypt.

Stylolophus shares with *Arsinoitherium* some remarkable features that are plesiomorphic, and more or less generalized among the Embrithopoda, Paenungulata, and Placentalia. Several of them are morphotypic and exclusive to the order Embrithopoda

Fig 24 here

among the Paenungulata: the hyperdilambdodont upper molars; lower molars with strongly lingual cristid obliqua (and related deep hypoflexid); hypoconulid lobe of M_3 small but present, lingually located, and linked to the postcingulid; M^3 lingually offset; and palate concave (arched) between the premolars. Other more generalized shared traits include the full placental dental formula, small canine, small and uniradicular first premolar, premolariform P_3 with weak metaconid and still distinct paracristid, lower molars lacking entocristid with postfossid widely open lingually, zygomatic arch diverging far posteriorly at the level of M^3. Some primitive features of the petrosal are also shared by *Stylolophus* and *Arsinoitherium,* such as the elongated crus commune*,* the very high divergence of the anterior and posterior semicircular canals (with respect to their apex), and the partial fusion of the posterior and lateral semicircular canals. The small and uniradicular canine (C^1_1) and first premolar (P^1_1) seen in both *Stylolophus* and *Arsinoitherium* characterize the Tethytheria (see Cladistic analysis).

One of the most remarkable differences of *Stylolophus* and *Arsinoitherium* lays in the anterior dentition. Andrews's reconstruction of the anterior dentition of *Arsinoitherium* displays a typical homodont battery of anterior tooth with all teeth, from I^1_1 to P^1_1, of similar size, orientation, and morphology, which are included in a crowded series (Andrews 1906: figs. 6b and 36; Fig. 24B). This contrasts with *Stylolophus* which has two distinctive enlarged and procumbent anterior incisors (Figs. 6-7, 24). I^1_1 is moreover the largest anterior tooth, and I_1 is hypsodont in *Stylolophus*. This seems to indicate noticeable divergent specializations of the anterior dentition in *Stylolophus* and *Arsinoitherium*. However, Andrews's reconstruction of the anterior dentition of *Arsinoitherium* (Andrews 1906; e.g., NHMUK M8463 see Fig. 24B) is mainly based on the posterior incisors and the canine, to the exclusion of the first incisor, which remains unknown in the genus. In *Arsinoitherium,* I^1 and I_1 are actually known only by their more or less well-preserved alveoli. A detailed

observation of the *Arsinoitherium* NHM and MNHN material reveals in fact that the anteriormost alveoli are not so similar in shape, size, and orientation. Several specimens show a more or less enlarged alveolus for the first incisor. Andrews (1906: 20) noted that in the upper tooth row "the anterior incisor, judging from its alveolus, is much larger than the others." He tentatively identified one isolated possible upper first incisor that has a higher crown than posterior teeth. Furthermore, several specimens of the lower jaw of *Arsinoitherium* preserving the symphysis display an anterior alveolus remarkably enlarged and procumbent. This is most noticeable in MNHN.F LBE 579 (Fig. 24D) referred to *A. zitelli*. The specimen NHMUK M8461b, holotype of *A. "andrewsi"* (junior synonym of *A. zitelli*), also shows an enlarged and procumbent anterior alveolus (Andrews 1906: pl. 4, fig.3). The detailed observation of some specimens such as NHMUK M8461b indicates that the alveolus and/or root of I_1 is more vertical anteriorly and more horizontal posteriorly. The strict procumbent condition of the alveoli of I_1 seen in MNHN.F LBE 579 might be a little exaggerated because the symphysis is broken and lacks the anteriormost part of the alveoli of $I_{1\text{-}2}$. This suggests that in *Arsinoitherium* the crown and uppermost part of the root of the first lower incisor are secondarily oriented vertically, with respect to the still procumbent posterior part of the root, to be fully integrated in an autapomorphic homodont anterior tooth battery characterized by crowded, subvertical, and similarly sized crowns.

Our comparisons of *Stylolophus* and *Arsinoitherium* indeed support that *Arsinoitherium* is secondarily specialized among Embrithopoda in his homodont anterior dentition. *Stylolophus* more closely approximates the embrithopod ancestral morphotype with the presence of enlarged and procumbent anterior incisors (Figs. 6-7) and a hypsodont first incisor (root hypsodonty). From this ancestral condition, *Arsinoitherium* evolved smaller and vertically oriented first incisors. The large size of the first incisor and the antero-posterior orientation (= procumbent) of the posterior part of its root are indeed probably

plesiomorphic in *Arsinoitherium*. It should be noted that the anterior incisors remain poorly known in early embrithopods; in particular, we do not know the distribution of the hypsodont condition of I_1 seen in *S. minor*.

Arsinoitherium further differs from *Stylolophus* by many other characters, in addition to its much larger size:

- Cheek teeth strongly hypsodont with a much higher crown;
- Upper molars: pseudolophodont pattern with longer and fully developed pseudolophs and absence of the lingual cusps, postmetacrista and postparacrista, and lingual cingulum; parastyle and mesostyle much less prominent and cuspate; labial and lingual roots fused as two transversely elongated roots, and presence of an additional lingual root between them;
- P^{2-4} with a hypocone;
- P^2_2 more molarized; P^2 has a lingual cusp and is three-rooted (two roots in *Stylolophus*); P_2 is two rooted (one root in *Stylolophus*);
- lower premolars compressed laterally and cutting with an extended mesio-distal crest;
- lower molars: occlusal outline more compressed mesio-distally, with reduced basins, and deep hypoflexid between trigonid and talonid; postmetacristid absent; hypoconulid lobe vestigial (very small) and lower in M_3;
- Skull: lacrimal foramen absent (present in S. *major*); infraorbital foramen and orbit located posterior; and absence of submaxillary fossa (in contrast to *S. major*);
- Petrosal and bony labyrinth (only known in *S. major*): subarcuata fossa absent, presence of a unique perilymphatic foramen (instead of separated aquaeductus cochleae and fenestra cochleae), semicircular canals broad and flattened in cross section, posterior semicircular canal oval, and absence of a lamina secundaria.

Most of these characters are derived in *Arsinoitherium.* However, some of the distinctive traits of *Arsinoitherium* are unexpectedly known in the generalized eutherian and placental condition. This includes the posterior orbit, the orbit rim made only by the jugal, and the weak zygomatic process of the squamosal. They might correspond to remarkable reversals in *Arsinoitherium,* as for the subvertical crown of I_1.

Enamel microstructure of *Stylolophus* by comparison with other embrithopods

Stylolophus minor and *S. major* share a one-layered Schmelzmuster formed by RE with numerous prisms with irregular and sinuous trajectories; this is an original derived feature of the two species that differs from the typical primitive RE in which prisms are parallel to one another rising exclusively radially away from the EDJ towards the OES. The two species differ by the prism density (reduced on *S. minor*) and the orientation of IPM crystallites relative to prisms near EDJ (~45° in *S. minor*, no angle in *S. major*).

Other embrithopods are also characterized by radial enamel, but they differ from *S. minor* and *S. major* in having a more complex Schmelzmuster. *Arsinoitherium* has a two-layered Schmelzmuster characterized by an inner layer with alternating stripes having different organization of the IPM, and an outer layer of RE (Koenigswald 2012; Vialle et al. 2013). Likewise, *Crivadiatherium* and *Hypsamania* also have a two-layered Schmelzmuster but here the inner layer is composed of modified radial enamel (MRE) consisting of prisms aligned in radial rows and thick inter-row sheets of IPM (Maas et al. 1998; Tabuce et al. 2007; Koenigswald 2012); the outer layer also consists of RE.

Noteworthy, Koenigswald (2012: 8) noted that *Crivadiatherium* can also present some RE patches in the MRE inner zone, suggesting that it is from this level of differentiation of tooth microstructure that the regular pattern of alternating stripes observed in *Arsinoitherium* may have been derived. *Arsinoitherium* has supposedly developed the more

derived enamel microstructure in embrithopods. Koenigswald (2012) also proposed that a one-layered Schmelzmuster formed by RE is plesiomorphic for embrithopods. This hypothesis was based on the morphology he observed on *Palaeoamasia*. Interestingly, we also observe a one-layered Schmelzmuster formed by RE in *S. minor* and *S. major*, supporting Koenigswald's hypothesis.

A further remark can be expressed about the development of MRE in embrithopods. According to Koenigswald (2012), the presence in *Palaeoamasia* of an inner zone where IPM show a slight tendency to develop thin sheets of IPM could prefigure the MRE of *Crivadiatherium* and *Hypsamania*. It is worth mentioning that the thin (*Palaeoamasia*) to thick (*Crivadiatherium* and *Hypsamania*) sheets of IPM are the direct consequence of a marked angle of IPM crystallites relative to prisms. Consequently, although *Stylolophus* does not develop thin sheets of IPM as *Palaeoamasia*, it is important to mention in *S. minor* the presence of a marked angle of ~45° between the prisms and the crystallites of the thin IPM, suggesting that this species could represent an early stage of *Palaeoamasia* enamel.

Anyway, *S. minor* and *S. major* significantly differ from *Palaeoamasia* and other embrithopods by the presence of prisms with irregular and sinuous trajectories that occur throughout the RE, especially in the middle and outer zones of the enamel layer. This type of prism trajectories found in both *S. minor* and *S. major* is very rare in mammals. According to our current knowledge, only some extinct hyracoids developed similar structures. Tabuce et al. (2017) mentioned indeed RE associated with isolated prisms or bundles of prisms that diverge from the general direction and return to it after a short distance in the stem hyracoid *Dimaitherium* Barrow et al., 2010 (single prism diverging), but also in 'saghatheriids' (*Megalohyrax* Andrews, 1903, and *Thyrohyrax* Meyer, 1973) and titanohyracids (*Titanohyrax* Matsumoto, 1922, and *Antilohyrax* Rasmussen and Simons, 2000) (small to large bundles). Importantly, the earliest and basalmost hyracoid, *Seggeurius*

amourensis Crochet, 1986, does not present rare single prism diverging, but a 'basic' radial enamel, suggesting that this enamel microstructure is primitive for hyracoids (Tabuce et al. 2017).

To conclude, *S. minor*, *S. major*, and many Paleogene hyracoids share a very peculiar enamel structure (i.e., presence of prisms with irregular and sinuous trajectories). However, the presence of a 'basic' radial enamel in *Seggeurius*, *Eritherium*, *Khamsaconus*, as well as in *Protosiren* might indicate it is an ancestral feature of the Paenungulata and that the character 'presence of prisms with irregular and sinuous trajectories' was convergently developed in some hyracoids and embrithopods.

CLADISTIC ANALYSIS

Matrix and parsimony analyses

The relationships of *S. minor* and *S. major* with the embrithopods and within a broad taxonomic sample including various afrotherians, euungulates, and eutherians, were first investigated by Gheerbrant et al. (2018), based on the cladistic analysis of a character matrix modified from Gheerbrant et al. (2016). The matrix studied by Gheerbrant et al. (2018) included all known embrithopod genera. The coding of the embrithopods was based on direct observations and on works of Andrews (1906), Court (1992), Pickford et al. (2008), Sanders et al. (2014), Erdal et al. (2016). The coding of Gheerbrant et al. (2018) followed here details several features related to hyperdilambdodont pattern that typifies the Embrithopoda (Electronic Supplementary Material).

In this study several changes and corrections were made in the matrix analyzed by Gheerbrant et al. (2018). The most important relate to: 1) a revision of the enamel characters (characters 204-207) following their study in *S. minor* and *S. major* by one of us

(RT) in this paper, and 2) the addition of the early proboscidean taxa *Barytherium* Andrews, 1901, and *Moeritherium* Andrews, 1901. Other corrections are mentioned in supplementary informations (Electronic Supplementary Material).

The resulting matrix analyzed here includes 35 taxa and 208 characters of which 48 are additive. In the matrix 27.5 % of character states are unknown (most) or inapplicable, and 3.5 % are polymorphic. The most poorly known coded taxa are *Crivadiatherium*, *Hypsamasia, Minchenella* Zhang, 1980, *Teilhardimys* Kretzoi and Kretzoi, 2000, and *Paschatherium* Russell, 1963. The parsimony and character analyses were developed with the help of the software TNT (1.5) (Goloboff et al. 2008) and Winclada (Nixon 1999). The cladistic analyses were made using different options (Table 13): 1) equal weighting (unweighted) and implied weighting analyses, and 2) ordered and unordered characters. See Electronic Supplementary Material for more details and results of our cladistic analyses. The characters numbering used in our description of our most parsimonious trees (MPTs) starts from 0 (default option in TNT).

Resulting topologies

Fig 25 here

The new analysis of the relationships of *Stylolophus* developed here provides consolidated and consistent results with those obtained in our preliminary study (Gheerbrant et al. 2018). It yields well-resolved MPTs and clarifies several points on the topology and the character transformations within especially the Paenungulata.

The shortest trees (MPTs) are obtained for the analysis of the matrix with unordered characters (**Table 13**). They yield similar topologies than analyses of the matrix with ordered characters, although the implied weighting analysis with unordered characters does not recover the clade Paenungulatomorpha (Gheerbrant et al. 2016). All our cladistic analyses and resulting MPTs recover 1) basal relationships of *Stylolophus* to the Embrithopoda; 2) a

sister-group relationship of the Embrithopoda to extant Tethytheria; and 3) the clades Tethytheria and Paenungulata (Fig. 25).

Table 13 here

The clade Paenungulatomorpha (stem and crown paenungulates: Gheerbrant et al. 2016) is recovered only in implied weighting analyses (Fig. 26; Electronic Supplementary Material: analysis 3; Table 13) and in the analyses excluding the Desmostylia (Electronic Supplementary Material; analyses 6-7). Desmostylia has indeed proved to have had an effect of long branch attraction with the Paenungulata (Gheerbrant et al. 2016, 2018). The equal weighting analysis of the matrix with ordered characters recovers the clade "Altungulata" instead of Paenungulatomorpha, i.e., a sister-group relationship of the Paenungulata and lophodont euungulates such as Perissodactyla. However, this node is weakly supported, with low Bremer support and standard Bootstrap (Electronic Supplementary Material).

Our discussion below on the relationships of *S. minor* and *S. major* and on the character evolution among embrithopods, paenungulates, and paenungulatomorphs is based on the MPTs found in the equal weighting analysis (Fig. 25) and the implied weighting analysis (Fig. 26), both with ordered characters.

Relationships of *S. minor* and *S. major*

In our MPTs (Figs. 25-26), the two Moroccan species *S. minor* and *S. major* are not related as sister-groups in a single exclusive clade, but they are rooted as two successive stem taxa of other embrithopods, which would make paraphyletic the genus *Stylolophus.* However, a generic clade *Sylolophus* is supported by a unique enamel pattern with the presence of prisms with irregular and sinuous trajectories within radial enamel (206-1), and it is found in trees with only one additional step in constrained analysis. Besides this generic clade *Stylolophus*, these trees have the same topology (Electronic Supplementary Material,

analysis 2). Most differences of *S. major* from *S. minor* actually correspond to a more advanced stage of evolution, and both species perfectly fit with the definition of a chronospecies in accordance with their relative stratigraphic and geographic provenance. Additional data, especially on the unknown lower dentition of *S. major,* will help to further test its congeneric status with *S. minor*.

Relationships with the Embrithopoda

Fig 26 here

The two new Moroccan species of *Stylolophus* are firmly related to the order Embrithopoda. This is actually the best supported clade in our cladistic analysis with the higher Bremer support in our MPTs, together with the Proboscidea (excepting *Eritherium*) (Electronic Supplementary Material). The order Embrithopoda including *Stylolophus* is indeed well characterized. The MPTs resulting from equal weighting and implied weighting analyses (Figs. 25-26) display 11 exclusive synapomorphies and 11 to 14 homoplastic synapomorphies at the node Embrithopoda (Supp. Figs. 9-10). The order Embrithopoda is the longest branch among paenungulates and paenungulatomorphs. Most recovered exclusive synapomorphies of the embrithopods - but not all - are related to the hyperdilambdodont pattern of upper molars; this includes characters of the stylar shelf, the ectoloph, and the styles (characters 96-1, 99-3, 104-2, 107-2, 112-2, 113-3). Other embrithopod synapomorphies seen in *Stylolophus* include the large metacone of M^3 (114-2), the reduced preprotocrista (119-1), the reduction of the metaconular pseudohypocone (122-1) and of the protocone (123-1), the M^3 lingually offset with respect to M^{1-2} (136-1), and the palate (pars maxillary) concave between the premolars (143-1). The most noticeable homoplastic features of *Stylolophus* that are exclusive to the order Embrithopoda among paenungulates are the small I^3 (67-1), and especially the lingual hypoconulid on M_{1-2} (41-1; convergence with Sirenia). The cristid obliqua contacting very lingually the trigonid of the

lower molars of *S. minor* (39-0) is also characteristic of the Embrithopoda among the Paenungulata.

It should be noted that the I_1 of *S. minor*, which is specialized as a hypsodont and enlarged tooth, is not recorded in our MPTs as a basal synapomorphy of the embrithopods, but it is instead an uninformative feature in our analysis. This is because the first incisor remains poorly known in early embrithopods and paenungulates.

Relationships within the Embrithopoda

Stylolophus minor and *S. major* are recovered as the most basal species within the Embrithopoda. This is in agreement with the fact that they are older than other described embrithopods, including *Palaeoamasia* and *Hypsamasia* (?early – middle Eocene*;* Maas et al. 1998; Erdal et al. 2016; Metais et al. 2017). The ancestral embrithopod morphotype, including *Stylolophus,* remains well typified and specialized, at least in dental morphology. The internal branches within the embrithopod tree are much shorter. The most remarkable specialized embrithopod traits are the hyperdilambdodont pattern, the M^3 shifted lingually, and the arched palate. They are found in *Stylolophus*, although in a more primitive condition. In fact, the most striking primitive feature of *Stylolophus* within Embrithopoda is its small size, especially for the type species *S. minor*.

Besides the small size, a substantial number of characters distinguish *Palaeoamasia* and other more advanced embrithopods from *Stylolophus*. However, they do not indicate great shift in evolutionary stage. The most remarkable characters correspond to the upper molars M^{1-2} with at least two lingual roots (128-2) and with fused mesial roots (129-1), which are the only known exclusive synapomorphies of *Palaeoamasia* and derived embrithopods. Homoplastic synapomorphies of *Palaeoamasia* and other embrithopods are linked to the more molarized P^2 (74-1, 75-1, 76-2) and P^3 (79-2). The node separating derived

embrithopods from *Palaeoamasia* includes *Namatherium* and corresponds to a more derived evolutionary stage related to a further specialized hyperdilambdodont pattern (108-2, 119-2, 122-2, all exclusive synapomorphies). It is also characterized by a deeper palate between premolars (143-2). The difference is especially true for both *Namatherium* and *Arsinoitherium.* The relationships of *Hypsamasia, Crivadiatherium, Namatherium*, and *Arsinoitherium* are unresolved in our analyses (Figs. 24-25). By contrast, Erdal et al. (2016) made *Namatherium* the sister-group to all other embrithopods (i.e., including *Palaeoamasia)*, although the authors noted that it is the weakest node in their analysis. In fact, Erdal et al. (2016: fig. 9B) found as in this work a sister-group relationship of *Palaeoamasia* to both *Namatherium* and *Arsinoitherium* using the matrix of Tabuce et al. (2007). The unresolved relationships of advanced embrithopods most likely relate to our poor knowledge of the palaeoamasiids, which are only known by dental remains. Our opinion is nevertheless that the family Palaeoamasiidae is most likely monophyletic.

In our analyses the embrithopods genera, including *Stylolophus,* are poorly autapomorphic, with the exception of *Arsinoitherium*. *Arsinoitherium* is remarkable in the fact that many of its autapomorphies are reversals within embrithopods, for example, 127-0, M^3 size similar to M^2; 157-01, posterior orbit; 158-0, orbit ventral rim formed by the jugal; 174-0, zygomatic arches narrow transversely (ACCTRAN optimization); and 176-0, weak lateral zygomatic process of the squamosal (ACCTRAN optimization). However, it should be noted that it is not known if the ventral rim of the orbit was formed by the jugal in *Stylolophus* as in *Arsinoitherium*.

Relationships within the Tethytheria

Along with the Paenungulata, the clade Tethytheria is the best supported supraordinal node in our analyses (Fig. 25; Electronic Supplementary Material). In all MPTs (equal weighting and implied weighting analyses), the order Embrithopoda including *Stylolophus* is included in

the supraordinal clade Tethytheria, which is restricted to the orders Embrithopoda, Sirenia, and Proboscidea. Within the Tethytheria, all our analyses also recover a sister-group relationship of the Embrithopoda to other tethytherian orders (i.e., Proboscidea + Sirenia) (Figs. 25-26; Electronic Supplementary Material). As a result, the order Embrithopoda has a stem tethytherian position.

The stem tethytherian position of the Embrithopoda is supported by five unambiguous synapomorphies of the two orders Sirenia and Proboscidea. The stronger among them are the presence of a molar postentoconule (125-1, RI= 100) and the reduced preparacrista (112-1, RI= 90). The coronoid process rising at M_3 level (55-1, RI=66) is also known in *Cambaytherium* and *Ocepeia*. The preparacrista oriented longitudinal (111-1, RI=58) is also known in euungulates. In addition, two exclusive ambiguous synapomorphies are unknown (optimizations) in the Sirenia: a large retromolar fossa (62-2, ACCTRAN) and a mesostyle located transversely close to paracone and metacone (106-1, DELTRAN). Other synapomorphies are very homoplastic. The presence of a coronoid foramen in Sirenia and Proboscidea might actually be more inclusive, as a synapomorphy of the whole Paenungulata (60-1).

The node Tethytheria including the Embrithopoda as sister-group to both the Sirenia and Proboscidea is supported by one unambiguous exclusive synapomorphy and 17 homoplastic synapomorphies of which the most important are the followings (Electronic Supplementary Material, Supp. Fig. 10):

- 8-4 (RI=100), lower canine very small; *Eritherium* shares this condition although the tooth is lost in other proboscideans;
- 11-2 (RI=55), P_1 small and simple; this state is also known in euungulates such as Phenacodontidae and *Hyopsodus*;

- 13-1 and 14-1, P_2 small and uniradicular; these characters are reversed in advanced embrithopods and proboscideans:
- 72-1 (RI=83), P^1 uniradicular; this character state is also known in Arctocyonidae and *Hyopsodus*;
- 91-1 (RI=66), absence of postprotocrista in P^{3-4}; this character is reversed in *Palaeoamasia*;
- 118-2 (RI=70), molar postprotocrista absent; this state is related to the bilophodont morphology and is convergent with the Perissodactyla and the Desmostylia; it is apparently reversed in *Palaeoamasia* and *Namatherium*;
- 147-1 (RI=62), wide nasal cavity (convergence with Desmostylia, and *Orycteropus*);
- 157-3 (RI=59), orbit anterior to molars; this is a convergence with Desmostylia;
- 161-1 (RI=58), infraorbital foramen close to the orbit; this is a convergence with Desmostylia;
- 169-1 (RI=88), zygomatic process high dorso-ventrally; this character remains unknown in *Stylolophus*.
- 181-1 (RI=83), external auditory meatus high above the tooth row; this is a convergence with the Desmostylia.

The clade Tethytheria is also supported by a few additional ambiguous synapomorphies:

- 40-2 (RI= 83; DELTRAN optimization), postcristid absent and hypoconulid cingular-like; this is a convergence with euungulates;
- 174 -1 (RI=71, ACCTRAN optimization), zygomatic arch widely divergent laterally; however, this trait is poorly known in early embrithopods and is reversed in *Arsinoitherium*.

It should be noted that within Tethytheria, *Eritherium* is found in stem position of the Proboscidea in the equal weighting analysis (Fig. 25) in accordance with the study of Gheerbrant (2009) and in contrast to Gheerbrant et al. (2018). However, the position of *Eritherium* changes to the stem group of both the Sirenia and the Proboscidea in the implied weighting analysis (Fig. 26). The sister-group relationship of the *Eritherium* and the Proboscidea is also recovered in the analysis with all characters unordered (equal weighting and implied weighting analyses; see Electronic Supplementary Material).

The sister-group relationship of the Embrithopoda and extant tethytherian orders of Sirenia and Proboscidea obtained here contrasts with the previous consensus hypothesis of a sister-group relationship of the Embrithopoda and Proboscidea (Tassy and Shoshani 1988; Court 1990, 1992b; Fischer and Tassy 1993; Asher et al. 2003). Court (1992b) identified seven synapomorphies of the Embrithopoda and Proboscidea in *Arsinoitherium*. Of these seven synapomorphies, five (ethmoidal foramen posterior, posttympanic process recurved toward the postglenoid process, perilymphatic foramen present, paroccipital process reduced, hypoglossal foramen absent) were shown to be convergent by Gheerbrant et al. (2005), which is confirmed by the present study. More recently, Benoit et al. (2013b) also showed the convergence of *Arsinoitherium* with Proboscidea in the petrosal and bony labyrinth morphology. The distribution of the two remaining synapomorphies of the Embrithopoda and Proboscidea identified by Court (1992b) (166-2, reduced orbital exposure of the palatine; 167-2, sphenopalatine foramen anterior) remains poorly known in both early embrithopods and proboscideans.

The stem tethytherian position of the Embrithopoda order including *Stylolophus* supported here implies an hyperdilambdodont specialization derived from an ancestral tethytherian morphotype closer to that of the paenungulates than to that of the crown tethytherians (especially proboscideans). This is consistent with the distinctive molar

specialization seen in the earliest known proboscideans and sirenians (e.g., reduced stylar shelf and ectoloph).

Supraordinal relationships above the Tethytheria

The clade Paenungulata is recovered in all our analyses (Figs. 25-26). It excludes *Phenacolophus* from the Paleocene of China, which was considered as a primitive relative of the Embrithopoda (McKenna and Manning 1977; McKenna and Bell 1997). Relationships of *Phenacolophus* and the Embrithopoda were already challenged based on enamel microstructure (Koenigswald 2012). The Paenungulata also excludes in our analysis the Anthracobunia (Anthracobunidae, Cambaytheriidae) and the Desmostylia in agreement with Rose et al. (2014) and Cooper et al. (2014). The cladistic analysis of *Stylolophus* and other embrithopods supports an ancestral dilambdodont morphotype in the Paenungulata and in the Tethytheria (see Gheerbrant et al. 2016), which is one important feature departing from the Desmostylia. Moreover, in our matrix the character hypocone, which is coded unknown in the Desmostylia because of its uncertain homology (see Gheerbrant et al. 2016), is optimized as present in resulting trees in contrast to the Paenungulata. It supports the convergence of the bilophodont molars in the Paenungulata on one side and in the Desmostylia and other Euungulata on the other side (see Gheerbrant et al. 2016). Bilophodonty was previously considered as an important synapomorphy relating Desmostylia and Paenungulata.

The clade Paenungulatomorpha that includes crown and stem Paenungulata (Gheerbrant et al. 2016) is found in the implied weighting analysis (Fig. 26), in analyses excluding the Desmostylia, and in the analysis constraining the clade Afrotheria (Table 11; Electronic Supplementary Material). It is supported by 21 unambiguous characters, including three exclusive synapomorphies (62-1, retromolar fossa present; 116-1, molar metaconule shifted lingually; 158-1, orbit bordered by a short process of the maxilla). The least

homoplastic synapomorphies (other than the exclusive synapomorphies) are the presence of an inflated tegmen tympani (195-1, RI=80), and the absence of true hypocone (93-0, RI=83). Other afrotherians such as the Macroscelidea are found related to Paenungulatomorpha in the implied weighting analysis excluding the Desmostylia (Electronic Supplementary Material).

DISCUSSION

Phylogeny

Our cladistic analysis supports the basalmost position of *Stylolophus* within embrithopods. *Stylolophus minor* and *S. major* are both the most primitive and earliest known embrithopods. The two Moroccan species nevertheless already have a well-specialized embrithopod morphology that is quite distinctive with respect to all other paenungulates. This is best illustrated by the hyperdilambdodont molar pattern and by other molar details such as the lingual hypoconulid, the cristid obliqua very lingual on the trigonid, the small and lingually located hypoconulid lobe in M_3, and the widely lingually open talonid. Some other interesting specialized embrithopod skull features are observed in *S. minor*, such as the palate significantly concave between the premolars. In addition, *S. major* shows a remarkable intranasal rostrum pattern with the occurrence of large paranasal sinuses, which is strongly reminiscent of the very large hollow air space developed in the nasal horn of *Arsinoitherium*. As a result, *S. minor* from the Ouled Abdoun phosphate basin shows that the ancestral morphotype of the order Embrithopoda was well established at least by the earliest Eocene.

A substantial number of features found in *Stylolophus* are retained in *Arsinoitherium* from the early Oligocene. *Arsinoitherium* is however much more derived in such features as

the hypsodont cheek teeth, advanced hyperdilambdodonty with a pseudolophodont pattern, molarized P^{2-4} bearing a hypocone, and petrosal morphology (subarcuata fossa absent, perilymphatic foramen, lamina secundaria absent). *Arsinoitherium* additionally differs from *Stylolophus* and other embrithopods by remarkable reversals. They include the biradicular P_2, the M^3 close in size to M^2, and the posterior orbit. The homodont anterior dentition with subvertical incisors reconstructed in *Arsinoitherium* also differs well from the enlarged and procumbent I_{1-2} seen in *Stylolophus.* Other likely major reversals of *Arsinoitherium*, such as the narrow zygomatic arches, are features still unknown in *Stylolophus.*

The Moroccan embrithopods *S. minor* and *S. major* are closely related. They differ mostly in the larger size of *S. major,* consistently with its higher stratigraphic provenance (Sillons A-B of Ouled Abdoun phosphate series, middle Ypresian, ca. 53-51 Ma). Their close morphological affinity, including one exclusive enamel feature (206-1), supports their congeneric position. In addition to its larger size, *S. major* shows some more specialized features that agree with a more derived chronospecies. *Stylolophus minor* and *S. major* belong indeed to one of the best-known mammal lineage discovered in the Eocene sequence of the phosphate deposits from Morocco. It adds to the Paleocene mammal lineage *Ocepeia daouiensis* (Selandian) - *O. grandis* (Thanetian) identified in the same Ouled Abdoun phosphate series (Gheerbrant et al. 2014).

The stem tethytherian position of the order Embrithopoda, as the sister-group to both the Sirenia and the Proboscidea, is most consistent with an ancestral dilambdodont morphotype in paenungulates and paenungulatomorphs (Gheerbrant et al. 2014, 2016) from which evolved the hyperdilambdodonty of the Embrithopoda (Gheerbrant et al. 2018, Fig. 4C). Such an ancestral dilambdodont morphotype, known especially in *Ocepeia* and early hyracoids such as *Seggeurius*, is characterized by a wide stylar shelf and a selenodont

ectoloph that is transversely extended and linked to enlarged stylar cusps. The hyperdilambdodont specialization corresponds to the trend for a further development of the labial molar structures. By contrast, the crown tethytherian orders Sirenia and Proboscidea both show an opposite early trend to reduce the labial structural elements (crests and stylar cusps) of the upper molar "primary trigon," in combination with the development of the lingual lophs (true bilophodonty) (Gheerbrant et al. 2018: fig. 4C). Our cladistic analysis (Fig. 26) accordingly recovers the clade Paenungulatomorpha gathering stem and crown paenungulates (Gheerbrant et al. 2016).

Study of the enamel microstructure of *Stylolophus* further supports that the Paenungulata and Euungulata represent two distinct and convergent ungulate-like placental radiations (e.g., Gheerbrant et al. 2016). Tabuce et al. (2017) have shown that the Paenungulata enamel microstructure is characterized by 1) the very weak development of HSB, which is found only in some advanced proboscideans, and 2) by original specializations of the radial enamel in different subtype patterns. This is well exemplified by the embrithopods which, despite their poor diversity, developed various radial enamel type: MRE (*Crivadiatherium*, *Hypsamasia*), ARE (*Arsinoitherium*), and 'RE with prisms having irregular and sinuous trajectories' (*S. minor* and *S. major*).

Paleobiogeographic significance

Stylolophus minor and *S. major* come respectively from the early Ypresian (ca. 56-54 Ma) and the middle Ypresian (early EECO interval, ca. 53-51 Ma; Yans et al. 2014; Kocsis et al. 2014; Gheerbrant et al. 2018) of Morocco. Before the discovery of *S. minor* and *S. major,* the earliest known embrithopods were found in the early-middle Eocene of Anatolia, Turkey. They are the palaeoamasiids *Palaeoamasia kansui* from the Eski-Celtek Formation (Amasya basin, Turkey), *Hypsamasia seni* from the Uzuncarsıdere Formation (Lülük Member, Haymana-Polatli Basin, Orhaniye sub-Basin, Turkey), and *Crivadiatherium* from the Lutetian (Hateg Basin, Romania). The Eski-Celtek Formation has yielded the stratigraphically best dated palaeoamasiids. The type locality of *Palaeoamasia kansui* in Eski-Celtek Formation was initially dated Ypresian, based on the occurrence above it of 1) a marine horizon with planktic foraminifera and of 2) the overlying Armutlu Formation bearing early Lutetian (ca. 47.8 Ma) planktic foraminifera (e.g., Sen and Heintz 1979; Sen 2013). *Palaeoamasia kansui* is also found in other local formations in Anatolia dated early middle Eocene (Sen 2013). According to Metais et al. (2017) the Eski-Celtek Formation is ?early Eocene. As a result, the current estimation of the age of *Palaeoamasia kansui* ranges from late Ypresian (ca. 49 Ma) to early Lutetian (ca. 47 Ma). The age of the continental Uzuncarsıdere Formation (=Kartal Formation in Kappelman et al. 1996: Maas et al. 1998) yielding *Hypsamasia seni* is less constrained. It was initially referred to the early-middle Eocene (Kappelman et al. 1996; Maas et al. 1998, 2001), and to the late Paleocene (Kazanci and Gokten 1986; Sen 2013). More recently, Metais et al. (2017), Licht et al. (2017), and Maga and Beck (2017) referred a middle-late Lutetian age (44-43 Ma) to the Uzuncarsıdere Formation mammal assemblage. Consequently, current stratigraphical data support a late Ypresian to Lutetian first occurrence of the palaeoamasiids in Anatolia, which postdates by a few million years the

Ouled Abdoun species *S. minor* and *S. major*. This is consistent with the relative evolutionary stage of the Moroccan and the Anatolian taxa, and the basal phylogenetic position of *Stylolophus* within the Embrithopoda.

The order Embrithopoda is monophyletic in our cladistic analyses, like in Erdal et al. (2016). Its distribution in both Arabo-Africa (*Stylolophus*, *Namatherium*, *Arsinoitherium*) and Eurasia (Palaeoamasiidae) indicates at least one dispersal event across the Neotethys during the Paleogene. The basal position and early age of *Stylolophus* reported here, together with the afrotherian/paenungulate/tethytherian relationships of the order, all indicate an early Cenozoic Arabo-African center of origin of the order Embrithopoda. It implies a northward dispersal of the stem palaeoamasiid in North Tethyan continental areas such as Anatolia, from which evolved *Palaeoamasia* and the family Palaeoamasiidae. Unfortunately, our analysis does not solve the question of the monophyly of the family Palaeoamasiidae, because all described species remain poorly know, only by dental remains. However, it is most likely to us that this is a single clade, originating from one trans-Tethyan dispersal founding event of an African stem relative close to *Stylolophus*. The palaeoamasiid Eurasian colonization might pertain to the Ypresian/Lutetian trans-Tethyan dispersal event between Arabo-Africa and Laurasia (Gheerbrant and Rage 2006), although we cannot exclude it is alternatively related to the earlier known Thanetian/Ypresian trans-Tethyan dispersal event. The Ypresian/Lutetian trans-Tethyan dispersal event is best consistent with the age, the close morphology, and the relative evolutionary stage of *S. major* and *Palaeoamasia kansui.* The ecological conditions in the northern Tethyan shores of Eurasia favored the Eocene local radiation of the Palaeoamasiidae, in parallel to that of the Arsinoitheriidae on the African southern side of the Mediterranean Neotethys. Interestingly, Licht et al. (2017) suggested that the palaeoamasiid biotopes, such as those recorded by the Uzuncarsıdere fauna and

deposits, were characterized by wet climatic conditions with a dry season, as part of Eocene monsoonal ecosystems extended on the Eurasian Tethyan shores.

CONCLUSION

The discovery of the earliest and basalmost embrithopods in the early Eocene of Morocco sheds new light on the early African radiation and phylogeny of ungulate-like placentals, and especially on the Tethytheria. The species S. *minor* and S*. major* belong to an early-middle Ypresian Ouled Abdoun embrithopod lineage that is characterized by a rapid increase in size (135-140 % in tooth size, 260 % in body size). These Moroccan species remain much smaller and more primitive than previously known embrithopods, including the palaeoamasiids.

The phylogenetic analysis of *Stylolophus* supports that the order Embrithopoda is a basal tethytherian offshoot that rapidly evolved and specialized in parallel to the early evolution of the crown tethytherian orders Proboscidea and Sirenia. By the beginning of the Eocene the Embrithopoda already acquired the autapomorphic hyperdilambdodont dental pattern and some specialized skull characters such as a developed nasal sinus system.

Stylolophus minor was sympatric and coeval with the early proboscidean *Phosphatherium escuilliei* found in the same early Ypresian Ouled Abdoun phosphate beds. Both species shows that the earliest known embrithopods were slightly larger and distinctly specialized with respect to contemporaneous early proboscideans*. Stylolophus minor* supports indeed an at least Paleocene origin and early evolution of the Embrithopoda. This is consistent with the stem tethytherian position of the Embrithopoda, and with the discovery of the earliest proboscidean *Eritherium* in the Selandian of the Ouled Abdoun phosphates series (Gheerbrant 2009). During the early Eocene, both the early embrithopods and

proboscideans rapidly evolved at least in size, as testified by *S. major* and *Daouitherium rebouli* Gheerbrant and Sudre, 2002 (Gheerbrant et al. 2002) from the Moroccan phosphate series. This might point out an early general trend of the Tethytheria to increase in size during the early-middle Ypresian, in correlation with global climatic warming events known at that time such as the ETM2-3 and EECO events. As for the proboscideans, the embrithopod trend to increase in size continued in Africa during the Eocene and Oligocene as evidenced by *Namatherium* and *Arsinoitherium*.

Stylolophus minor helps to recognize within the Tethytheria two major divergent structural trends in the evolution of the upper molar lophodonty (Gheerbrant et al. 2018: fig. 4C): 1) development of labial cusps (styles) and crests (ectoloph), forming the pseudolophs (extended preparacrista and premetacrista) in the Embrithopoda; and 2) development of the lingual crests and cusps, forming protoloph and metaloph in crown tethytherians (Sirenia and Proboscidea). These two trends are antagonistic in the Tethytheria. By contrast, the Hyracoidea retained both trends with the evolution of more or less specialized and combined selenodonty and lophodonty in several lineages.

The embrithopods distribution is one of the most demonstrative mammalian evidences of trans-Tethyan dispersals between the Arabo-African Island and Eurasia during the Paleogene. The early and basalmost embrithopods *S. minor* and *S. major* are new evidence of the Arabo-African origin of the order, in agreement with its paenungulate and afrotherian supraordinal relationships. It supports an Ypresian/Lutetian trans-Tethyan dispersal to Eurasia at the origin of the palaeoamasiids in Eurasia. This dispersal event is correlative with an important global eustatic drop (Gheerbrant et Rage 2006; Vandenberghe et al. 2012).

ACKNOWLEDGEMENTS

We thank P. Brewer for helping with the comparison of the *Arsinoitherium* material from the NHM collections (London) and for providing photographs of this material (Fig. 24 A-B). We thank L. Cazes and P. Loubry (CR2P) for the photographs of the material (all other figures). We thank R. Vacant, Y. Despres and J. Zajac (CR2P) for the preparation and casting of the *Stylolophus* specimens. We thank F. Escuillié (OCP DEK/GE 667), S. Xerri (OCP DEK/GE 668) for donation of specimens to the OCP collection, and for making them available for study. We thank N. Longrich (University of Bath) for donation of specimen MHNM.KHG.228 to MHNM collection (Marrakech) and for making it available for study. We thank C. Letenneur and F. Goussard (CR2P) for the drawings and 3 D digital reconstructions of *Stylolophus* material (Figs. 7, 9, 10, 14; and suppl. Inf. Figures). We thank E. Louis (CR2P) for drawings of figures 19a, 22b. We thank H. Cappetta for the determination of the selachian taxa found in the matrix of the *Stylolophus* specimens. The *Stylolophus* specimens were CT scanned at the « AST -RX, plateau d'accès scientifique à la tomographie à rayons X du MNHN, UMS 2700 outils et méthodes de la systématique intégrative CNRS -MNHN, PARIS.» We thank the Office Chérifien des phosphates (OCP S.A., Morocco) for making available and supporting the study of the material in their collections. We thank the two reviewers and the editor for corrections and comments that helped to improve this paper.

REFERENCES

Andrews CW (1904) III. Further Notes on the Mammals of the Eocene of Egypt. Geol Mag 1:109–115

Andrews CW (1906) A descriptive catalogue of the Tertiary Vertebrata of the Fayûm, Egypt. Trustees of the British Museum, London

Asher RJ, Novacek MJ, Geisler JH (2003) Relationships of endemic African mammals and their fossil relatives based on morphological and molecular evidence. J Mammal Evol 10:131-194

Beadnell HJL (1902) A preliminary note on *Arsinoitherium zitteli* Beadnell, from the upper Eocene strata of Egypt. National Printing Department, Cairo

Benoit J, Ben Haj Ali M, Adnet S, Essid EM, Hayet K, Marivaux L, Merzeraud G, Merigeaud S, Vianey-Liaud M, Tabuce R (2013a) Cranial remain from Tunisia provides new clues for the origin and evolution of Sirenia (Mammalia, Afrotheria) in Africa. PLoS One 8:e54307

Benoit J, Crochet J-Y, Mahboubi M, Jaeger J-J, Bensalah M, Adaci M, Tabuce R (2016) New material of *Seggeurius amourensis* (Paenungulata, Hyracoidea), including a partial skull with intact basicranium. J Vertebr Paleontol 36 (1):e1034358

Benoit J, Merigeaud S, Tabuce R (2013b) Homoplasy in the ear region of Tethytheria and the systematic position of Embrithopoda (Mammalia, Afrotheria). Geobios 46:357-370

Billet G, Muizon C de (2013) External and internal anatomy of a petrosal from the late Paleocene of Itaboraí, Brazil, referred to Notoungulata (Placentalia). J Vertebr Paleontol 33:455-469

Cooper LN, Seiffert ER, Clementz M, Madar SI, Bajpai S, Hussain ST, Thewissen JGM (2014) Anthracobunids from the middle Eocene of India and Pakistan are stem perissodactyls. PLoS One 9:e109232

Court N (1990) Periotic anatomy of *Arsinoitherium* (Mammalia, Embrithopoda) and its phylogenetic implications. J Vertebr Paleontol 10:170-182

Court N (1992a) A unique form of dental bilophodonty and a functional interpretation of peculiarities in the masticatory system of *Arsinoitherium* (Mammalia, Embrithopoda). Hist Biol 6:91-111

Court N (1992b) The skull of *Arsinoitherium* (Mammalia, Embrithopoda) and the higher order interrelationships of ungulates. Palaeovertebrata 22:1-43

Court N (1994) The periotic of *Moeritherium* (Mammalia, Proboscidea): homology or homoplasy in the ear region of Tethytheria McKenna, 1975? Zool J Linn Soc Lond 112:13-28

Damuth J (1990) Problems in estimating body masses of archaic ungulates using dental measurements. In: Damuth J, Macfadden BJ (eds) Body Size in Mammalian Paleobiology:Estimation and Biological Implication. Cambridge University Press, Cambridge, pp 229253

David R, Stoessel A, Berthoz A, Spoor F, Bennequin D (2016) Assessing morphology and function of the semicircular duct system: introducing new in-situ visualization and software toolbox. Sci Rep 6:32772

Ekdale EG (2011) Morphological variation in the ear region of Pleistocene Elephantimorpha (Mammalia, Proboscidea) from central Texas. J Morphol 272:452-464

Erdal O, Antoine P-O, Sen S (2016) New material of *Palaeoamasia kansui* (Embrithopoda, Mammalia) from the Eocene of Turkey and a phylogenetic analysis of Embrithopoda at the species level. Palaeontology 59:631-655

Fischer MS, Tassy P (1993) The interrelation between Proboscidea, Sirenia, Hyracoidea, and Mesaxonia:the morphological evidence. In:Szalay FS, Novacek MJ, McKenna MC (eds) Mammal Phylogeny. Placentals. Springer-Verlag, New-York, USA, pp 217-234

Gannon PJ, Eden AR, Laitman JT (1988) The subarcuate fossa and cerebellum of extant primates: comparative study of a skull-brain interface. Am J Phys Anthropol 77:143-164

Gheerbrant E (2009) Paleocene emergence of elephant relatives and the rapid radiation of African ungulates. Proc Natl Acad Sci USA 106:10717–10721

Gheerbrant E, Amaghzaz M, Bouya B, Goussard F, Letenneur C (2014) *Ocepeia* (middle Paleocene of Morocco): the oldest skull of an afrotherian mammal. PLoS One 9:e89739

Gheerbrant E, Filippo A, Schmitt A (2016) Convergence of afrotherian and laurasiatherian ungulate-like mammals: first morphological evidence from the Paleocene of Morocco. PLoS One 11:e0157556

Gheerbrant E, Rage J-C (2006) Paleobiogeography of Africa: how distinct from Gondwana and Laurasia? Palaeogeogr Palaeoclimatol Palaeoecol 241:224-246

Gheerbrant E, Schmitt A, Kocsis L (2018) Early African fossils elucidate the origin of embrithopod mammals. Curr Biol 28:2167-2173

Gheerbrant E, Sudre J, Cappetta H, Bignot G (1998) *Phosphatherium escuilliei* du Thanétien du Bassin des Ouled Abdoun (Maroc), plus ancien proboscidien (Mammalia) d'Afrique. Geobios 30:247-269

Gheerbrant E, Sudre J, Cappetta H, Iarochene M, Amaghzaz M, Bouya B (2002) A new large mammal from the Ypresian of Morocco: evidence of surprising diversity of early proboscideans. Acta Palaeontol Pol 47:493-506

Gheerbrant E, Sudre J, Tassy P, Amaghzaz M, Bouya B, Iarochene M (2005) Nouvelles données sur *Phosphatherium escuilliei* de l'Eocène inférieur du Maroc, apports à la phylogénie des Proboscidea et des ongulés lophodontes. Geodiversitas 27:239-333

Goloboff PA, Farris JS, Nixon KC (2008) TNT, a free program for phylogenetic analysis. Cladistics 24:774-786

Kappelman J, Maas MC, Sen S, Alpagut B, Fortelius M, Lunkka J-P (1996) A new Early Tertiary mammalian fauna from Turkey and its paleobiogeographic significance. J Vertebr Paleontol 16:592-595

Kazanci N, Gokten E (1986) Sedimentary characteristics of terrestrial Paleocene deposits in northern Ankara Region, Turkey. Communications of the Faculty of Sciences, University of Ankara 4:153-163

Koç C, Türkmen I (2002) Sedimentological characteristics of the coal-bearing Eocene deposits at the north of Suluova (Amasya). Bulletin of Earth Sciences Application and Research Centre of Hacettepe University 26:101-117

Kocsis L, Gheerbrant E, Mouflih M, Cappetta H, Ulianov A, Chiaradia M, Bardet N (2016) Gradual changes in upwelled seawater conditions (redox, pH) from the Late Cretaceous through early Paleogene at the northwest coast of Africa: Negative Ce anomaly trend recorded in fossil bio-apatite. Chem Geol 421:44-54

Kocsis L, Gheerbrant E, Mouflih M, Cappetta H, Yans J, Amaghzaz M (2014) Comprehensive stable isotope investigation of marine biogenic apatite from the late Cretaceous–early Eocene phosphate series of Morocco. Palaeogeogr Palaeoclimatol Palaeoecol 394:74-88

Koenigswald W von (2012) Unique differentiation of radial enamel in *Arsinoitherium* (Embrithopoda, Tethytheria). Hist Biol 25:183-192

Krombach GA, Schmitz-Rode T, Prescher A, DiMartino E, Weidner J, Günther RW (2002) The petromastoid canal on computed tomography. Eur Radiol 12:2770-2775

Licht A, Coster P, Ocakoğlu F, Campbell C, Métais G, Mulch A, Taylor M, Kappelman J, Beard KC (2017) Tectonostratigraphy of the Orhaniye Basin, Turkey: implications for collision chronology and Paleogene biogeography of central Anatolia. J Asian Earth Sci 143:45-58

Maas MC, Thewissen JGM, Kappelman J (1998) *Hypsamasia seni* (Mammalia: Embrithopoda) and other mammals from the Eocene Kartal Formation of Turkey. Bull Carnegie Mus Nat Hist 34:286-297

Maas MC, Thewissen JGM, Sen S, Kazanci N, Kappelman J (2001) Enigmatic new ungulates from the early middle Eocene of central Anatolia, Turkey. J Vertebr Paleontol 21:578-590

Maga AM, Beck RMD (2017) Skeleton of an unusual, cat-sized marsupial relative (Metatheria: Marsupialiformes) from the middle Eocene (Lutetian:44-43 million years ago) of Turkey. PLoS One 12:e0181712

McKenna MC, Bell SK (1997) Classification of Mammals Above the Species Level. Columbia University Press, New York

McKenna MC, Manning EM (1977) Affinities and palaeobiogeographic significance of the Mongolian Paleogene genus *Phenacolophus*. Geobios Mem sp 1:61-85

Métais G, Erdal O, Erturaç K, Beard KC (2017) Tarsal morphology of the pleuraspidotheriid mammal *Hilalia* from the middle Eocene of Turkey. Acta Palaeontol Pol 62:173-179

Nixon KC (1999) Winclada (BETA) Version 0.9.9. Software published by the author, Ithaca

O'Leary MA (2010) An anatomical and phylogenetic study of the osteology of the petrosal of extant and extinct artiodactylans (Mammalia) and relatives. Bull Am Mus Nat Hist 59:1-206

Ozansoy F (1966) Türkiye Senozoik çağlarında fosil insan formu problemi ve biostratigrafik dayanakları. Ankara University Dil ve Tarih Cografya Fakultesi 172, 1–104.

Pickford M (1986) Première découverte d'une faune mammalienne terrestre paléogène d'Afrique sub-saharienne. CR Acad Sci Ser II A 302:1205-1210

Pickford M (2015) Large ungulates from the basal Oligocene of Oman:1-Embrithopoda. Span J Palaeontol 30, 33–42

Pickford M (2017) *Arsinoitherium* (Embrithopoda) and other large mammals and plants from the Oligocene of Tunisia. Foss Impr 73:172-181

Pickford M, Senut B, Morales J, Mein P, Sanchez IM (2008) Mammalia from the Lutetian of Namibia. Memoir Geol Survey Namibia 20:465-514

Radulesco C, Iliesco G, Iliesco M (1976) Un Embrithopode nouveau (Mammalia) dans le Paléogène de la dépression de Haţeg (Roumanie) et la géologie de la région. Neues Jahrb Geol Pa, Mh 11:690-698

Radulesco C, Samson P (1987) Eocene mammals from Romania with a review of embrithopods. In: Petrescu I (ed) The Eocene from the Transylvanian Basin. Universitatea Babes-Bolyai, Cluj-Napoca, Romania, pp 135-142

Radulesco C, Sudre J (1985) *Crivadiatherium iliescui* n. sp., nouvel embrithopode (Mammalia) dans le Paléogène ancien de la dépression de Hateg (Roumanie). Palaeovertebrata 15:139-157

Rasmussen DT, Gutierrez M (2009) A mammalian fauna from the late Oligocene of northwestern Kenya. Palaeontogr Abh A:1–52

Rose KD, Holbrook LT, Rana RS, Kumar K, Jones KE, Ahren HE, Smith T (2014) Early Eocene fossils suggest that the mammalian order Perissodactyla originated in India. Nat Comm 5:1-9

Sanders WJ, Kappelman J, Rasmussen DT (2004) New large-bodied mammals from the late Oligocene site of Chilga, Ethiopia. Acta Palaeontol Pol 49:365-392

Sanders WJ, Nemec W, Aldinucci M, Janbu NE, Ghinassi M (2014) Latest evidence of *Palaeoamasia* (Mammalia, Embrithopoda) in Turkish Anatolia. J Vertebr Paleontol 34:1155-1164

Sanders WJ, Rasmussen DT, Kappelman J (2010) Embrithopoda. In: Werdelin L, Sanders WJ (eds) Cenozoic Mammals of Africa. University of California Press, Berkeley, pp 115-122

Savage RJG, Domning DP, Thewissen JGM (1994) Fossil Sirenia of the west Atlantic and Caribbean region. V. The most primitive known sirenian, *Prorastomus sirenoides* Owen, 1855. J Vertebr Paleontol 14:427-449

Schmitt A, Gheerbrant E (2016) The ear region of earliest known elephant relatives: new light on the ancestral morphotype of proboscideans and afrotherians. J Anat 228:137–152

Seiffert ER (2007) A new estimate of afrotherian phylogeny based on simultaneous analysis of genomic, morphological, and fossil evidence. BMC Evol Biol 7:1-13

Sen S (2013) Dispersal of African mammals in Eurasia during the Cenozoic: ways and whys. Geobios 46:159–172

Sen S, Heintz E (1979) *Palaeoamasia kansui* Ozansoy 1966, Embrithopode (Mammalia) de l'Eocène d'Anatolie. Ann Paleontol 65:73-91

Simpson GG (1945) The principles of classification and a classification of mammals. Bull Amer Mus Nat Hist 85:1-350

Tabuce R, Marivaux L, Adaci M, Bensalah M, Hartenberger J-L, Mahboubi M, Mebrouk F, Tafforeau P, Jaeger J-J (2007) Early Tertiary mammals from North Africa reinforce the molecular Afrotheria clade. P Roy Soc B 274:1159-1166

Tabuce R, Seiffert ER, Gheerbrant E, Alloing-Séguier L, Koenigswald W von (2017) Tooth enamel microstructure of living and extinct hyracoids reveals unique enamel types among mammals. J Mammal Evol 24:91-110

Tassy P, Shoshani J (1988) The Tethytheria:elephants and their relatives. In: Benton MC (ed) The Phylogeny and Classification of the Tetrapods. Volume 2: Mammals. Clarendon Press, Oxford, pp 283-315

Thomas H, Roger J, Sen S, Bourdillon de Grissac C, Al-Sulaimani Z (1989) Découverte de vertébrés fossiles dans l'Oligocène inférieur du Dhofar (Sultanat d'Oman). Geobios 22:101-120

Thomas H, Roger J, Sen S, Pickford M, Gheerbrant E, Al-Sulaimani Z, Al-Busaidi S (1999) Oligocene and Miocene terrestrial vertebrates in the southern Arabian Peninsula (Sultanate of Oman) and their geodynamic and palaeogeographic settings. In: Whybrow PJ, Hill A (eds) Fossil Vertebrates of Arabia. Yale University Press, New Haven, pp 430-442

Vandenberghe N, Hilgen FJ, Speijer RP (2012) The Paleogene Period. In: Gradstein FM, Ogg JG, Schmitz MD, Ogg GM (eds) The Geological Time Scale 2012. Elsevier Science, Oxford, pp 855-921

Vialle N, Merzeraud G, Delmer C, Feist M, Jiquel S, Marivaux L, Ramdarshan A, Vianey-Liaud M, Essid EM, Marzougui W, Hayet KA, Tabuce R (2013) Discovery of an embrithopod mammal (*Arsinoitherium*?) in the late Eocene of Tunisia. J Afr Earth Sci 87:86-92

Westerhold T, Röhl U, Donner B, Zachos JC (2018) Global extent of early Eocene hyperthermal events: a new Pacific benthic foraminiferal isotope record from Shatsky Rise (ODP Site 1209). Paleoceanogr Paleoclimatol Palaeoecol 33:626-642

Wight AWR (1980) Paleogene vertebrate fauna and regressive sediments of Dur at Talhah, Southern Sirt Basin, Libya. In: Salem MJ, Busrewil MT (eds) The Geology of Lybia. Academic Press, London, pp 309-325

Yans J, Amaghzaz M, Bouya B, Cappetta H, Iacumin P, Kocsis L, Mouflih M, Selloum O, Sen S, Storme J-Y, Gheerbrant E (2014) First carbon isotope chemostratigraphy of the Ouled Abdoun phosphate basin, Morocco; implications for dating and evolution of earliest African placental mammals. Gondwana Res 25:257-269

Tables

Table 1. Scan parameters of the studied specimens

Specimen	Voltage	Current	Exposure	Voxel size
MNHN.F PM53 maxilla	225 kV	250 µA	200 ms	0.20 mm
MNHN.F PM53 petrosal	150 kV	270 µA	200 ms	0.01407810 mm
MNHN.F PM30	150 kV	185 µA	200 ms	0.20 mm
OCP DEK/GE 667	115 kV	330 µA	500 ms	0.08101174 mm
OCP DEK/GE 668	120kV	300 µA	500ms	0.04170082 mm

Table 2**.** Stratigraphic ranges of the selachian species found in the matrix of *Stylolophus minor* (determinations H. Cappetta), specimen OCP DEK/GE 668; ranges actualized by H. Cappetta (pers. com. EG 04 2016). Notes: ([1]) extension up to Bed 0 but not in the "sillons" in the Ouled Abdoun basin phosphate series.

Taxa	Danian	Thanetian	Early Ypresian	Middle Ypresian	Late Ypresian
Abdounia cf. *A. baugei*	-	-	**+**	+	+
Chiloscyllium meraense	-	-	**+**	+	+
Premontreia subulidens	+	+	**+**	+ ([1])	-

Table 3. Measurements of the upper teeth of *Stylolophus minor* (mm). * estimate; L= left; R= right.

Locus	Specimen	Length	Width
M^3	OCP DEK/GE 667 (R)	15	16
M^2	OCP DEK/GE 667 (R)	13	15.5
M^1	OCP DEK/GE 667 (R)	12	13
M^1	OCP DEK/GE 667 (L)	12	13
P^4	OCP DEK/GE 667 (R)	9.6	12
P^3	OCP DEK/GE 667 (L)	9	9
P^2	OCP DEK/GE 667 (L)	7	5
P^1 alveolus	OCP DEK/GE 667 (L)	*3.5	*4
C^1 alveolus	OCP DEK/GE 667 (L)	*5.5	*3
I^3 alveolus	OCP DEK/GE 667 (L)	*4	*2.7
I^3 alveolus	OCP DEK/GE 667 (R)	4.5	4
I^2 alveolus	OCP DEK/GE 667 (R)	7	5.5
I^1 alveolus	OCP DEK/GE 667 (R)	*11	*10.5

Table 4. Length of the upper tooth row of *Stylolophus minor* (mm; * estimate).

Tooth series	specimen	Length
M^3-P^4	OCP DEK/GE 667	49
M^{1-3}	OCP DEK/GE 667	40
M^{2-3}	OCP DEK/GE 667	29
M^{1-2}	OCP DEK/GE 667	25.5
P^3-P^2	OCP DEK/GE 667	15.2
P^3-I^3	OCP DEK/GE 667	*32.2
P^3-C^1	OCP DEK/GE 667	*20.8
I^{1-3} (minimal length)	OCP DEK/GE 667	*24
M^3-C^1	OCP DEK/GE 667	*77

Table 5. Measurements of the lower teeth of *Stylolophus minor* (mm). * estimate; alv: measurement from the alveolus. Measurements of M_2 and P_4 in MNHN.F PM30 were made on the 3D digital models reconstructed from the tomographies.

specimen	Locus	L	Ltrig	Ltal	Wtrig	Wtal	H
OCP DEK/GE 668	I_1 (alv)	*9			*6		*23
OCP DEK/GE 668	I_2 (alv)	*9.2	-		*5		?
OCP DEK/GE 668	I_3 (alv)	5.2	-	-	-	-	?
OCP DEK/GE 668	C_1 (alv)	4.5	-	-	-	-	?
OCP DEK/GE 668	P_1	5.2	-	-	2.7		-
OCP DEK/GE 668	P_2	?	?	?	?	?	?
OCP DEK/GE 668	P_3	8.2	5.4	2.4	4.7	5.6	6.4
OCP DEK/GE 668	P_4	8.5	5	3.6	6.6	6.5	8
OCP DEK/GE 668	M_1	10.4	5.4	5.4	*7.3	7.1	?
OCP DEK/GE 668	M_2	12.7	6	7.1	9.2	8.5	9.1 – 11
OCP DEK/GE 668	M_3	16.4	6.5	9.8	10.3	8.7	9.8-10.5
MHNM.KHG 228	M_3	19	8.4	11.5	10.8	9.2	10
MNHN.F PM30	P_4	8.4	*5.3	*3.9	*4.3	*3.7	?
MNHN.F PM30	M_1	*11.3	5.2	6	7.5	7	8.5-9.2
MNHN.F PM30	M_2	12.9	5.2	8.7	7.7	7.3	?
MNHN.F PM30	M_3	?	?	?	?	?	?
MNHN.F PM30	dP_4	?	?	*4.7	?	5.6	?

Table 6. Length of lower tooth row of *Stylolophus minor* (mm).

Tooth series	specimen	Length
P_3-M_3	OCP DEK/GE 668	54
P_4-M_3	OCP DEK/GE 668	46
M_{1-3}	OCP DEK/GE 668	38.5
M_{1-2}	OCP DEK/GE 668	22
P_{3-4}	OCP DEK/GE 668	16.5
C_1-M_3 (estimate)	OCP DEK/GE 668	*71

Table 7. Measurements of the dentary of *Stylolophus minor* (mm). H= height; W= width; L= length.

	Specimen	Dimensions
Corpus: H below M_2	OCP DEK/GE 668	26
Corpus: H below M_3	OCP DEK/GE 668	28.2
Corpus: H below M_3	MHNM.KHG.228	36.5
Corpus: W at M_2 level	OCP DEK/GE 668	13.7
Mand. symphysis: LxH	OCP DEK/GE 668	32.5x16.2
Dentary: L max	OCP DEK/GE 668	150

Table 8. Body mass estimate of *Stylolophus minor* based on dental measurements (equations of Damuth 1990 for non-selenodont ungulates), i.e., length of the molar series, and measurements on each molar. The best estimates are in bold. All values are given in kilograms. Note that 1) the lower jaw OCP DEK/GE 668 belongs to a smaller individual by 10 % than individual OCP DEK/GE 667 (upper jaw), based on teeth length; 2) MHNM.KHG.228 (lower jaw) belongs to a large and probably male individual based on the larger teeth and the deeper corpus with respect to OCP DEK/GE 668.

Specimen	Teeth	Length	Width	Surface
OCP DEK/GE 668	M_{1-3}	**25.94**	**--**	**--**
OCP DEK/GE 668	M_1	18.37	19.44	19.00
OCP DEK/GE 668	M_2	25.10	28.90	27.46
OCP DEK/GE 668	M_3	39.24	37.07	41.79
MHNM.KHG.228	M_3	59.33	57.97	54.97
OCP DEK/GE 667	M^{1-3}	**30.63**	--	--
OCP DEK/GE 667	M^1	29.26	30.61	29.23
OCP DEK/GE 667	M^2	47.26	46.98	45.83
OCP DEK/GE 667	M^3	37.26	42.85	39.93

Table 9. Summary of the characters of the petrosal of *Stylolophus major,* and their comparison with other early paenungulates and stem relatives.

	Stylolophus major	*Arsinoitherium*	*Eritherium*	*Phosphatherium*	*Seggeurius*	*Ocepeia*
Subarcuate fossa	moderately deep	absent	deep	moderately deep	moderately deep	deep
Perilymphatic foramen	likely divided	undivided	divided	divided	divided	divided
Tegmen tympani	likely inflated	flat	inflated	less developed	inflated	inflated
Crus commune	elongated	elongated	elongated	elongated	elongated	elongated
Semicircular canals	very thin	thick	thin	thin	thin	thin
Posterior and lateral canals	partially fused	not fused	partially fused	well fused	not fused	partially fused
Flattening of the canals	absent	present	absent	absent	absent	absent
Lamina secundaria	present	absent	present	present	present	present

Table 10. Measurements of the upper teeth of *Stylolophus major* (mm). * estimate (minimal length). L= left; R= right.

Locus	Specimen	Length	Width
M^3	MNHN.F PM53 (L)	22.5	31
M^3	MNHN.F PM53 (R)	*21.6	?
M^2	MNHN.F PM53 (L)	19.3	20
M^1	MNHN.F PM53 (L)	15	*17
P^4	MNHN.F PM53 (L)	?	?
$P^{4?}$	MNHN.F PM53 (R)	?	?
P^2	MNHN.F PM53 (R)	10.2	7.5

Table 11. Length of the upper tooth row of *Stylolophus major* (mm). * estimate (minimal length).

Tooth series	specimen	Length
M^3-P^4	MNHN.F PM53	*65
M^{1-3}	MNHN.F PM53	55.3
M^{2-3}	MNHN.F PM53	42
M^{1-2}	MNHN.F PM53	34.4

Table 12. Body mass estimate of *Stylolophus major* based on dental measurement (allometric Equations of Damuth 1990 for non-selenodont ungulates) of the upper molars, i.e., length of the molar series, and measurements on individual molars. Best estimates in bold (based on molar row length). All values given in kilograms.

Specimen	Teeth	Length	Width	Surface
MNHN.F PM53	M^{1-3}	**88.17**	--	--
MNHN.F PM53	M^1	58.57	65.93	60.49
MNHN.F PM53	M^2	128.26	104.94	111.72
MNHN.F PM53	M^3	123.73	94.28	106.63

Table 13 – Cladistic analyses of *Stylolophus* relationships performed in this work. All parsimony analyses were made with the "traditional search" command of TNT. Matrix with 35 taxa, 208 characters, 9 uninformative characters (inactivated for calculation of the indices), 48 additive (ordered) characters (Electronic Supplementary Material).

Ana-lysis	Type of analysis and constraint	Trees number	Trees Length	RI; CI	Comments (topology)
1	"Traditional search", 48 characters ordered	30	952	60.6; 35.4	Clades: "Altungulata"; Embrithopoda**: sister-group to (Proboscidea + Sirenia)**; *Eritherium* sister-group to Proboscidea
2	Idem, 1, Clade *Stylolophus* constrained	30	953	60.6; 35.4	Idem 1
3	Idem 1 with "Implied Weighting" option	5	964	59.9; 35	Clades: Paenungulatomorpha; **Embrithopoda sister-group to (Proboscidea, Sirenia);** *Eritherium* sister-group to (Proboscidea, Sirenia)
4	Idem 1, clade Afrotheria constrained	50	963	59.9; 35	Clades: Paenungulatomorpha; **Embrithopoda sister-group to (Proboscidea, Sirenia);** *Eritherium* sister-group to (Proboscidea, Sirenia)
5	Idem 4 with "Implied Weighting" option	5	975	59.2; 34.6	Idem 4
6	Analysis excluding Desmostylia, "Traditional search", 48 characters ordered	60	915	**63.2; 37**	Clades: Paenungulatomorpha; **Embrithopoda sister-group to (Sirenia, Proboscidea),** *Eritherium* sister-group to (Proboscidea, Sirenia)
7	Idem 6 with "Implied Weighting" option	10	924	61.2; 36.4	Idem 6 + Macroscelidea sister-group to Paenungulatomorpha
8	No character ordered, unweighted analysis	20	**886**	58.8; **37.7**	Clades: "Altungulata"; Embrithopoda**: sister-group to (Proboscidea + Sirenia)**; *Eritherium* sister-group to Proboscidea
9	idem 8 with "Implied Weighting"option	10	903	57.6; 37	Idem 8, with **clade *Stylolophus***.

Caption of figures

Figure 1. *Stylolophus minor.* Specimen OCP DEK/GE 667. Right premaxilla in ventral stereophotographic view (A), medial view (B), and lateral view (C). Note the large alveolus for I^1. Scale bar= 10 mm.

Figure 2. *Stylolophus minor.* Specimen OCP DEK/GE 667. Anterior part of left maxilla with P^{2-3} and alveoli in ventral stereophotographic view (A), medial view (B), and lateral view (C). A', detail of P^{2-3} in occlusal view. Scale bar= 10 mm.

Figure 3. *Stylolophus minor.* Specimen OCP DEK/GE 667. Posterior part of right maxilla with P^4, M^{1-3}, in occlusal stereophotographic view (A), lateral view (B), and medial view (C). Right isolated M^2 in occlusal stereophotographic view (E), lingual view (F), and labial view (G). Scale bar= 10 mm.

Figure 4. *Stylolophus minor.* Reconstruction of the upper dentition and the palate in ventral view. (A). Sketch of the occlusal outline of the cheek teeth P^{2-4}, M^{1-3} and outline of anterior teeth alveoli (I^{1-3}, C, P^1). (B). Outline and 3D digital model from CT scans reconstructing part of the palate and the upper dentition (from the premaxilla and maxilla fragments); in red: the anterior alveoli. Note the full placental dental formula, the enlarged anterior incisor, the hyperdilambdodont molar pattern and the concave palate between premolars and anterior teeth. Scale bar= 10 mm.

Figure 5. *Stylolophus minor.* Specimen OCP DEK/GE 667. Anterior fragment of left nasal in dorsal (A) and ventral views. c. ethm.: ethmoidal crest. Scale bar= 10 mm.

Figure 6. *Stylolophus minor.* Specimen OCP DEK/GE 668, holotype. Right lower jaw in labial (A), lingual (B), and occlusal (stereophotography) views (C). D. Stereophotographic front view of the jaw showing the roots of the large and proclive I_1 and I_2. €. Posterior view of the broken symphyseal part of the jaw showing the open root of I_1. al= alveolus; r= root; sy= symphysis. Scale bar= 10 mm.

Figure 7. *Stylolophus minor.* 3D digital model of the lower jaw OCP DEK/GE 668 (holotype) showing by transparency the roots (I_{1-2}) or the alveoli (I_3, C_1) of the teeth. (A), Occlusal view. (B), Lingual

view. (C), Labial view. r i1: Detail of the root of I_1 in its natural orientation in the jaw (tooth anteriorly tilted), with outline by transparency of the large and open pulp canal. D. Apical view of the root of I_1 showing the open pulp canal. al p2: alveolus of P_2 (damaged). Scale bar= 10 mm.

Figure 8. *Stylolophus minor.* Specimen MHNM.KHG 228, distal fragment of right lower dentary with M_3 in occlusal (A), lingual (B), and labial views (C). A: stereophotography. mf: mandibular foramen. Scale bar= 20 mm.

Figure 9. *Stylolophus minor.* Reconstruction of the lower tooth row and lower jaw from the holotype. (A), occlusal sketch of lower teeth and outline of alveoli (in grey). (B), 3D digital model reconstructing the lower jaw in occlusal view from the CT scans of OCP DEK/GE 668; in red the place of the alveolus of P_2 (broken). Scale bar= 10 mm.

Figure 10. *Stylolophus minor.* Reconstruction of the lower jaw in strict lateral view with I_{1-3} (reconstructed), C_1 (reconstructed), P_1, P_2 (reconstructed), P_{3-4}, M_{1-3}. Note the enlarged I_{1-2} (crown size redrawn following relative size of the roots; see Fig. 7). Drawing C. Letenneur. Scale-bar= 20 mm.

Figure 11. *Stylolophus minor.* Specimen MNHN.F PM30, fragment of right dentary with erupted M_1 and broken talonid of dP_4, and with unerupted germs of P_4 and M_2. (A-C), photographs in occlusal stereoview (A), lingual view (B), and labial view (C). (D- G), CT scans 3D digital models in occlusal (D, E), lingual (F), and labial (G) views; (F-G), views through the bone by transparency to display the tooth germs. Scale bar= 10 mm.

Figure 12. *Stylolophus minor.* Occlusal sketch of lower teeth: Comparison of OCP DEK/GE 668 (A) and MNHN.F PM30 (B). (A), P_{3-4}, M_{1-3}, specimen OCP DEK/GE 668 in reversed (mirror) view. (B), M_1, and talonid of dP_4, specimen MNHN.F PM30. Scale bar= 10 mm.

Figure 13. ***Stylolophus minor.*** Enamel microstructure. OCP DEK/GE 667 (=PM96), left M1, vertical section on the labial flank of the parastyle (UM-ENAM 584). (A), The one-layered Schmelzmuster is formed by radial enamel with an important amount of interprismatic matrix which completely encloses prisms. Prisms are not densely packed and have a slightly curved course from the

enamel dentine junction (EDJ) to the outer enamel surface (OES). (B-C), details of the outer part of the enamel section showing prisms with irregular and sinuous trajectories (B) and a similar orientation of the prism long axes and crystallites of the interprismatic matrix (C). (D), detail of the inner part of the enamel section showing an angle of ~45° between the prisms and the crystallites of the interprismatic matrix.

Figure 14. *Stylolophus minor.* Composite 3D digital reconstruction of the rostrum with upper and lower jaws in occlusion from the CT scans of the various fragments of the skull OCP DEK/GE 667 and the lower jaw OCP DEK/GE 668. (A), Lateral view; (B), The same with outline of the skull (missing parts) and with the bones make transparent to show the roots morphology; (C), Rostral view. In red: The reconstructed empty alveoli; note the large anterior incisor roots. Scale-bar= 20 mm.

Figure 15. *Stylolophus minor.* Occlusal sketch of the reconstructed upper and lower dentition based on OCP DEK/GE 667 (skull) and OCP DEK/GE 668 (lower jaw). The size of the lower dentition OCP DEK/GE 668 was enlarged by 10 % to fit with OCP DEK/GE 667, which belongs to a slightly larger individual. Scale bar= 10 mm.

Figure 16. *Stylolophus major*, n. sp. Holotype, MNHN.F PM53, maxilla and upper dentition. (A-C), left maxilla with P^4 (broken) and M^{1-3}. (A), sketch of the occlusal view of P^4 - M^3, and occlusal stereophotographic view of the maxilla and its preserved teeth P^4 - M^3; (B), Labial view; C. Medial view. (D), left P^2 in occlusal stereophotographic view; (E), isolated and broken right M^3 in occlusal stereophotographic view. Scale-bar= 20 mm.

Figure 17. *Stylolophus major,* n. sp. Holotype, MNHN.F PM53, maxilla and upper dentition. (A), Drawing of P^4, M^{1-3}. (B), 3D digital model of the maxilla and upper dentition in ventral view; (C), 3D digital model of the maxilla and upper dentition in dorsal view. (D), The same with the bone made transparent to show the roots morphology; note the labiolingually elongated metacone root on M^3. Iof: infraorbital foramen; Orb: Orbit; M3 post root: posterior root of M^3. Scale-bar= 10 mm.

Figure 18. *Stylolophus major*, n. sp. Holotype, MNHN.F PM53, fragment of the rostrum, mostly right side, with the right nasal, the right frontal, the anterior part of the right parietal, and part of the right orbito-temporal fossa. (A), lateral view; (B), dorsal view; (C1-2), medial view (C2: detail of paranasal sinuses). NA: nasal; FR: frontal; PA: Parietal; OS: orbitosphenoid; cr. orbito.: crista orbito-temporalis; Parana sin.: paranasal sinuses; FR sin.: frontal sinus; postorb. proc.: postorbital process; postorb constr: postorbital constriction; Nas. sut.: nasal suture. Scale-bar= 10 mm.

Figure. 19. *Stylolophus major*, n. sp. MNHN.F PM53 (holotype), left petrosal in cerebellar (A), and tympanic (B) views with details of the cochlea (C), the vestibule (D), and the lateral semicircular canal (E). Legends: aa anterior ampulla, ac aquaeductus cochleae, act apical turn of the cochlea, av aquaeductus vestibuli, cc base of the crus commune, co cochlea, ct crista transversa, ctp? caudal tympanic process (possibly), d? undetermined depression, ea eminentia arcuata, fai foramen acusticum inferior, fas foramen acusticum superior, fs fossa subarcuata, ls lamina secundaria, lsc lateral semicircular canal, pa posterior ampulla, pc prefacial commissure, pet, petromastoid canal, sf? sulcus facialis (possibly), st scala tympani, sv scala vestibuli, ve vestibule. Scale-bars= 1 and 5 mm.

Figure. 20. *Stylolophus major*, n. sp. 3D reconstruction of the bony labyrinth from specimen MNHN.F PM53 (holotype) (A-D) compared with the bony labyrinth of *Arsinoitherium zitteli* (mirrored, E-H) in lateral (A, E), anterior (B, F), posterior (C, G) and dorsal (D, H) views. Legends: aa anterior ampulla, asc anterior semicircular canal, atc apical cochlear turn, av aquaeductus vestibuli, btc basal cochlear turn, cc crus commune, ccr crus commune ridge, co cochlea, la lateral ampulla, ls lamina secundaria, lsc lateral semicircular canal, pa posterior ampulla, psc posterior semicircular canal. Scale-bar= 4 mm.

Figure 21. *Stylolophus major,* n. sp. MNHN.F PM53 (holotype), left petrosal (A) in cerebellar view; comparison with other early paenungulates: *Seggeurius* (right petrosal mirrored, B), *Eritherium* (C), *Phosphatherium* (right petrosal mirrored, D). a.c. aquaeductus cochleae, a.v. aquaeductus

vestibuli, f.a.i. foramen acusticum inferior, f.a.p. foramen acusticum posterior, f.s. fossa subarcuata, p.c. petromastoid canal. Scale-bar= 4 mm.

Figure 22 Comparison of the upper teeth of *S. minor* and *S. major*, n. sp., at the same scale. (A), Occlusal sketch of P^4, M^{1-3} preserved in OCP DEK/GE 667, hypodigm of *S. minor*. (B), Occlusal sketch of P^4, M^{1-3} preserved in MNHN.F PM53, holotype of *S. major*. Scale-bar= 10 mm.

Figure 23. *Stylolophus major,* n. sp. Enamel microstructure. MNHN.F PM53 (holotype), right M3, transverse section on the mesial flank of the metacone (UM-ENAM 582). (A), The one-layered Schmelzmuster is formed by radial enamel from the enamel dentine junction (EDJ) to the outer enamel surface (OES); prisms are densely packed. (B), Prisms present, especially near the OES, irregular deviations for short distance from the general order. (C), The interprismatic matrix crystallites show the same orientation as the long axis of prisms from the EDJ to the OES.

Figure 24. Comparison of the lower jaw of *Arsinoitherium zitelli* (A-D) and *Stylolophus minor* (E). (A-B), *Arsinoitherium zitelli,* skull NHMUK M8463 and detail of the right lower jaw in lateral view. (C-D), *Arsinoitherium zitelli,* lower jaw MNHN.F LBE579 in occlusal and rostral views showing the large and mostly horizontal alveoli for roots of I_{1-2}. (E), rostral stereoview of the lower jaw of *S. minor,* specimen OCP DEK/GE 668 (holotype), showing the large and mostly horizontal anterior incisor roots of I_{1-2}. al: alveolus; i1: first lower incisor; i2: second lower incisor. Scale-bars= 10 mm, 5 cm, 10 cm.

Figure 25. Relationships of *Stylolophus*. Most parsimonious tree resulting from equal weighting cladistic analysis with ordered features, and using TNT software. Strict consensus of 30 MPTs. Bremer index > 1 are indicated at the nodes. Retention index RI: 60.6; Consistency Index CI: 35.4. Tree length L: 952 steps. The matrix and details of the analysis, are provided in Suppl. Info. Text S1. The distribution of characters at nodes and branches is provided in Suppl. Inf. Fig. 7.

Figure 26. Relationships of *Stylolophus*. Single most parsimonious tree resulting from implied weighting parsimony analysis with ordered features, and using TNT software. Strict consensus of five MPTs. Relative Bremer index > 10 (out of 100) are indicated at the nodes. Retention index RI:

59.9; consistency Index CI: 35. Tree length L: 964 steps. The matrix and details of the cladistic analysis are provided in Suppl. Info. Text S1. The distribution of characters at nodes and branches is provided in Suppl. Inf. Fig. 8.

Caption of Tables

Table 1. Scan parameters of the studied specimens.

Table 2. Stratigraphic ranges of the selachian species found in the matrix of *Stylolophus minor*, specimen OCP DEK/GE 668; ranges actualized by H. Cappetta (pers. com. EG, 04. 2016). Notes: ([1]) extension up to Bed 0 but not in the "sillons" in the Ouled Abdoun basin phosphate series.

Table 3. Measurements of the upper teeth of *Stylolophus minor* (mm). *, estimate; L= left; R= right

Table 4. Length of the upper tooth row of *Stylolophus minor* (mm; * estimate)

Table 5. Measurements of the lower teeth of *Stylolophus minor* (mm). *, estimate; alv: measurement after the alveolus. Measurements of M_2 and P_4 in MNHN.F PM30, were made on the 3D digital models reconstructed from the tomographies.

Table 6. Length of lower tooth row of *Stylolophus minor* (mm).

Table 7. Measurements of the dentary of *Stylolophus minor* (mm). H= height; W= width; L= length.

Table 8. Body mass estimate of *S. minor* based on dental measurement (equations of Damuth (1990) for non-selenodont ungulates), i.e. length of the molar series, and measurements on individual molars. In bold the best estimates. All values given in kilograms. Note that 1) the lower jaw OCP DEK/GE 668 belongs to a smaller individual by 10 % than individual OCP DEK/GE 667 (upper jaw), based on teeth length; 2) MHNM.KHG.228 (lower jaw) belongs to a large and probably male individual based on the larger teeth and the deeper corpus with respect to OCP DEK/GE 668.

Table 9. Summary of the characters of the petrosal of *S. major*, n. sp., and their comparison with other early paenungulates and stem relatives**.**

Table 10. Measurements of the upper teeth of *Stylolophus major,* n. sp. (mm). * estimate (minimal length). L= left; R= right.

Table 11. Length of the upper tooth row of *Stylolophus major,* n. sp. (mm).

Table 12. Body mass estimated of *S. major*, n. sp. based on dental measurement (allometric equations of Damuth (1990) for non-selenodont ungulates) of the upper molars, i.e. length of the molar series, and measurements on individual molars. In bold the best estimates. All values given in kilograms**.**

Table 13. Cladistic analyses of *Stylolophus* relationships performed in this work. All parsimony analyses were made with the "traditional search" command of TNT. Matrix with 35 taxa. 208 characters, 9 uninformative characters (inactivated for calculation of the indices), 48 additive (ordered) characters (**Electronic Supplementary Material, S1 and S2**).

Caption of Electronic Supplementary Material

Suppl. Fig. 1. ***Stylolophus minor.*** 3D digital model of the right maxilla with P^4, M^{1-3}, specimen OCP DEK/GE 667 (caution: note that the teeth are wrongly labelled "M4-1" in the pdf, instated M3-1, P4). The root morphology of the teeth can be seen by hiding the bone.

Suppl. Fig. 2. ***Stylolophus minor.*** 3D digital model of the right dentary OCP DEK/GE 668 bearing M_{1-3}, P_{3-4}, P_1, root of I_{1-2}, and alveoli of C_1 and I_1 (alveolus of P_2 broken). The root morphology of the teeth (e.g., open root of I_1) can be seen by hiding the bone.

Suppl. Fig. 3. ***Stylolophus minor.*** Composite reconstruction of the rostrum with upper and lower dentition in occlusion, from specimens OCP DEK/GE 667 and OCP DEK/GE 668. 3D digital model reconstructed from the CT scans. Each element (teeth), bone (e.g., dentary, premaxilla) and specimen can be hidden separately.

Suppl. Fig. 4. ***Stylolophus minor.*** 3D digital model of the right dentary MHNM.KHG.228 bearing M_3 and posterior alveoli of M_2.

Suppl. Fig. 5. ***Stylolophus minor.*** CT scan sagittal section of the dentary MHNM.KHG.228 showing the absence of coronoid foramen and canal, the roots of M/3 and the position of the mandibular foramen (md. f.) and canal (md can.).

Suppl. Fig. 6. ***Stylolophus minor.*** Reconstruction of the occlusion of the M_3 of MHNM.KHG.228 and M^{3-2} of specimen OCP DEK/GE 667 (3D digital models). A, labial view; B, lingual view. Although MHNM.KHG.228 is distinguished by a large size among the specimens referred to *Stylolophus minor*, this reconstruction shows that the specimen fits in occlusion with specimen of the hypodigm of the species with only minor correction of tooth size (6.3 %).

Suppl. Fig. 7. ***Stylolophus major***. Holotype (specimen MNHN.F PM53), 3D digital model of the left maxilla with P4, M1-3. The root morphology of the teeth can be seen by hiding the bone.

Suppl. Fig. 8. Strict consensus of most parsimonious trees obtained from the analysis of *Stylolophus* in equal weighting default option and with ordered characters (see Fig. 25). Unambiguous synapomorphies are indicated at the nodes and branches. Black circles are non-homoplastic synapomorphies.

Suppl. Fig. 9. Strict consensus of most parsimonious trees obtained from the analysis of *Stylolophus* in obtained from the analysis of *Stylolophus* with Implied Weighting option and ordered characters (see Fig. 26). The unambiguous synapomorphies are indicated at the nodes and branches. Black circles are non-homoplastic synapomorphies.

Electronic Supplementary Material S1. Phylogenetic analysis of the relationships of *Stylolophus*.

Electronic Supplementary Material S2. TNT/Hennig character matrix analyzed for the cladistic study of the relationships of *Stylolophus*.

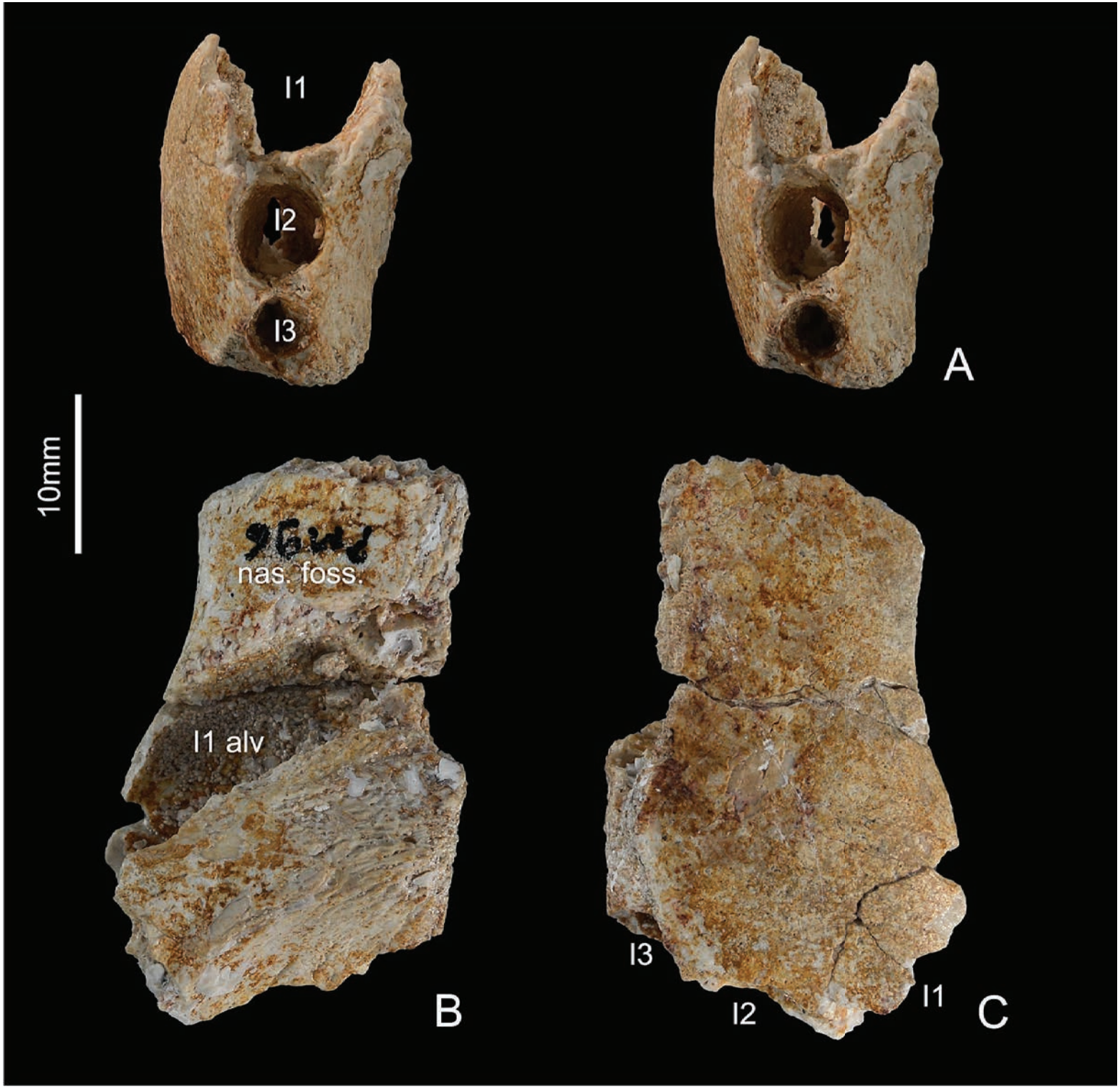
I1
I2
I3
A
10mm
nas. foss.
I1 alv
B
I3
I2
I1
C

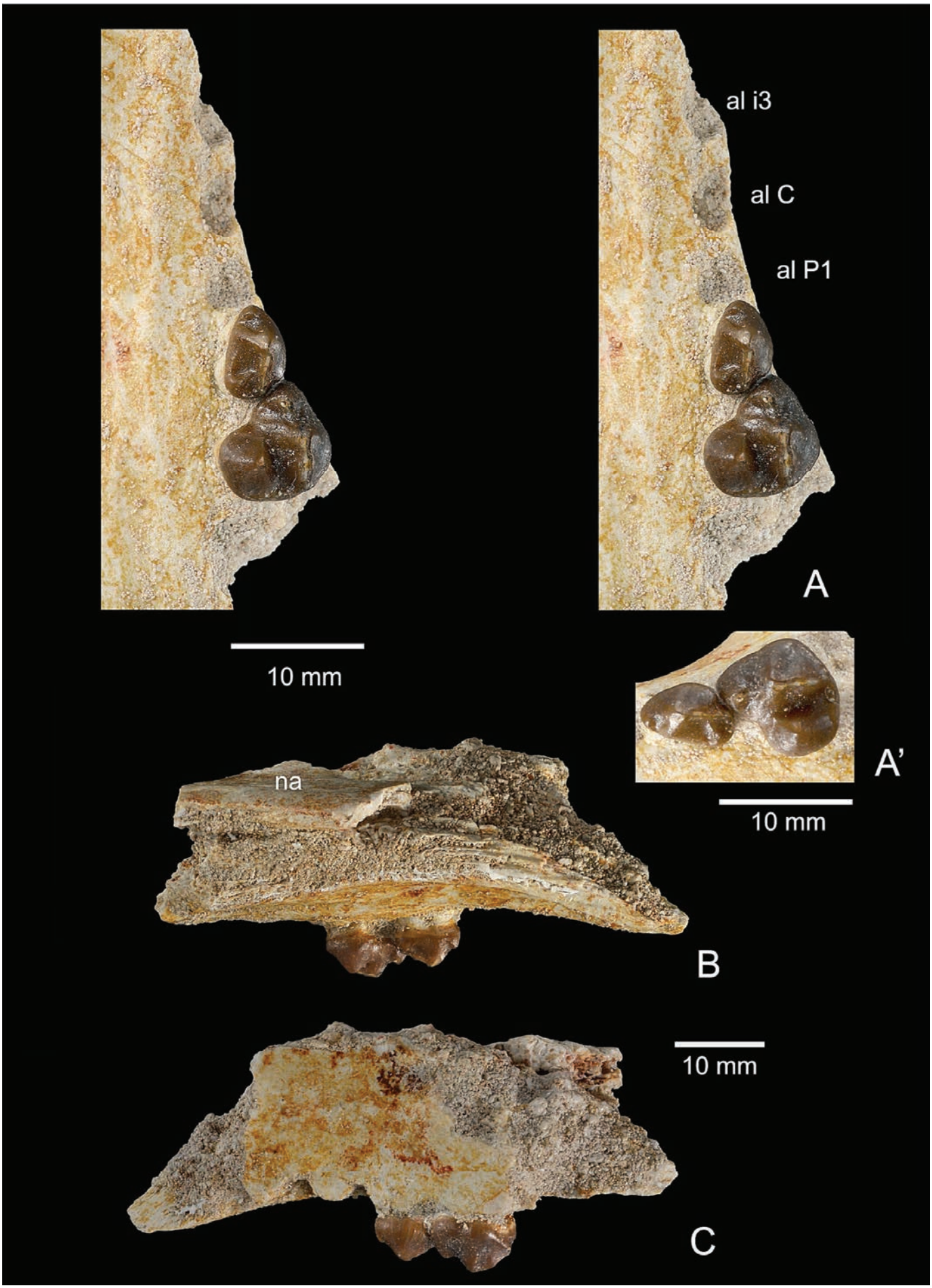
al i3
al C
al P1
A
10 mm
A'
10 mm
na
B
10 mm
C

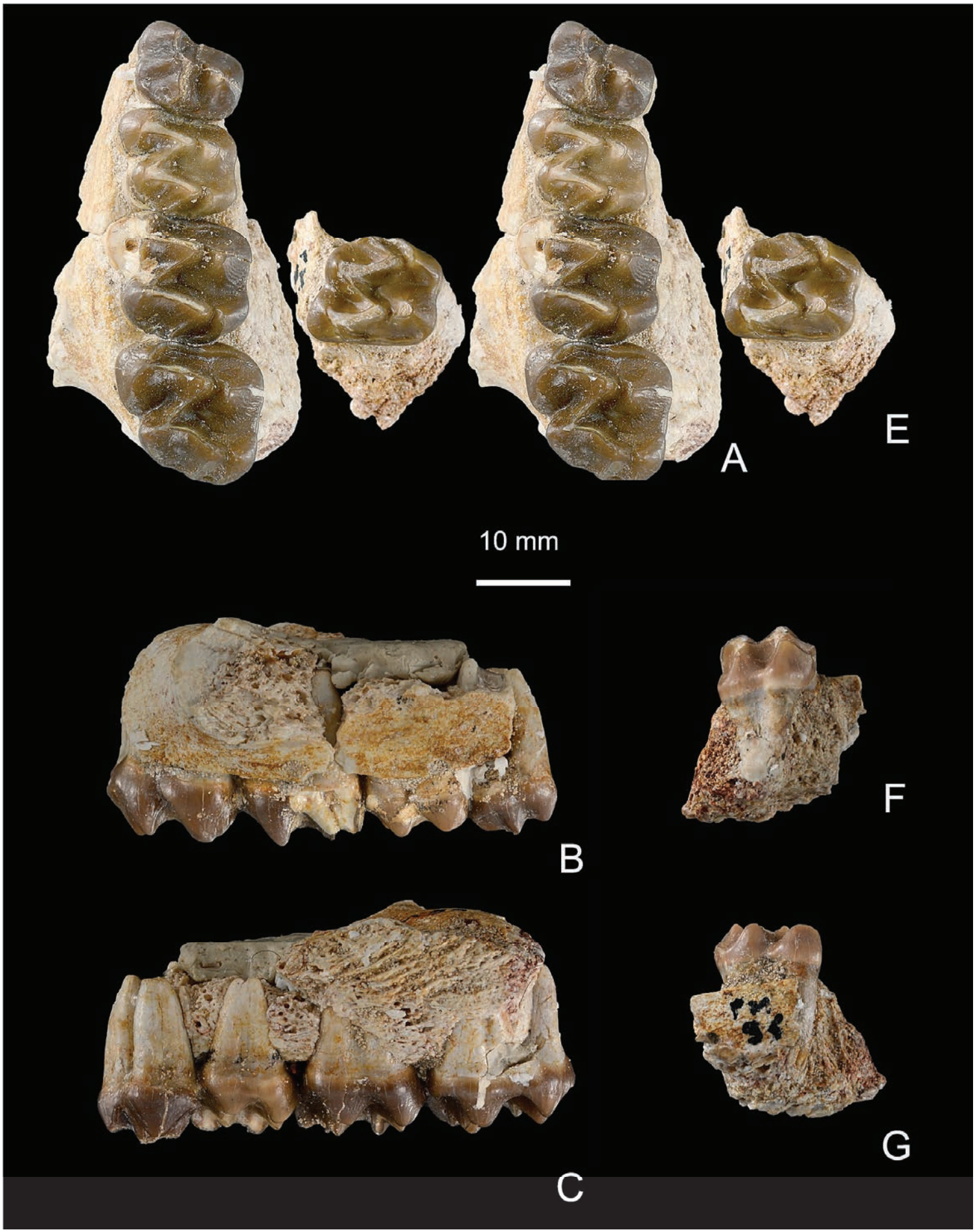
A
E
10 mm
B
F
C
G

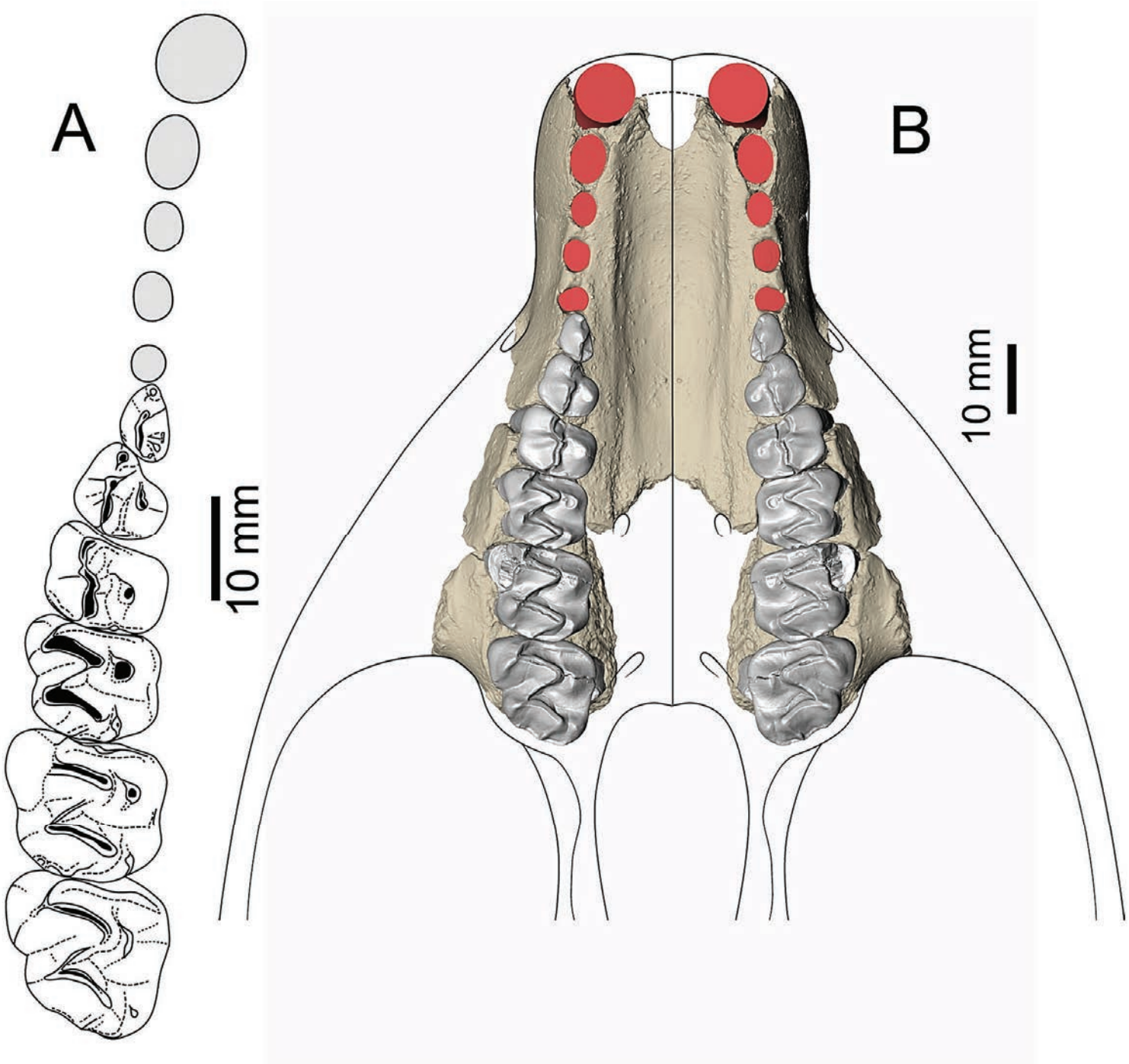
A
10 mm
B
10 mm

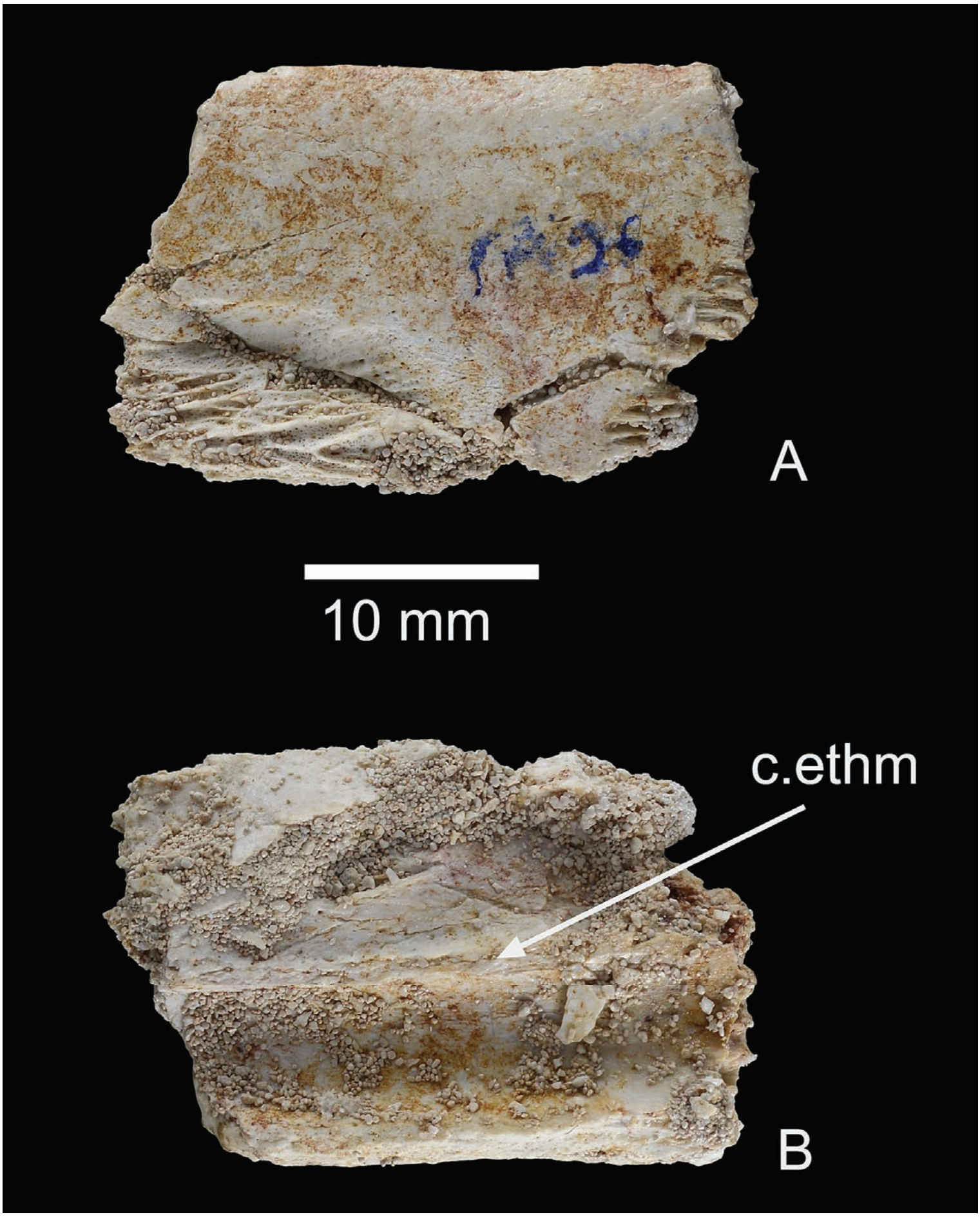
A
10 mm
c.ethm
B

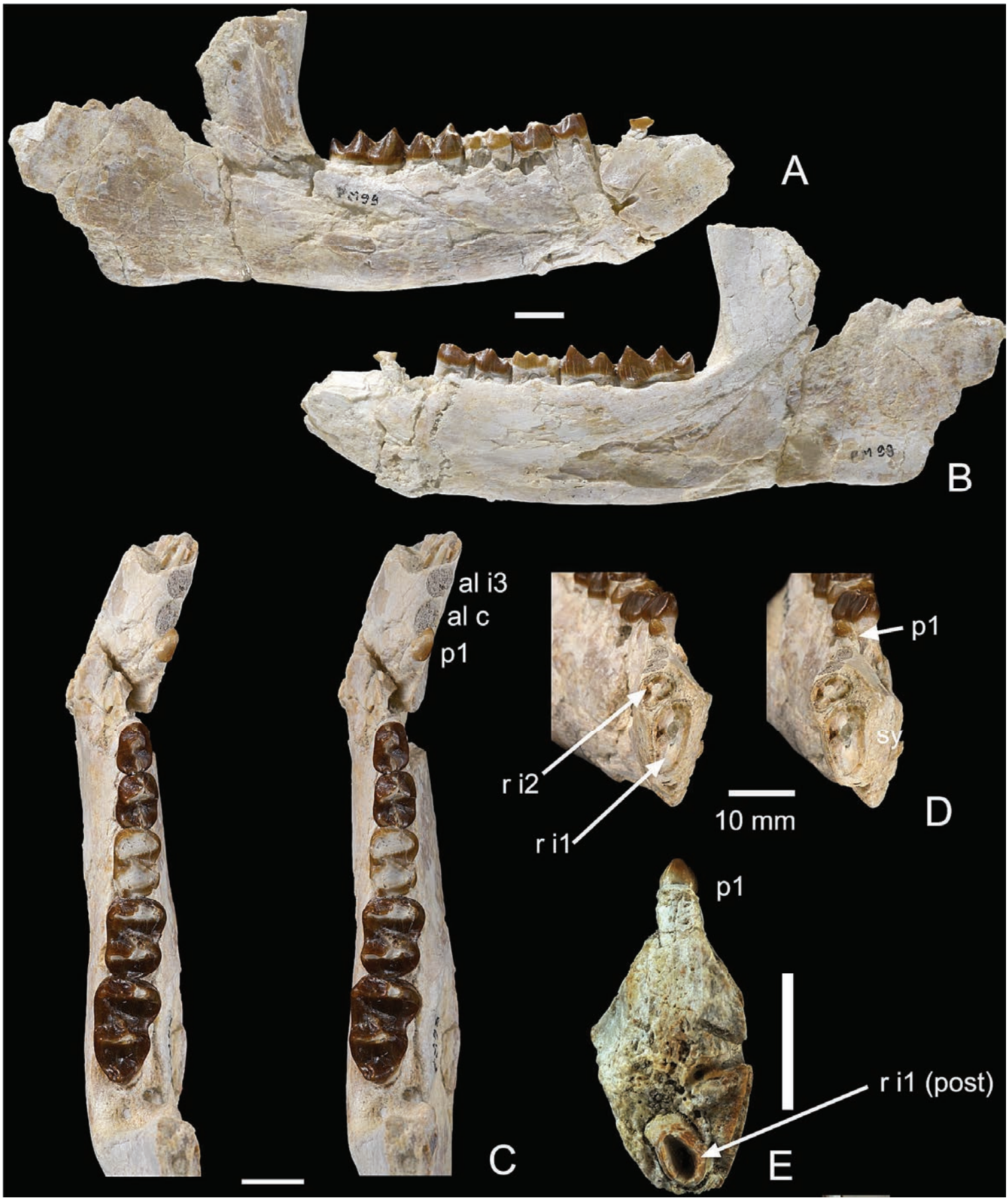
A
B
al i3
al c
p1
C
r i2
r i1
p1
sy
D
10 mm
p1
r i1 (post)
E

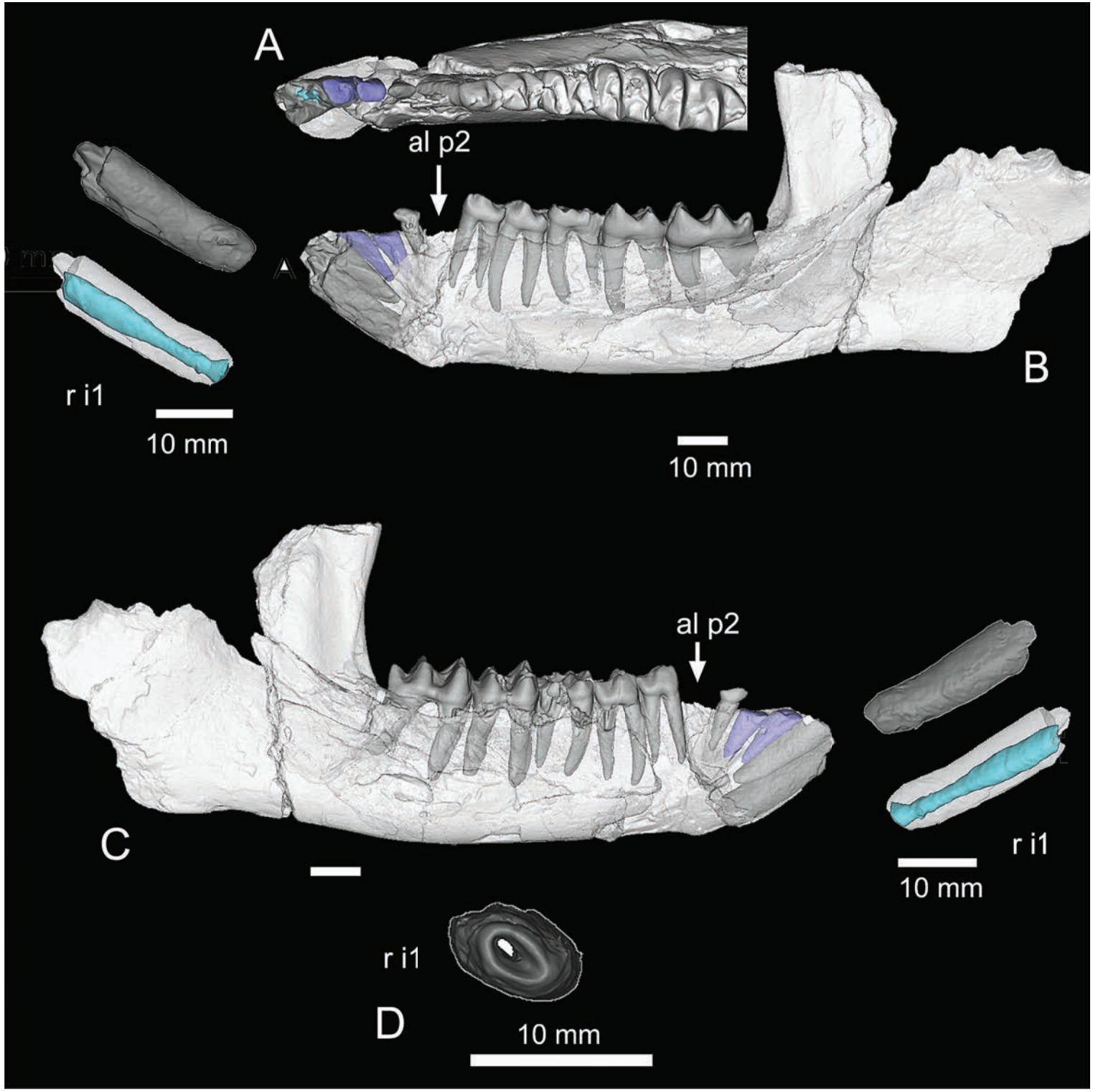
A
al p2
r i1
10 mm
B
10 mm
al p2
C
r i1
10 mm
r i1
D
10 mm

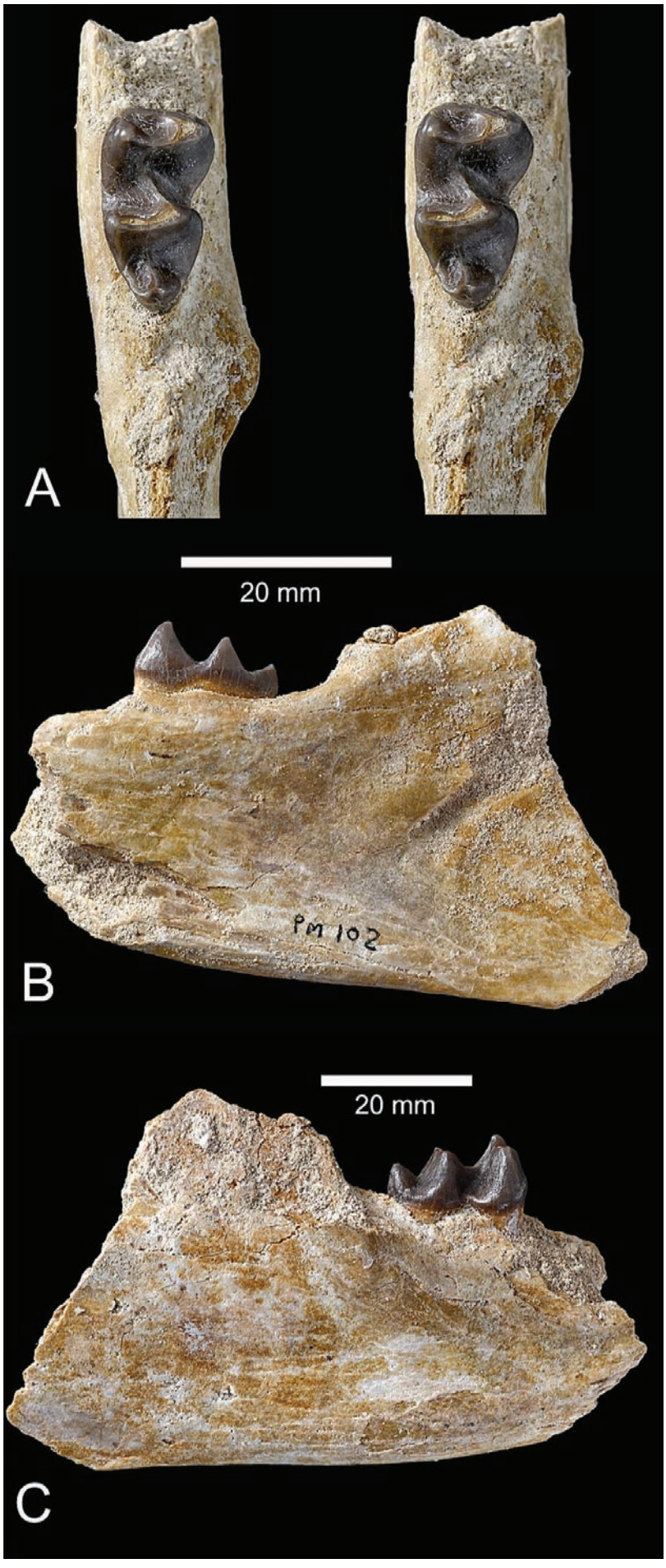
A
20 mm
PM 102
B
20 mm
C

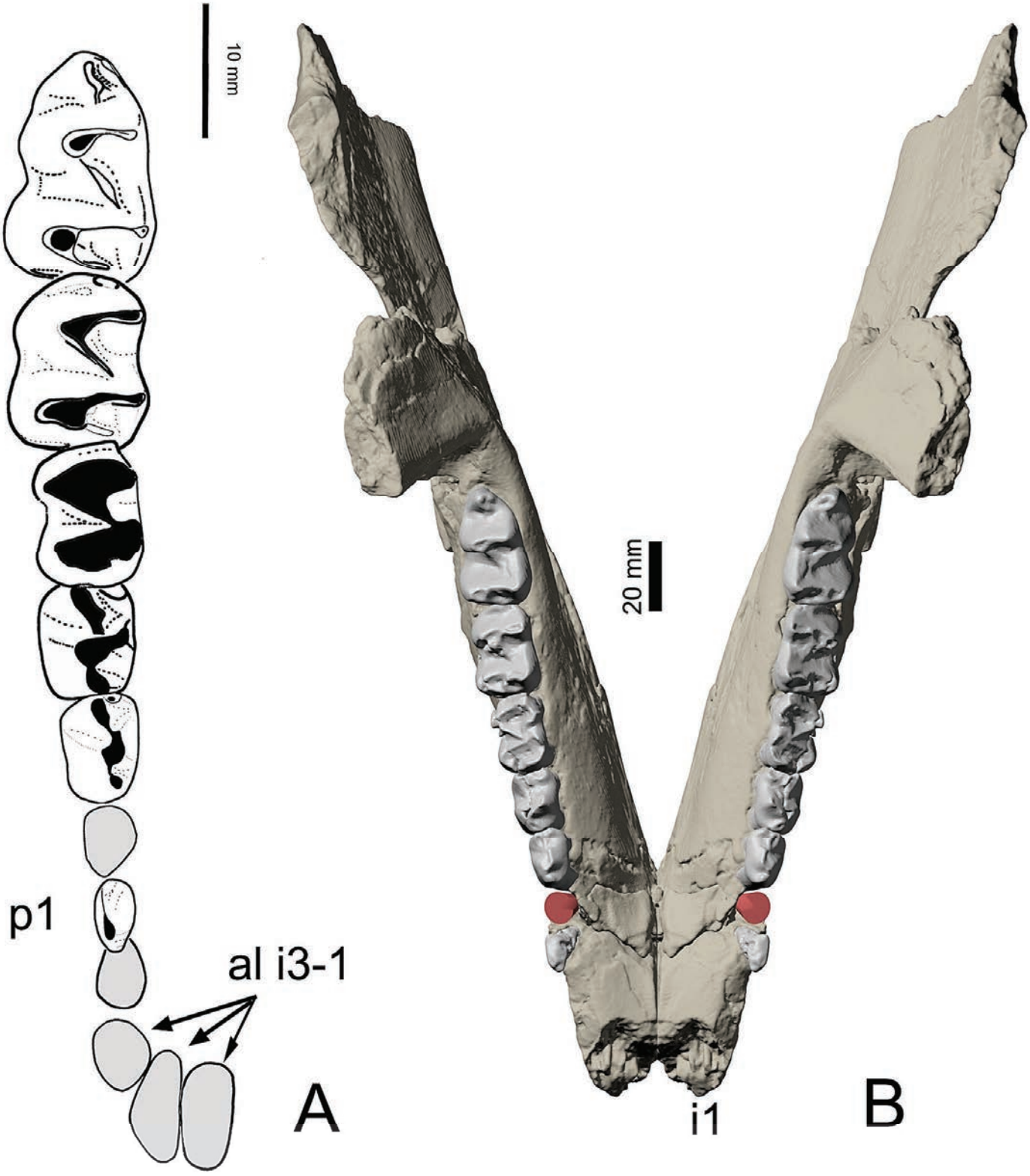
10 mm
p1
al i3-1
A
20 mm
i1
B

20 mm

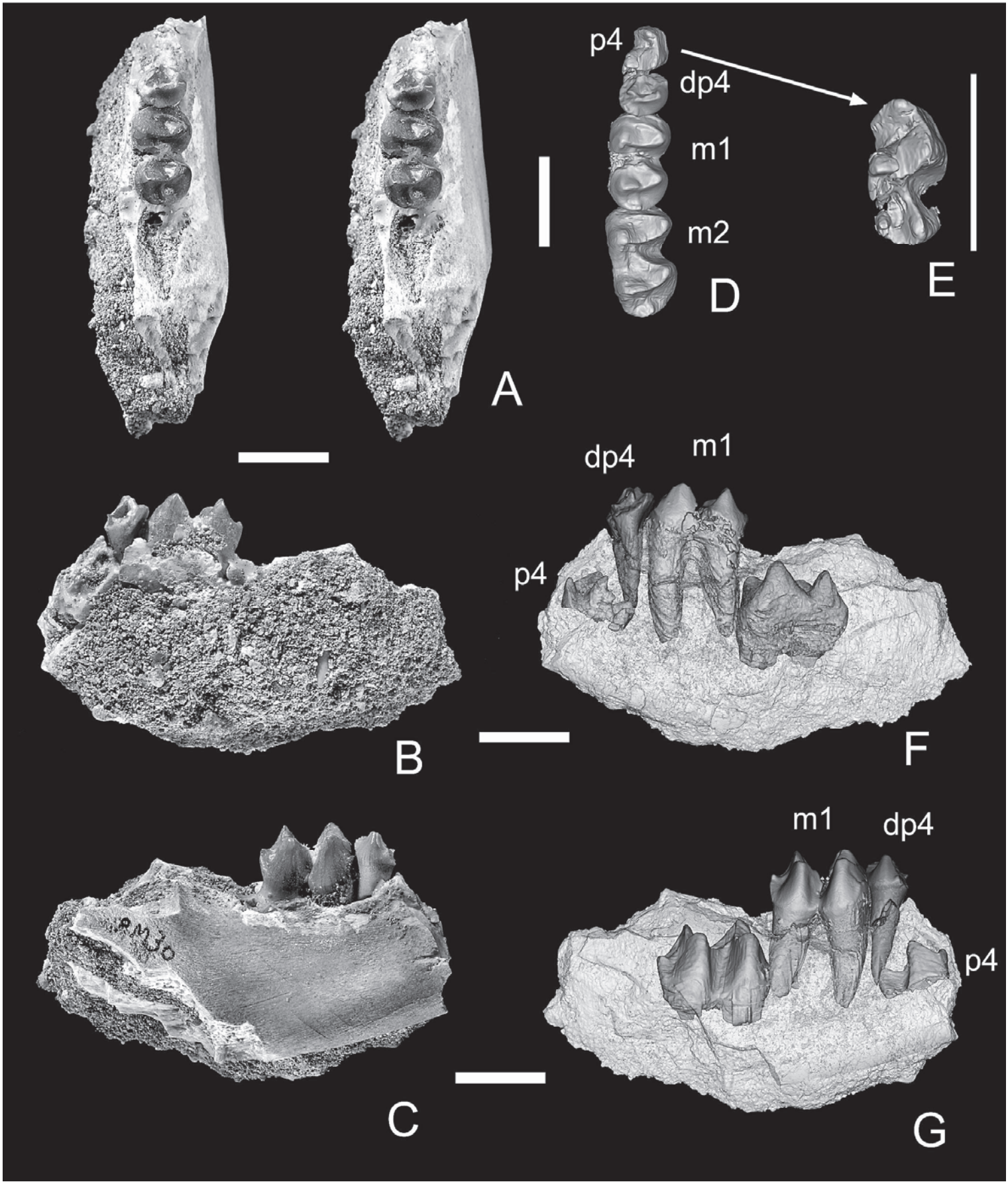
p4
dp4
m1
m2
D
E
A
dp4
m1
p4
B
F
m1
dp4
p4
C
G

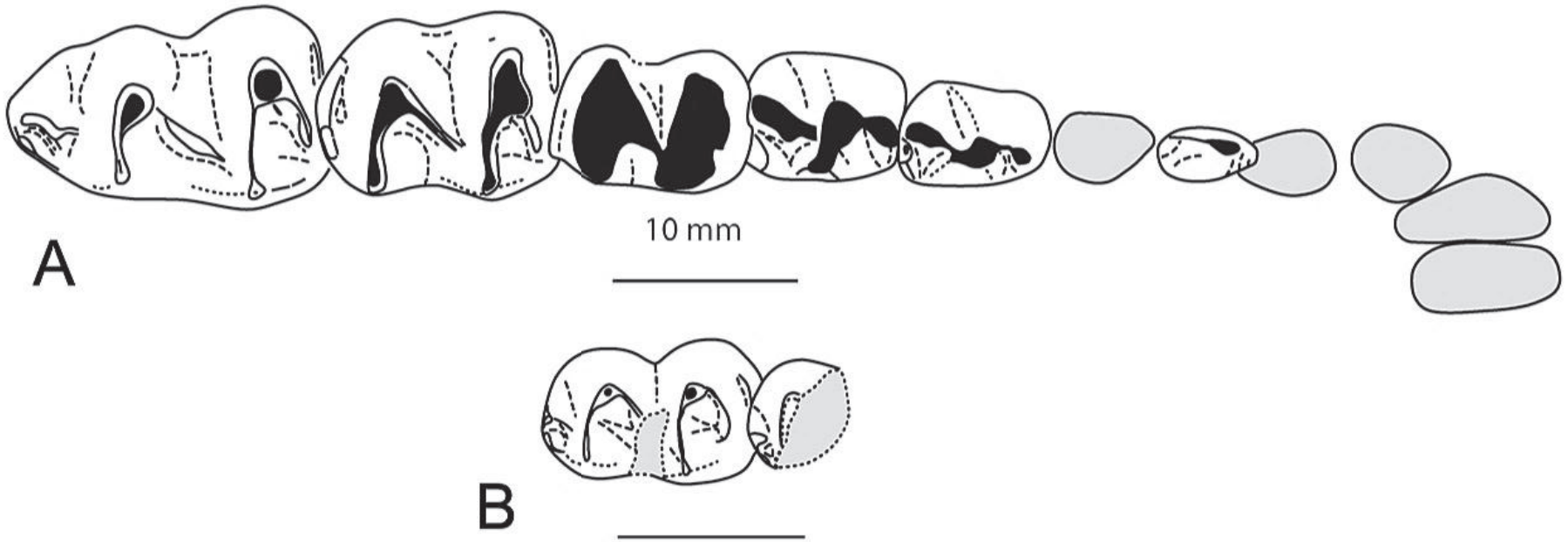
A
10 mm
B

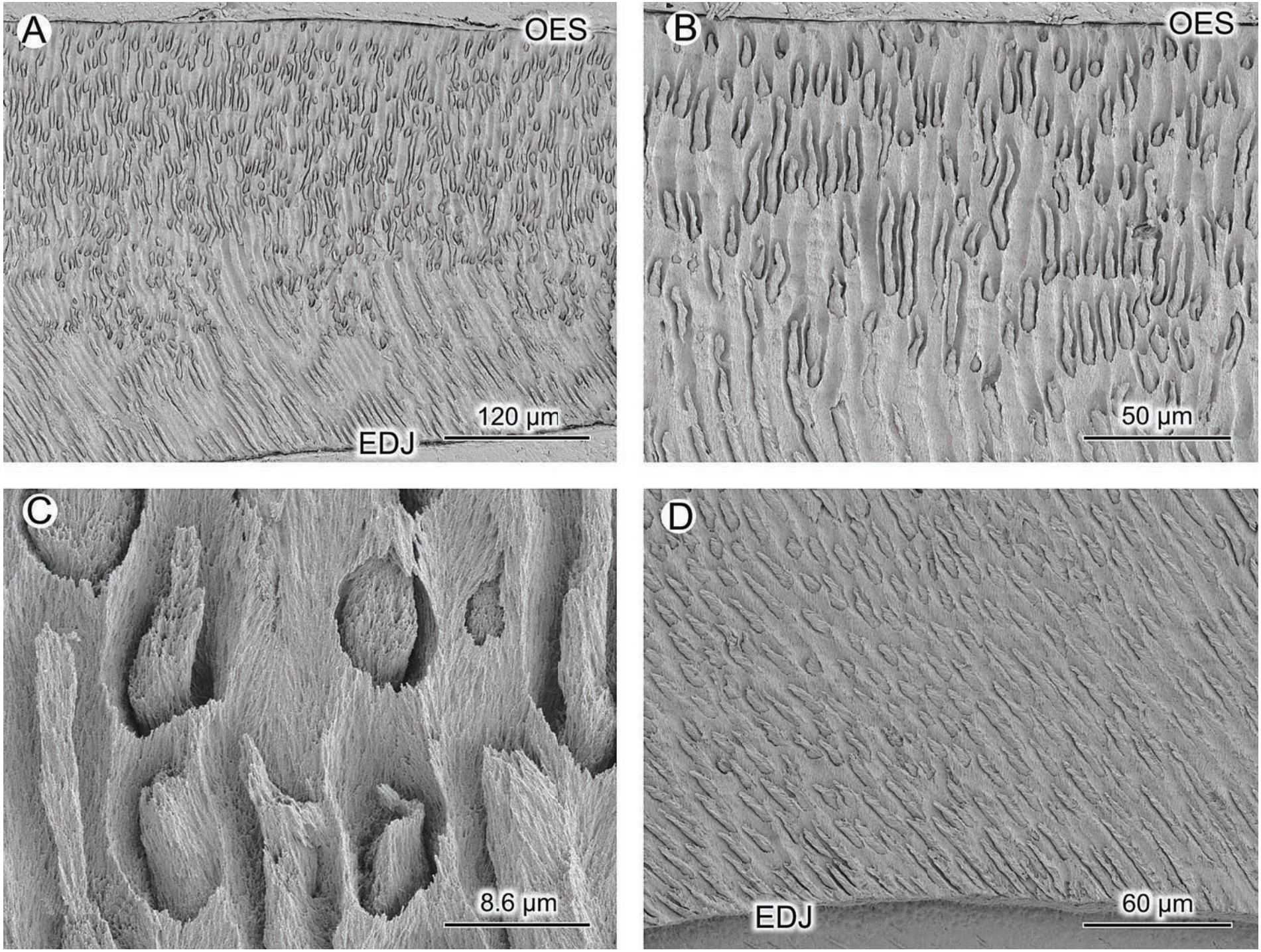
A
OES
EDJ
120 µm
B
OES
50 µm
C
8.6 µm
D
EDJ
60 µm

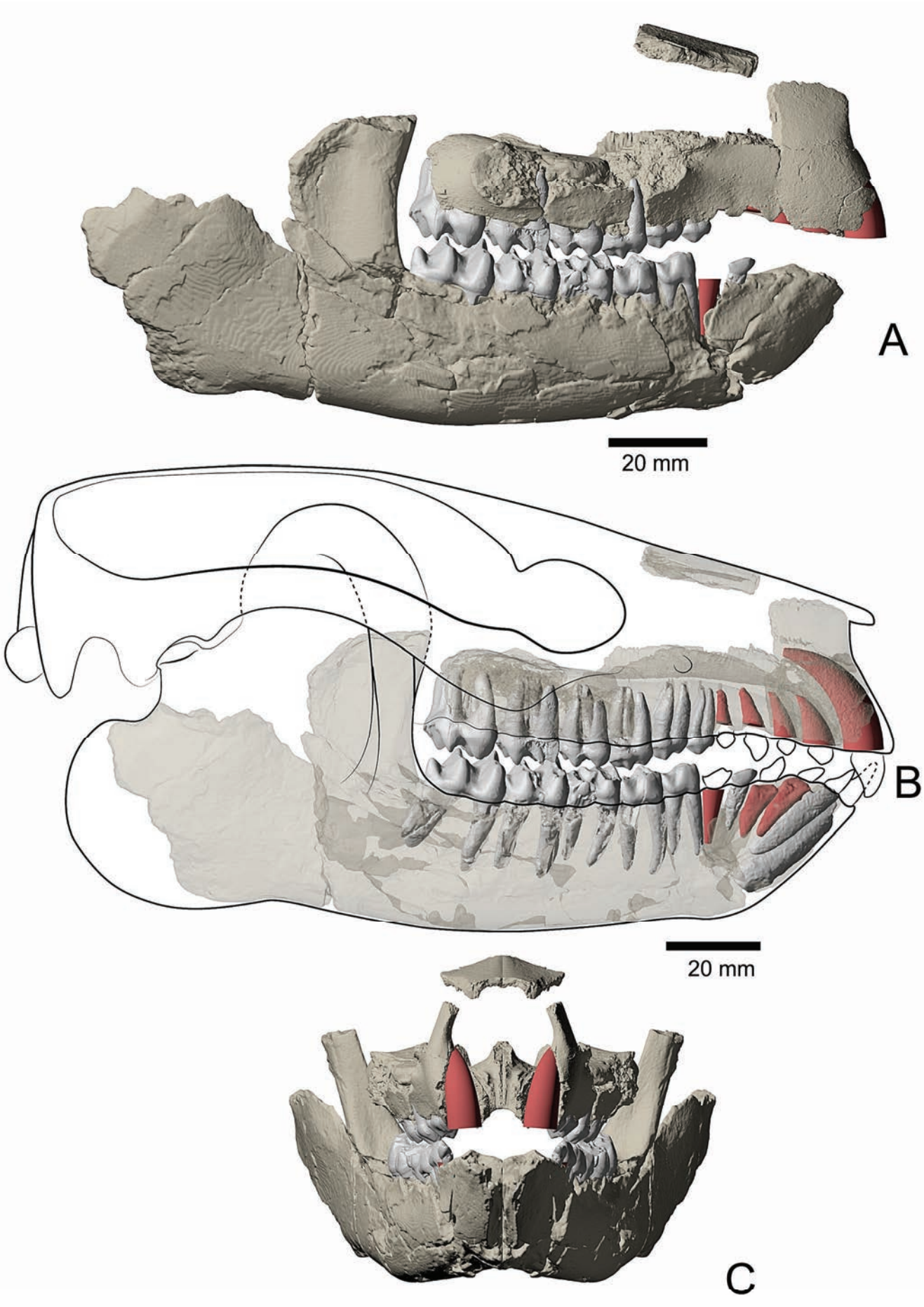
A
20 mm
B
20 mm
C


10 mm

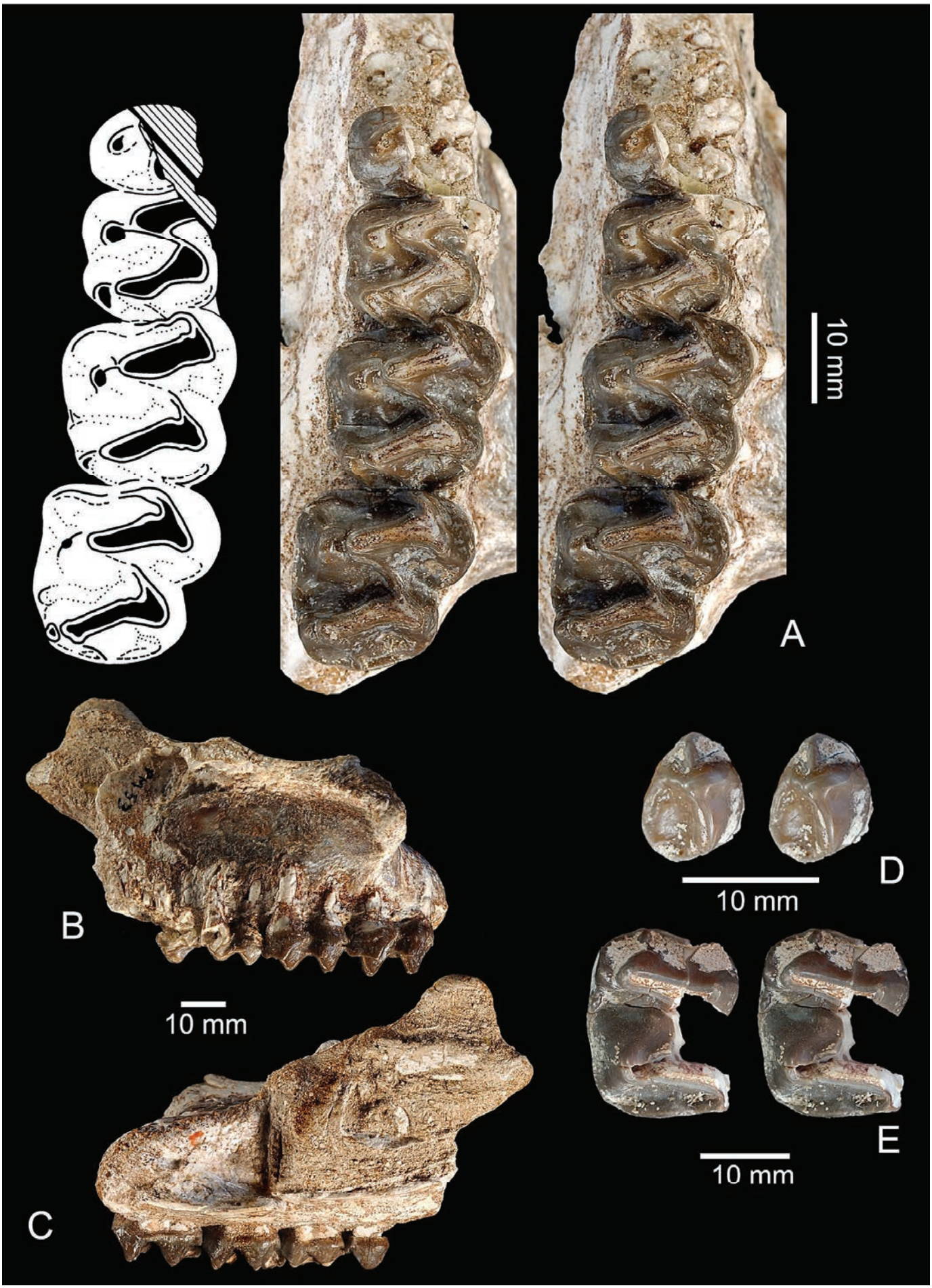
10 mm
A
B
10 mm
C
D
10 mm
E
10 mm

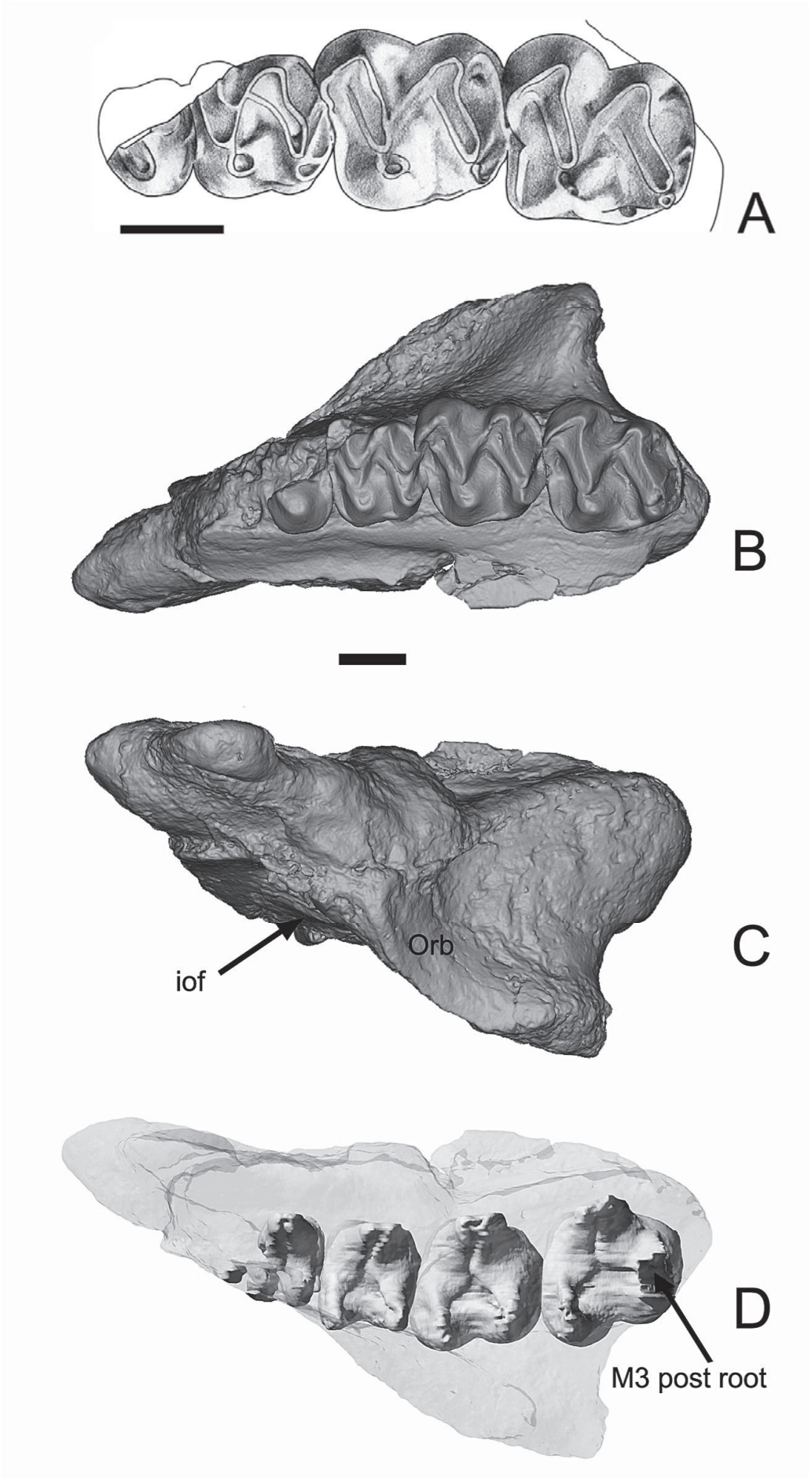
A
B
Orb
iof
C
D
M3 post root

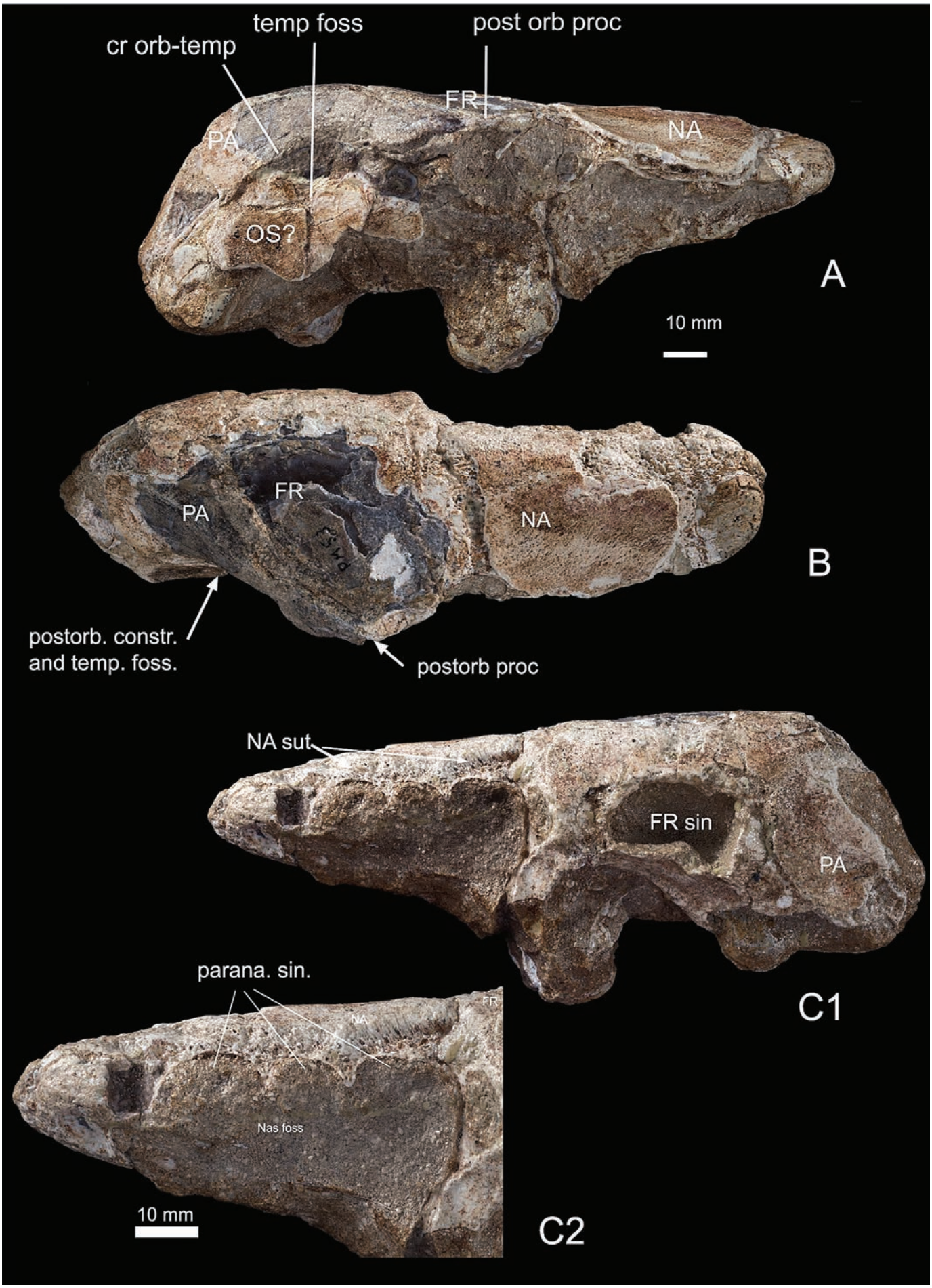
cr orb-temp
temp foss
post orb proc
FR
PA
NA
OS?
A
10 mm
FR
PA
NA
B
postorb. constr.
and temp. foss.
postorb proc
NA sut
FR sin
PA
C1
parana. sin.
FR
NA
Nas foss
10 mm
C2

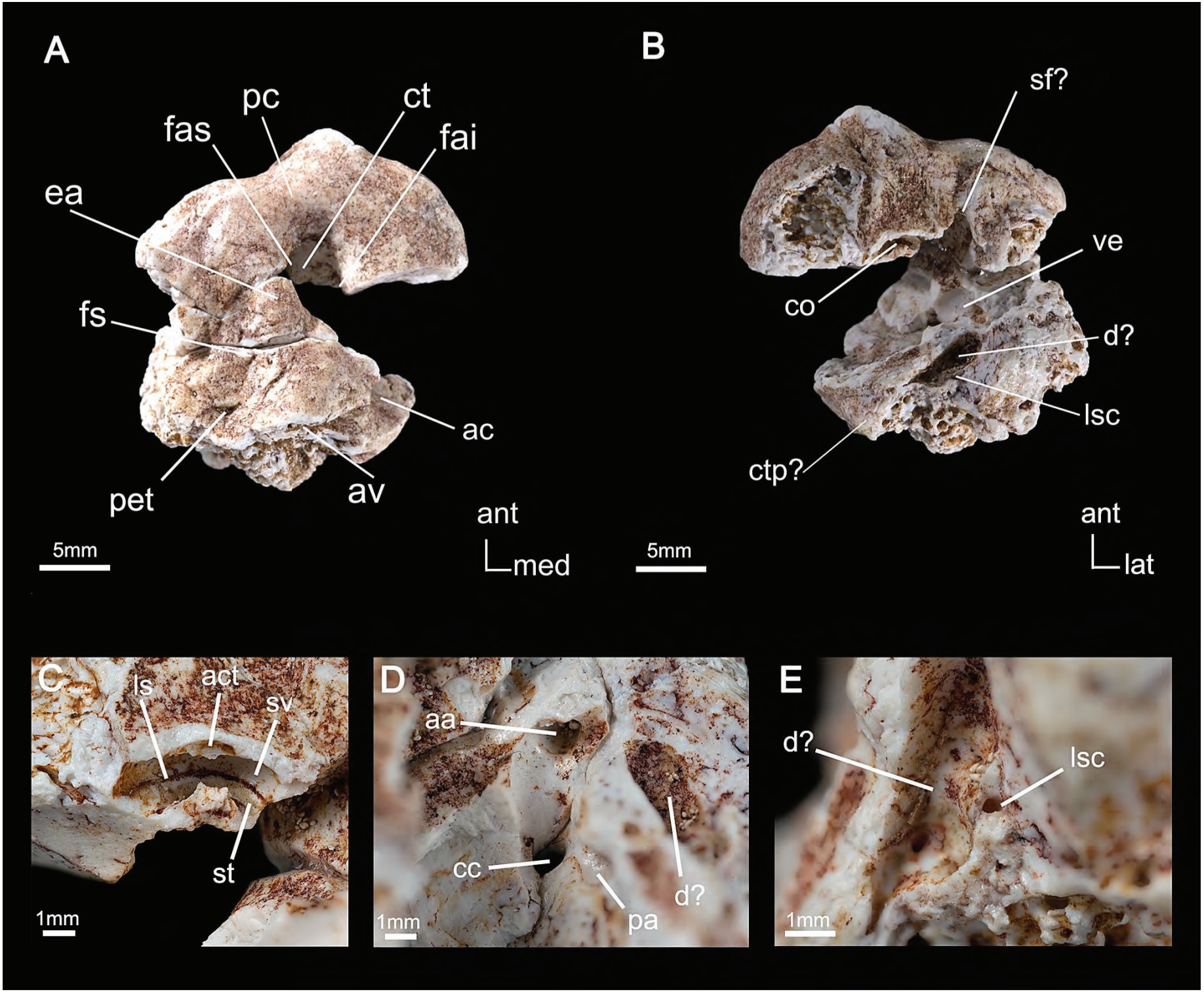
A
pc
ct
fas
fai
ea
fs
ac
pet
av
ant
med
5mm
B
sf?
ve
co
d?
lsc
ctp?
ant
lat
5mm
C
ls
act
sv
st
1mm
D
aa
cc
d?
pa
1mm
E
d?
lsc
1mm

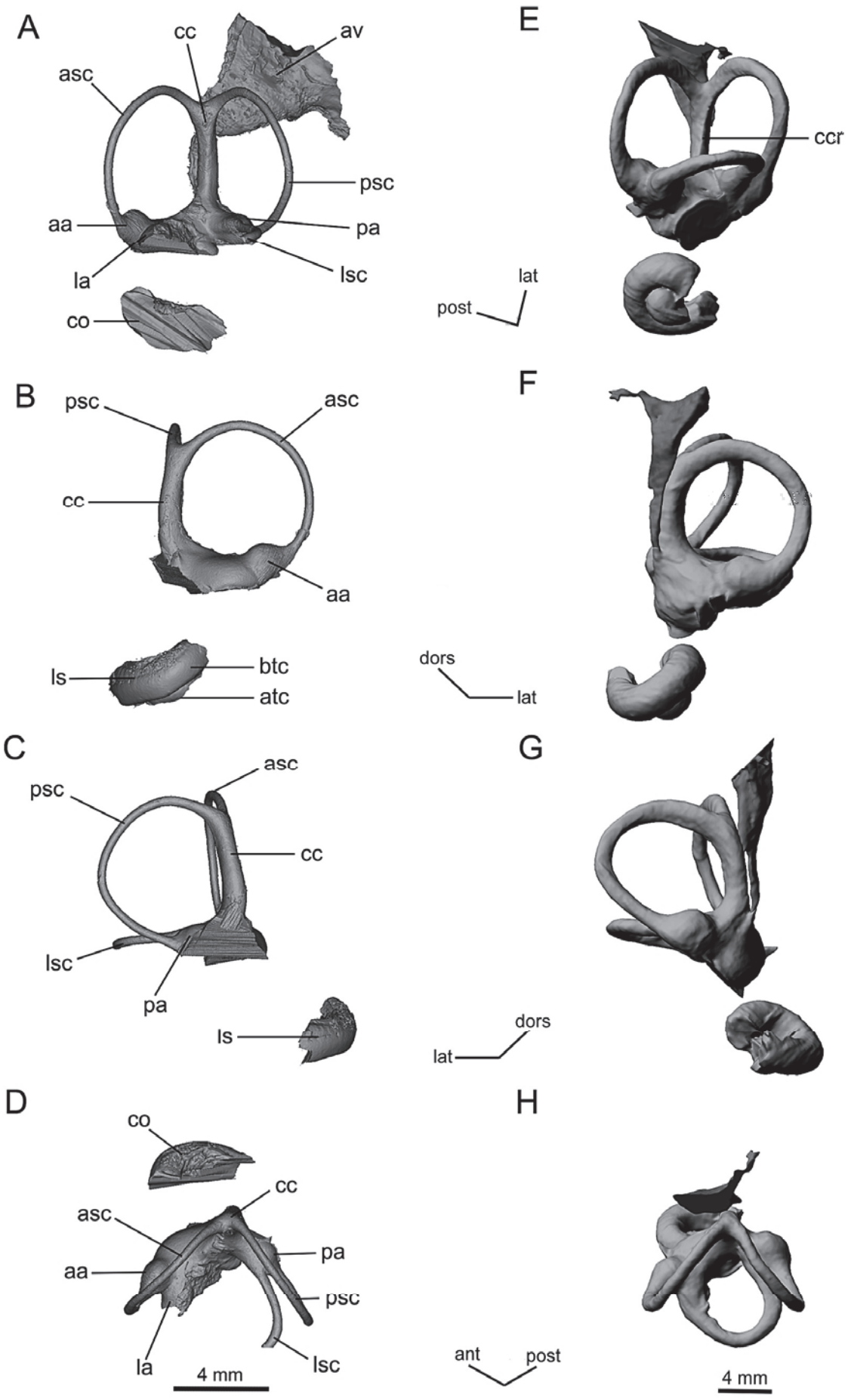
A
cc
av
asc
psc
aa
pa
la
lsc
co
B
psc
asc
cc
aa
ls
btc
atc
C
asc
psc
cc
lsc
pa
ls
D
co
cc
asc
pa
aa
psc
la
lsc
4 mm
E
ccr
lat
post
F
dors
lat
G
dors
lat
H
ant
post
4 mm

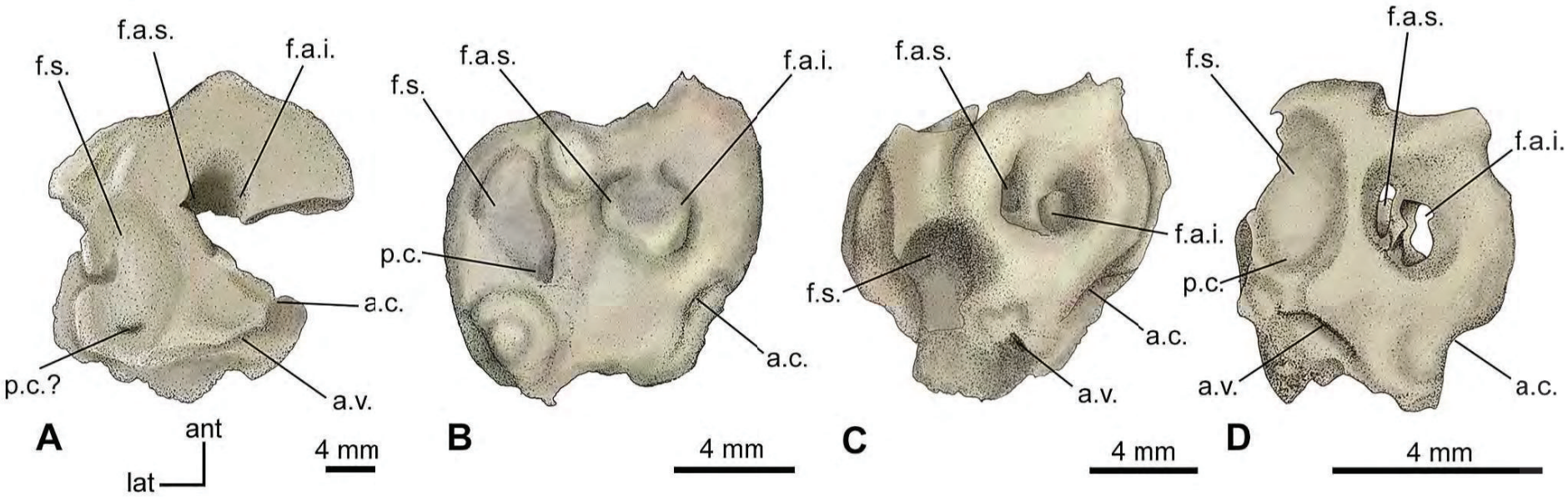
f.a.s.
f.s.
f.a.i.
p.c.?
a.c.
a.v.
A
ant
lat
4 mm
f.a.s.
f.s.
f.a.i.
p.c.
a.c.
B
4 mm
f.a.s.
f.a.i.
f.s.
a.c.
a.v.
C
4 mm
f.a.s.
f.s.
f.a.i.
p.c.
a.v.
a.c.
D
4 mm

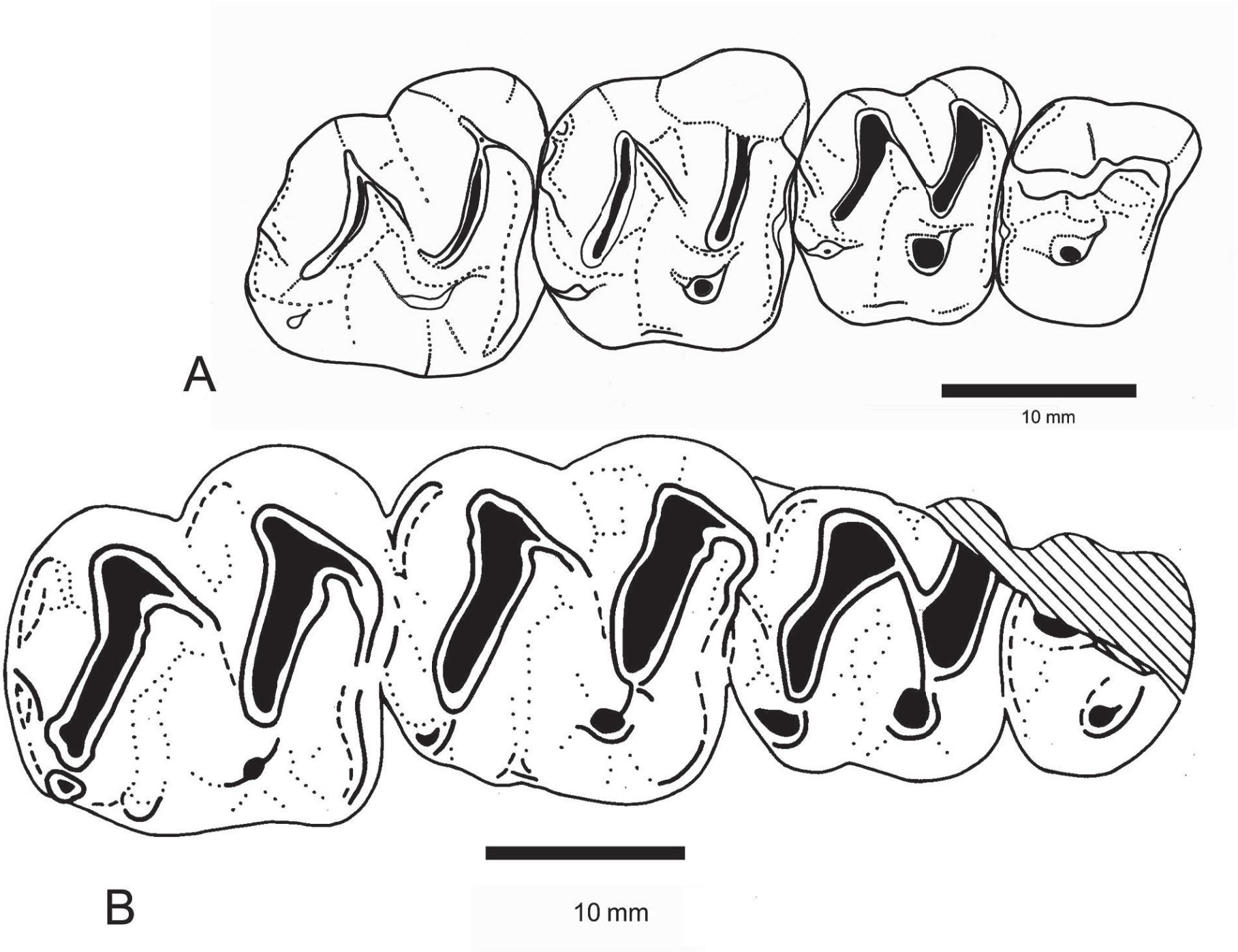
A
10 mm
B
10 mm

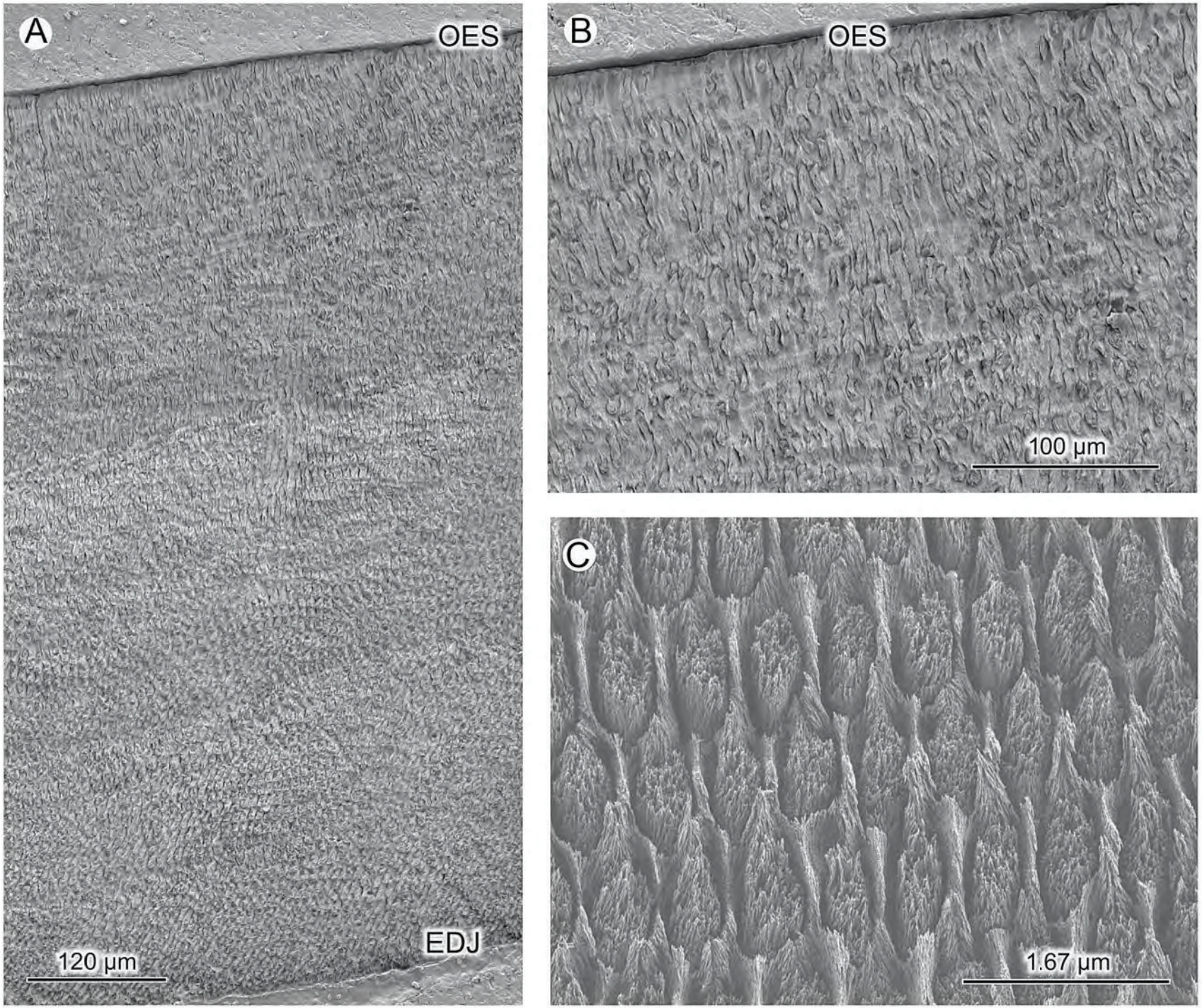
A
OES
EDJ
120 µm
B
OES
100 µm
C
1.67 µm

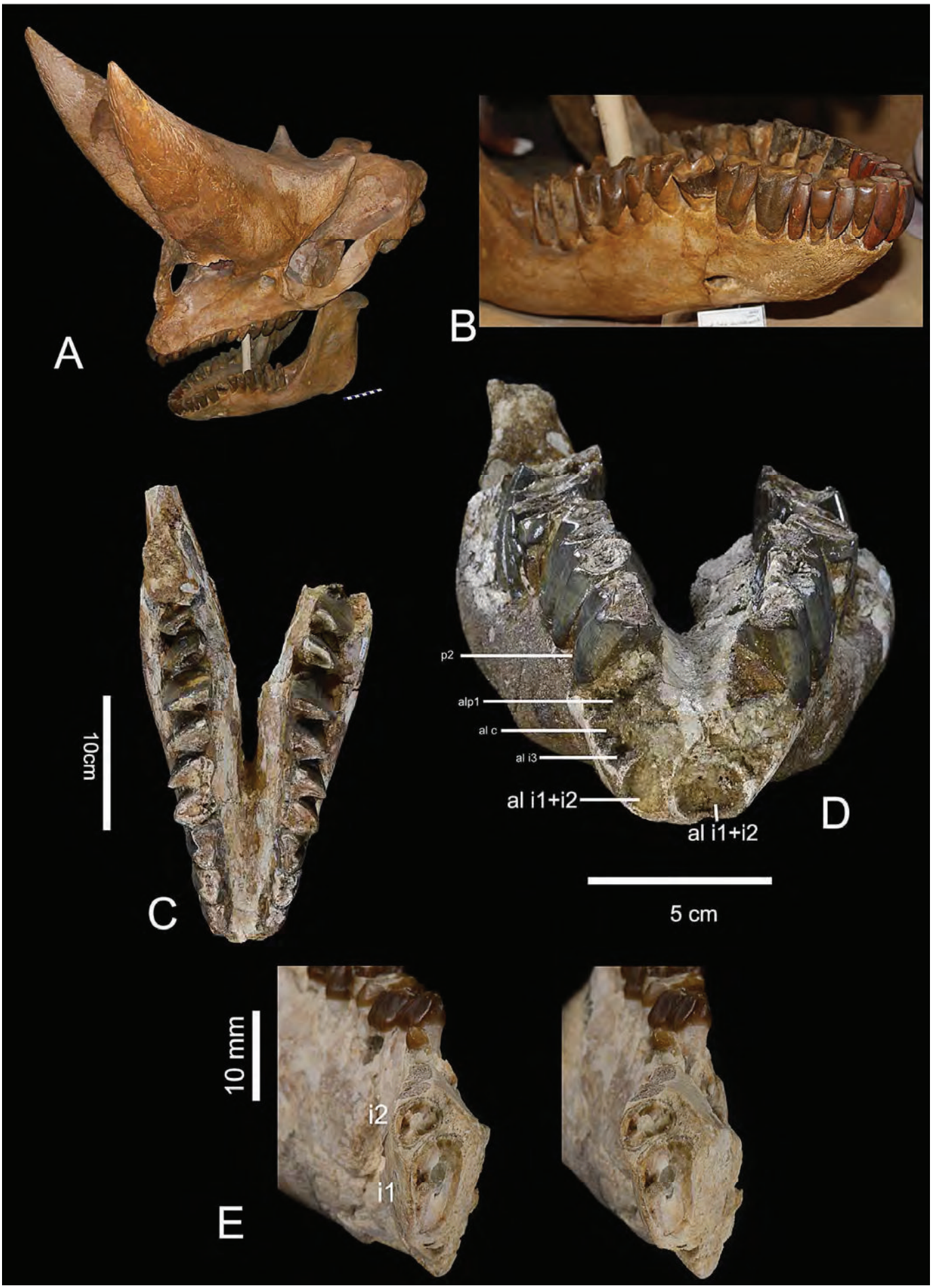
A
B
C
10cm
D
p2
alp1
al c
al i3
al i1+i2
al i1+i2
5 cm
E
10 mm
i2
i1

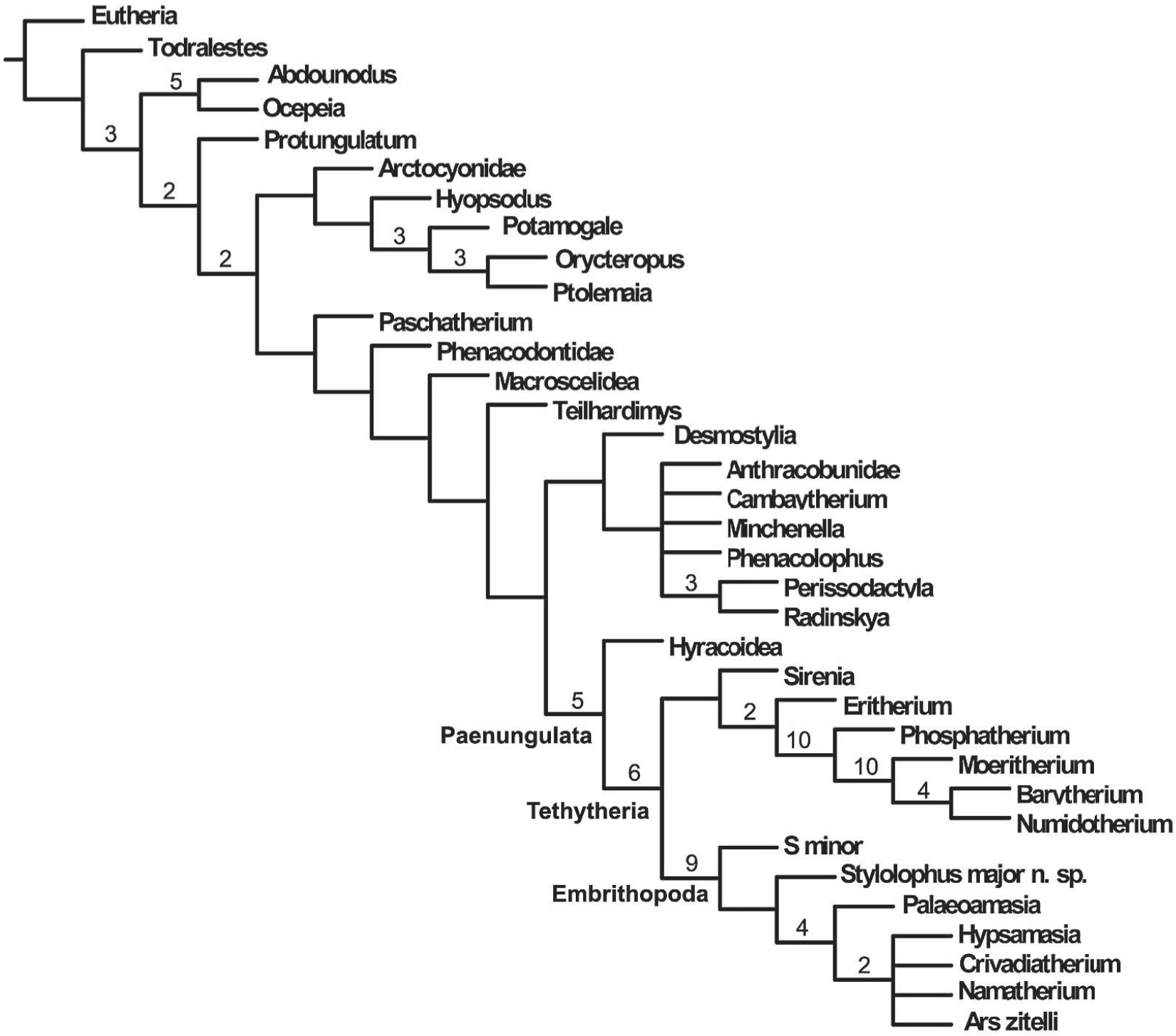
Eutheria
Todralestes
5
Abdounodus
Ocepeia
3
Protungulatum
2
Arctocyonidae
Hyopsodus
3
Potamogale
2
3
Orycteropus
Ptolemaia
Paschatherium
Phenacodontidae
Macroscelidea
Teilhardimys
Desmostylia
Anthracobunidae
Cambaytherium
Minchenella
Phenacolophus
3
Perissodactyla
Radinskya
Hyracoidea
Sirenia
5
2
Eritherium
Paenungulata
10
Phosphatherium
10
Moeritherium
6
4
Barytherium
Numidotherium
Tethytheria
S minor
9
Stylolophus major n. sp.
Embrithopoda
Palaeoamasia
4
Hypsamasia
2
Crivadiatherium
Namatherium
Ars zitelli

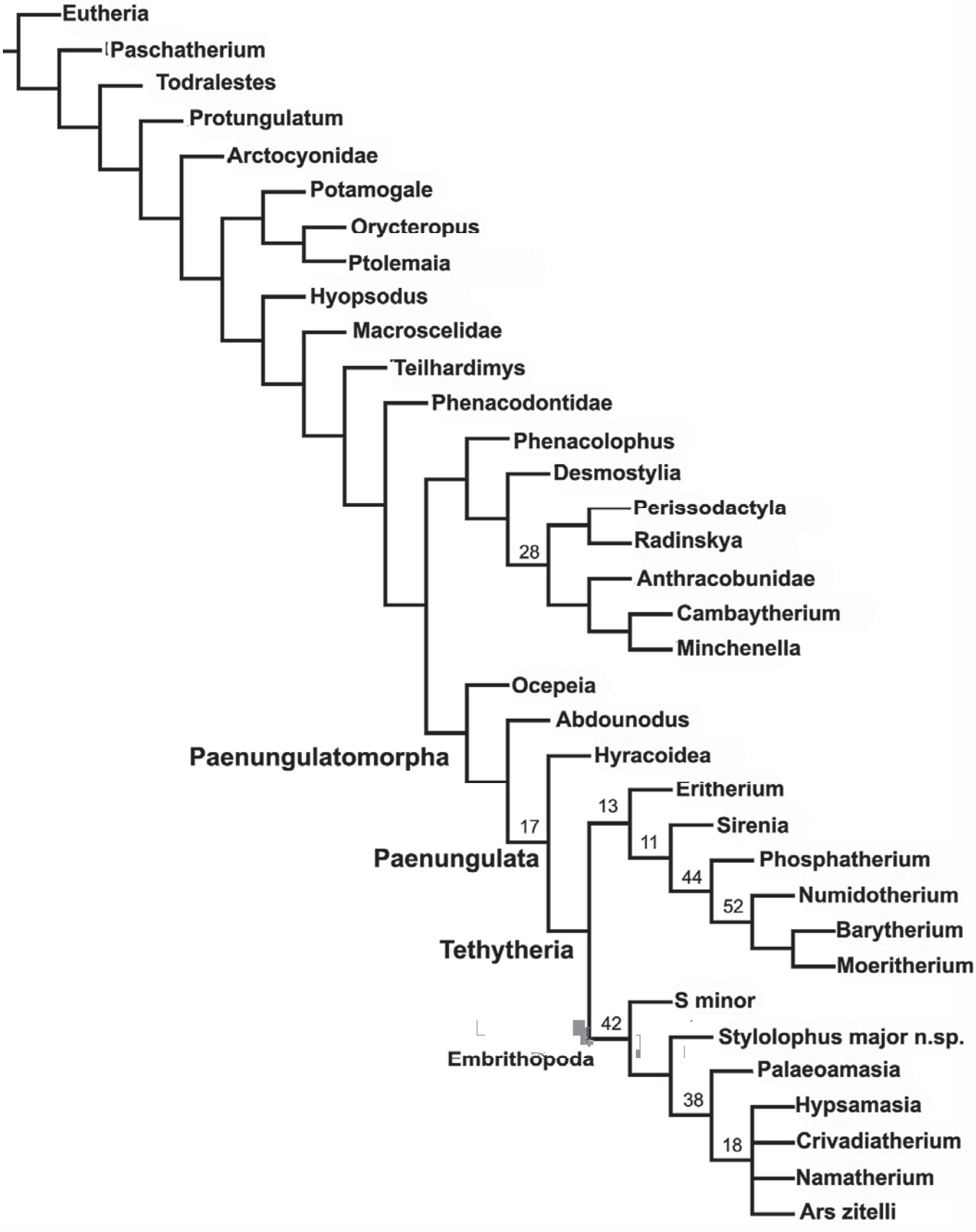
Eutheria
Paschatherium
Todralestes
Protungulatum
Arctocyonidae
Potamogale
Orycteropus
Ptolemaia
Hyopsodus
Macroscelidae
Teilhardimys
Phenacodontidae
Phenacolophus
Desmostylia
Perissodactyla
Radinskya
28
Anthracobunidae
Cambaytherium
Minchenella
Ocepeia
Abdounodus
Paenungulatomorpha
Hyracoidea
Eritherium
13
17
Sirenia
11
Paenungulata
Phosphatherium
44
Numidotherium
52
Barytherium
Tethytheria
Moeritherium
S minor
42
Stylolophus major n.sp.
Embrithopoda
Palaeoamasia
38
Hypsamasia
18
Crivadiatherium
Namatherium
Ars zitelli